

DOE/BC/14885-10
(DE95000180)

DEVELOPMENT OF COST-EFFECTIVE
SURFACTANT FLOODING TECHNOLOGY

Annual Report for the Period
September 30, 1993 to September 29, 1994

By
G. Pope
K. Sepehmoori

August 1995

Performed Under Contract No. DE-AC22-92BC14885

The University of Texas
Austin, Texas



**Bartlesville Project Office
U. S. DEPARTMENT OF ENERGY
Bartlesville, Oklahoma**

DISCLAIMER

This report was prepared as an account of work sponsored by an agency of the United States Government. Neither the United States Government nor any agency thereof, nor any of their employees, makes any warranty, expressed or implied, or assumes any legal liability or responsibility for the accuracy, completeness, or usefulness of any information, apparatus, product, or process disclosed, or represents that its use would not infringe privately owned rights. Reference herein to any specific commercial product, process, or service by trade name, trademark, manufacturer, or otherwise does not necessarily constitute or imply its endorsement, recommendation, or favoring by the United States Government or any agency thereof. The views and opinions of authors expressed herein do not necessarily state or reflect those of the United States Government.

This report has been reproduced directly from the best available copy.

Available to DOE and DOE contractors from the Office of Scientific and Technical Information, P.O. Box 62, Oak Ridge, TN 37831; prices available from (615) 576-8401.

Available to the public from the National Technical Information Service, U.S. Department of Commerce, 5285 Port Royal Rd., Springfield VA 22161

DOE/BC/14885-10
Distribution Category UC-122

Development of Cost-Effective
Surfactant Flooding Technology

Annual Report for the Period
September 30, 1993 to September 29, 1994

By
G. Pope
K. Sepehrnoori

August 1995

Work Performed Under Contract No. DE-AC22-92BC14885

Prepared for
U.S. Department of Energy
Assistant Secretary for Fossil Energy

Jerry Casteel, Project Manager
Bartlesville Project Office
P.O. Box 1398
Bartlesville, OK 74005

Prepared by
The University of Texas
Center for Petroleum and Geosystems Engineering
Dept. of Petroleum Engineering
Austin, TX 78712

TABLE OF CONTENTS

LIST OF TABLES	IV
LIST OF FIGURES	V
ABSTRACT	1
EXECUTIVE SUMMARY	1
UTCHEM MODELING ENHANCEMENTS	3
TASK 1. HIGH-RESOLUTION, FULLY IMPLICIT, COMPOSITIONAL SIMULATION	4
Introduction	4
Physical and Mathematical Model	5
Governing equations and constitutive relations	5
Finite-difference schemes	6
Solution schemes	6
Simulation Results and Analyses	7
Three-dimensional convection-diffusion problem	7
Three-dimensional polymerflood with horizontal well	8
Two-dimensional, cross-sectional polymerflood	8
Summary, Conclusions, and Future Work	9
TASK 2. OPTIMIZATION OF SURFACTANT FLOODING	9
Introduction	9
Subtask 2.1 Stochastic Simulation of Surfactant Flooding	10
Subtask 2.2 Evaluation of Surfactant Flooding using Horizontal Wells	10
Subtask 2.3 Evaluation of Low Tension Polymerflooding	10
Reservoir Description	11
Reservoir I	11
Reservoir II	11
Reservoir III	12
Horizontal Wells with Vertical Drainholes	12
Residual Oil Saturation Dependence on Permeability	12
Reservoir I	13
Reservoir II	13
Reservoir III	14
Low-Tension Polymerflooding	15
Reservoir I	15
Reservoir II	16
Reservoir III	16
Summary, Conclusions, and Future Work	17
NOMENCLATURE	18
Greek Symbols	18
Subscripts and Superscripts	18
REFERENCES	19

LIST OF TABLES

Tables

- 1.1 Potential Rate Allocation Method and Solution Scheme for Multicell Well
- 2.1 Simulation Input Data for Reservoir I
- 2.2 Schedule of Injection Conditions for Reservoir I
- 2.3 Simulation Input Data for Reservoir II
- 2.4 Simulation Input Data for Reservoir III

LIST OF FIGURES

Figures

- 1.1 Gridpoints Used in the High-Order Finite-Difference Scheme
- 1.2 Matrix Structure for a Three-Dimensional, Two-Component Problem Using the Fully Implicit High-Order Method with 5x5x3 Gridblocks
- 1.3 Schematic of Well Patterns
- 1.4 Simulation of a Three-Dimensional Tracer Convection-Diffusion Using the IMPES Simulator and the Fully Implicit Simulator
- 1.5 Simulation of a Three-Dimensional Tracer Convection-Diffusion Using the IMPES Simulator
- 1.6 Simulation of a Three-Dimensional Tracer Convection-Diffusion Using the Fully Implicit Simulator
- 1.7 Simulation of a Three-Dimensional Tracer Convection-Diffusion for a Peclet Number of 50 Using the Fully Implicit Simulator with the High-Order Scheme Without TVD Flux-Limiting and the Low-Order Scheme
- 1.8 Simulation of a Three-Dimensional Tracer Convection-Diffusion for a Peclet Number of 500 Using the Fully Implicit Simulator with the High-Order Scheme Without TVD Flux-Limiting and the Low-Order Scheme
- 1.9 Schematic of Nonuniform Grids and the Expansion Ratio
- 1.10 Simulation of a Three-Dimensional Tracer Convection-Diffusion Using the IMPES Simulator with Nonuniform Grids
- 1.11 Simulation of a Three-Dimensional Tracer Convection-Diffusion Using the IMPES Simulator with Nonuniform Grids
- 1.12 Simulation of a Three-Dimensional Polymerflood with Horizontal Well Using the Fully Implicit Simulator and the Fully Implicit Simulator
- 1.13 Simulation of a Three-Dimensional Polymerflood with Horizontal Well Using the IMPES Simulator
- 1.14 Simulation of a Three-Dimensional Polymerflood with Horizontal Well Using the Fully Implicit Simulator
- 1.15 Simulation of a Two-Dimensional, Cross-Sectional Polymerflood Using the IMPES Simulator and the Fully Implicit Simulator
- 1.16 Oil Recovery and Normalized Effluent Polymer Concentration of Simulating a Two-Dimensional, Cross-Sectional Polymerflood Using the IMPES Simulator
- 1.17 Water Cut of Simulating a Two-Dimensional, Cross-Sectional Polymerflood Using the IMPES Simulator

- 1.18 Oil Recovery and Normalized Effluent Polymer Concentration of Simulating a Two-Dimensional, Cross-Sectional Polymerflood Using the Fully Implicit Simulator
- 1.19 Water Cut of Simulating a Two-Dimensional, Cross-Sectional Polymerflood Using the Fully Implicit Simulator
- 1.20 Simulation of a Two-Dimensional, Cross-Sectional Polymerflood with a High Vertical Permeability
- 1.21 Water Saturation and Polymer Concentration Distributions with a High Vertical Permeability Using the Mobility Rate Allocation Method
- 1.22 Water Saturation and Polymer Concentration Distributions with a High Vertical Permeability Using the Potential Rate Allocation Method
- 1.23 Simulation of a Two-Dimensional, Cross-Sectional Polymerflood with a Low Vertical Permeability
- 1.24 Water Saturation and Polymer Concentration Distributions with a Low Vertical Permeability Using the Mobility Rate Allocation Method
- 1.25 Water Saturation and Polymer Concentration Distributions with a Low Vertical Permeability Using the Potential Rate Allocation Method
- 2.1 Sketch of the Quarter Five-Spot Showing the Horizontal Injection Wellbore for Reservoir I
- 2.2 Simulation Gridblocks for Reservoir II
- 2.3 Sketch of the Quarter Five-Spot Showing the Horizontal Injection Wellbore Along the x direction and Vertical Drainholes for Reservoir I
- 2.4 Cumulative Oil Produced versus Time for Surfactant Floods One with the Horizontal Injection Wellbore Placed Along the x direction and the Other Placed Along the y direction for Reservoir I
- 2.5 Cumulative Oil Produced versus Pore Volumes Injected for Surfactant Floods One with the Horizontal Injection Wellbore Placed Along the x direction and the Other Placed Along the y direction for Reservoir I
- 2.6 Cumulative Oil Produced versus Time for Surfactant Floods One with the Horizontal Injection Wellbore Placed Along the x direction and with and without Drainholes for Reservoir I
- 2.7 Cumulative Oil Produced versus Pore Volumes Injected for Surfactant Floods One with the Horizontal Injection Wellbore Placed Along the x direction and with and without Drainholes for Reservoir I
- 2.8 Plot of S_{orw} as a Function of Permeability for Reservoir I
- 2.9 Capillary Desaturation Curves for Permeability-dependent S_{orw} (Case 3: $S_{orw} = \exp(-1.1859127k^{0.04})$) for Reservoir I

- 2.10 Capillary Desaturation Curves for Permeability-dependent S_{orw} (Case 4: $S_{orw} = \exp(-0.941164k^{0.1})$) for Reservoir I
- 2.11 Effect of Distributed S_{orw} on Oil Recovery for Reservoir I
- 2.12 Effect of Distributed S_{orw} on Oil Recovery for Reservoir I
- 2.13 Oil Concentration Distribution at 0.75 Pore Volumes Injected (1,976 days) for Case 1 for Reservoir I
- 2.14 Oil Concentration Distribution at 0.75 Pore Volumes Injected (1,976 days) for Case 2 for Reservoir I
- 2.15 Oil Concentration Distribution at 0.75 Pore Volumes Injected (1,976 days) for Case 3 for Reservoir I
- 2.16 Oil Concentration Distribution at 0.75 Pore Volumes Injected (1,976 days) for Case 4 for Reservoir I
- 2.17 Oil Concentration Distribution at 2.75 Pore Volumes Injected (7,241 days) for Case 1 for Reservoir I
- 2.18 Oil Concentration Distribution at 2.75 Pore Volumes Injected (7,241 days) for Case 2 for Reservoir I
- 2.19 Oil Concentration Distribution at 2.75 Pore Volumes Injected (7,241 days) for Case 3 for Reservoir I
- 2.20 Oil Concentration Distribution at 2.75 Pore Volumes Injected (7,241 days) for Case 4 for Reservoir I
- 2.21 Plot of Residual Oil Saturation (S_{orw}) as a Function of Permeability for Reservoir II
- 2.22 Capillary Desaturation Curves for Permeability-dependent S_{orw} ($S_{orw} = \exp(-0.88222k^{0.125})$) for Reservoir II
- 2.23 Capillary Desaturation Curves for Permeability-dependent S_{orw} ($S_{orw} = \exp(-1.1048k^{0.0625})$) for Reservoir II
- 2.24 Capillary Desaturation Curves for Permeability-dependent S_{orw} ($S_{orw} = \exp(-0.5665k^{0.25})$) for Reservoir II
- 2.25 Effect of Residual Oil Saturation on Chemical Flood Oil Recovery for Reservoir II
- 2.26 Effect of Residual Oil Saturation on Chemical Flood Oil Recovery for Reservoir II
- 2.27 Effect of Residual Oil Saturation on Oil Production Rate for Reservoir II
- 2.28 Effect of Residual Saturation on Tertiary Cumulative Oil Production for Reservoir II
- 2.29 Effect of Residual Saturation on Tertiary Cumulative Oil Production for Reservoir II
- 2.30 Plot of Residual Oil Saturation (S_{orw}) as a Function of Permeability for Reservoir III

- 2.31 Capillary Desaturation Curves for Permeability-dependent S_{orw} (Case 3: $S_{orw} = \exp(-0.0161865k^{0.5})$) for Reservoir III
- 2.32 Capillary Desaturation Curves for Permeability-dependent S_{orw} (Case 4: $S_{orw} = \exp(-0.001752905k^{0.075})$) for Reservoir III
- 2.33 Capillary Desaturation Curves for Permeability-dependent S_{orw} (Case 5: $S_{orw} = \exp(-0.2336038k^{0.2})$) for Reservoir III
- 2.34 Effect of Distributed S_{orw} on Oil Recovery for Reservoir III
- 2.35 Effect of Distributed S_{orw} on Oil Rate for Reservoir III
- 2.36 Effect of Distributed S_{orw} on Water Cut for Reservoir III
- 2.37 Oil Concentration Distribution at 0.5 PV Injected (84 days) for Reservoir III
- 2.38 Oil Concentration Distribution for LTPF at 1.8 PV Injected (303 days) for Reservoir III
- 2.39 Effect of Competitive Adsorption on Oil Recovery for Reservoir I
- 2.40 Effect of Competitive Adsorption on Oil Recovery for Reservoir I
- 2.41 History of Effluent Surfactant Concentration for Reservoir I
- 2.42 Surfactant Adsorption with and without Competition from Polymer for Reservoir I
- 2.43 Effect of Polymer Preflooding on Oil Recovery for Reservoir I
- 2.44 Effect of Polymer Preflooding on Surfactant Adsorption for Reservoir I
- 2.45 Effect of Competitive Adsorption on Oil Recovery for Reservoir II
- 2.46 Effect of Competitive Adsorption on Effluent Surfactant Concentration for Reservoir II
- 2.47 Effect of Competitive Adsorption on Surfactant Adsorption for Reservoir II
- 2.48 Effect of Competitive Adsorption on Oil Recovery for Reservoir II
- 2.49 Effect of Competitive Adsorption on Effluent Surfactant Concentration for Reservoir II
- 2.50 Effect of Competitive Adsorption on Surfactant Adsorption for Reservoir II
- 2.51 Surfactant Adsorption Isotherm for Reservoir II
- 2.52 Effect of Competitive Adsorption on Oil Recovery for Reservoir III
- 2.53 Oil Concentration Profiles for Base Case for Reservoir III
- 2.54 Profiles of Surfactant Concentration Overlaid by Temperature Contours in °F for Reservoir III

- 2.55 Profiles of Surfactant Concentration Overlaid by Polymer Concentration Contours in wt% for Reservoir III
- 2.56 Surfactant Adsorption with and without Competition from Polymer for Reservoir III
- 2.57 Effect of Polymer Preflooding on Oil Recovery for Reservoir III
- 2.58 Effect of Polymer Preflooding on Oil Cut for Reservoir III
- 2.59 Effect of Polymer Preflooding on Effluent Surfactant Concentration for Reservoir III
- 2.60 Effect of Polymer Preflooding on Surfactant Adsorption for Reservoir III
- 2.61 Profiles of Surfactant Concentration Overlaid by Polymer Concentration Contours in wt% for Reservoir III

ABSTRACT

This research consists of the parallel development of a new chemical flooding simulator and the application of our existing UTCHEM simulation code to model surfactant flooding. The new code is based upon a completely new numerical method that combines for the first time higher-order finite-difference methods, flux limiters, and implicit algorithms. Results indicate that this approach has significant advantages in some problems and will likely enable us to simulate much larger and more realistic chemical floods once it is fully developed. Additional improvements have also been made to the UTCHEM code, and it has been applied to the study of stochastic reservoirs with and without horizontal wells to evaluate methods to reduce the cost and risk of surfactant flooding. During the second year of this contract, we have already made significant progress on both of these tasks and are ahead of schedule on both of them.

EXECUTIVE SUMMARY

The objective of this research is to develop cost-effective surfactant flooding technology by using surfactant simulation studies to evaluate and optimize alternative design strategies taking into account reservoir characteristics, process chemistry, and process design options such as horizontal wells. Task 1 is the development of an improved numerical method for our simulator that will enable us to solve a wider class of these difficult simulation problems accurately and affordably. Task 2 is to apply numerical simulation to better understand and optimize the design of surfactant flooding to reduce its cost and risk.

A new algorithm that is fully implicit and higher-order in both time and space has been developed and used in our simulator under development. This algorithm combines the best features of several recent numerical schemes, since it is both accurate and stable. We reported the basic structure and some preliminary results of the simulator last year. The algorithm and the simulator were verified by the good agreement between numerical results and analytical solutions. The preliminary results on several one- and two-dimensional test problems with known solutions look very good compared to standard finite-difference methods used in reservoir simulation, including our own version of the total variation diminishing (TVD) flux-limited, higher-order, implicit pressure-explicit saturation method (IMPES) now used in UTCHEM. Our work this year has focused on code development and extension of our implicit method to three-dimensional problems involving more physical-chemical properties with nonuniform grids and horizontal well options. Results of two-dimensional, cross-sectional and three-dimensional simulations reported here continually show the merits of our numerical method and the simulator.

UTCHEM development has continued and several significant improvements have been made in the code during the past year. These improvements have the combined effect of making the code more versatile and efficient, which serves not only our needs better but those of a large number of external users. These users consist of not only the industrial sponsors of our enhanced oil recovery research at The University of Texas at Austin, but also a large and increasing number of academic users who use our code in a variety of oil recovery research. These users now include the following organizations:

ADREF	Amoco Production Co.
ARAMCO	Arco Oil & Gas Co.
BP Exploration, Inc.	Chevron Oil Field Research Co.
Clemson University	Conoco, Inc.
Cray Research	DOE
Duke University	Elf Aquitaine
EPA	Exxon Production Research Company
Idaho National Engineering Laboratories (EG&G)	Institute for Energy Technology

INTERA, Inc.	INTEVEP, S.A.
Japan National Oil Corp.	Japan Petroleum Exploration Co., Ltd.
Louisiana State University.	Marathon Oil Company
Mobil Exploration and Producing Services	New Mexico Petroleum Recovery Research Center
Norsk Hydro	Oryx Energy Co.
Oxy USA, Inc.	Pacific Northwest Laboratories
PETROBRAS	Rice University
Rogaland Research Institute	Sandia National Laboratories
Santa Fe Energy Resources	Schlumberger Well Services
Scientific Computing Associates, Inc.	Shell Development Co.
Shengli Geological Research Institute	Stanford University
Statoil	Technical University of Clausthal, Germany
Technical University of Denmark	Texaco, Inc.
Texas A&M University	Union Pacific Resources
Université Laval (Quebec, Canada)	University of Buenos Aires
University of Florida	University of Kansas
University of Michigan	University of Mining and Metallurgy - Poland
University of Oklahoma	University of São Paulo
University of Wyoming	UNOCAL
Xinjiang Research Institute of Exploration and Development	

A significant effort is required to provide the code and its documentation to these users as well as some support on its use. However, we do benefit from feedback from these users and occasionally even add new features to the code. In addition to these application users, we also have a major collaborative research effort with the Computational and Applied Mathematics group led by Professor Mary Wheeler at Rice University to port UTCHEM to massively parallel computers as well as to develop new algorithms for future use. This research is sponsored by the High Performance Computing and Communications program of the federal government. This research is targeted at the use of massively parallel computers to solve Grand Challenge problems, which in our case means flow in permeable media problems with applications to both oil recovery and groundwater remediation. Some of our most recent UTCHEM development targeted to contaminant cleanup is sponsored by the Environmental Protection Agency. This effort includes such things as the addition of local mesh refinement, which will be very valuable to all of our applications. Thus, there is a large leverage on the research funds provided by this grant, among other benefits to this related activity.

The potential of improving surfactant flooding using horizontal wells has been systematically investigated. The potential for horizontal wells to accelerate the oil production and thus improve the discounted cash flow may seem obvious, but the precise improvement depends on many complex factors such as vertical permeability ratio and can only be assessed using realistic simulations. We performed the simulations for several reservoir descriptions including layered and stochastic. The location of the horizontal well is very important with respect to both the sweep efficiency and injectivity and must be in a good location to produce the desired results. The vertical permeability must be moderate to high for horizontal wells to give good results, although vertical drainholes off the horizontal injector can potentially give good results even for low vertical permeability. The combination of vertical producer and horizontal injector, under some conditions, does appear to have economic merit. However, these conditions are clear only after a careful study with realistic reservoir and process descriptions.

In an attempt to include more realistic rock and fluid properties in the evaluation of surfactant flooding in different reservoir descriptions with properties suitable for surfactant flooding, we used permeability-dependent waterflood residual oil saturation rather than uniform residual saturations. Several permeability-residual oil saturation correlations were used. The

simulation results for the three reservoirs studied here indicate that the tertiary oil recovered is more sensitive to the amount of target oil at the time of chemical flood than to the distribution of the oil saturation.

To evaluate the potential of improving the cost effectiveness of surfactant flooding, we performed, for the first time, low-tension polymerflood (LTPF) simulations taking into account competitive surfactant and polymer adsorption. These results indicate that the oil recovery is still good for the small amount of chemical used. The results might be too optimistic and are shown here only to illustrate the trend. The actual results will depend on the specific adsorption isotherms for the reservoir formation, surfactant and polymer solutions, and many other factors. More realistic results and the economic impact of LTPF will be the subject of our future reports.

UTCHEM MODELING ENHANCEMENTS

UTCHEM development has continued and several significant improvements have been made in the code during the past year. These improvements have the combined effect of making the code more versatile and efficient, which better serves not only our needs but those of a large number of external users in both petroleum, subsurface, and environmental engineering. The enhancements in UTCHEM include the following:

- The development of a single-level adaptive grid refinement. The implementation strategy for grid refinement is based on domain decomposition where each zone is treated independently (Edwards, 1995).
- A dual porosity formulation to model tracer transport in fractured media (Liang 1995; Liang *et al.*, 1995).
- An option to calculate the interfacial tension between microemulsion/oil and microemulsion/brine using Chun Huh relationship (Huh, 1980). The only option previously available was based on Healy and Reed (1975).
- An option to calculate the capillary pressure and relative permeability functions using van Genuchten (1980) and Parker *et al.* (1987) models.
- Temperature-dependent surfactant phase behavior. Both the height of the binodal curve and the effective salinity are shifted to model the shift in surfactant/oil/water phase behavior with temperature.
- The component numbering scheme presently in UTCHEM has been changed to allow additional aqueous species. We also plan to simplify the input requirements for the geochemical option by using a preprocessor. The preprocessor will allow the users to set up an input file for the geochemistry subroutine of UTCHEM that includes any set of species and elements in a database.
- Options of chromium malonate gel and silicate gel systems for the application of in-depth gel treatment in addition to the previous option of polymer/chromium chloride gel (Kim, 1995).
- Allow for competitive surfactant adsorption in the presence of polymer. This option was added to adequately simulate the low tension polymer flooding. The surfactant adsorption model was modified such that the adsorbed surfactant concentration is reduced as a function of polymer concentration (Wu, 1996).

TASK 1. HIGH-RESOLUTION, FULLY IMPLICIT, COMPOSITIONAL SIMULATION

Introduction

The objective of this research is to develop cost-effective surfactant flooding technology by using surfactant simulation studies to evaluate and optimize alternative design strategies taking into account reservoir characteristics, process chemistry, and process design options such as horizontal wells. Task 1 is the development of an improved numerical method for our simulator that will enable us to solve a wider class of these difficult simulation problems accurately and affordably.

A high-resolution total variation diminishing (TVD) finite-difference scheme has been developed and used for years in our multidimensional, multicomponent, multiphase, finite-difference, IMPES-type compositional simulators. A variety of simulation results have shown that this scheme gives convergent, higher-order, accurate solutions. However, a restriction on the timestep size is always needed to ensure stability because of the IMPES formulation. This restriction sometimes can be very severe, which means in some cases simulations are of high cost or even infeasible. It is well-known that the fully implicit method is the most stable method. The standard approach, however, usually adopts lower-order finite-difference schemes for both the temporal and spatial discretizations because of computational requirements and difficulties in the program coding and the implementation of the physical property models. The advantage of the methods thus are overshadowed by the increased amount of numerical dispersion associated with large truncation error, which is detrimental to accurate field simulation and process design. This is important in all reservoir simulation problems, but it is especially important in surfactant flooding because of its complex behavior and high cost. We need accurate field simulation so that we can design the floods at a minimum cost and risk.

The solution to this dilemma, and what we have done in Task 1, is to develop a new fully implicit algorithm. It is second-order correct in time and uses a third-order finite-difference method to discretize the first-order space derivatives and a new total variation diminishing flux limiter to constrain the gradients of the fluxes to obtain accurate, oscillation-free numerical solutions (Saad *et al.*, 1990; Datta Gupta *et al.*, 1991; Liu *et al.*, 1994). This algorithm combines the best features of several recent numerical schemes, since it is both stable and accurate and can be easily generalized to multidimensional, multicomponent, multiphase flow problems such as those arising in the simulation of compositional chemical flow problems that are the specific focus of this project. Improved computing technologies, including large-scale vector and parallel architectures, and the development of more efficient and robust solution solvers have made the application of this fully implicit algorithm more realistic.

We have reported the basic structure and some preliminary results of the simulator last year. The algorithm and the simulator were verified by the good agreement between numerical results and analytical solutions. The preliminary results look very good compared to the use of standard finite-difference methods. With both using TVD high-order schemes, the fully implicit method is compared with the IMPES method. Using the fully implicit method, the first-order spatial discretization scheme is compared with the high-order spatial discretization scheme, and the high-order scheme is compared with the TVD high-order scheme. The results demonstrate that the TVD high-order scheme with a fully implicit method is more stable than that with an IMPES method. Using the fully implicit method, the TVD high-order scheme is more accurate than the lower-order spatial discretization scheme and the high-order spatial discretization scheme without TVD flux-limiting. The computational efficiency of the simulator can be greatly improved by using suitable timestepping algorithms and effective solution solvers to solve the linear system of equations, which represents the most costly aspect of a fully implicit simulator.

Our work this year has focused on code development and extension of our implicit method to three-dimensional problems involving more physical-chemical properties with nonuniform grids and horizontal well options. Results of two-dimensional, cross-sectional and three-dimensional simulations reported here continue to show the merits of our numerical method.

Physical and Mathematical Model

We will only give a brief description of the physical and mathematical model and basic structure of the simulator. A detailed description of the governing differential equations and equations describing the numerical method were presented in last year's report and can be found in references: Pope and Nelson (1978), Datta Gupta *et al.* (1986), Camilleri *et al.* (1987), Bhuyan *et al.* (1988), Saad (1989), Liu *et al.* (1994) and Delshad *et al.* (1995).

Governing equations and constitutive relations

In an oil reservoir, molecular species can undergo transport within phases and exchange across phase boundaries. For example, many EOR processes rely on the effects of interphase mass transfer to alter fluid properties in ways that benefit oil production. The simulation of any of these phenomena requires a fully compositional formulation. For a chemical flooding compositional simulator that models multiphase, multicomponent, three-dimensional flow in porous media, the basic governing equations consist of a mass conservation equation for each component, an energy balance, Darcy's law generalized for multiphase flow, and an overall mass conservation or continuity equation that determines the pressure. The equations allow for slight compressibility of fluid and rock, velocity-dependent dispersion, adsorption, chemical reactions, and complex phase-behavior effects including varying phase viscosities and relative permeabilities. The basic governing equations are complemented by a number of constitutive relations that relate the number of phases present and their compositions, saturations, densities, viscosities, interfacial tensions, and capillary pressures to the overall component concentrations and pressure. Further constitutive relations determine adsorption, residual saturation, and relative permeability. The total number of equations equals the total number of unknowns.

The initial value of concentration of each component must be specified at each point in the reservoir. For compressible flow cases, the initial pressure distribution is also required. The pressure equation is parabolic in nature and requires either the pressure or its normal derivative to be specified at each point on the boundary. The conservation equations have a hyperbolic element, associated with the convective terms, which requires that the composition of any fluid entering through the boundary be specified but requires no boundary condition on outflow boundaries, nor on any boundary through which no flow is allowed. Physical dispersion introduces a parabolic element to these equations and when present requires composition or its normal derivative to be specified on all boundaries through which dispersive flux is possible. The basic boundary condition assumed in the simulator is no flow and no dispersive flux through all boundaries.

The inflow and outflow conditions in the simulator are specified as well conditions. The ways in which wells are handled in the simulator have a significant impact on the simulation results. In an areal flow, the well model is interpreted as a point-source or -sink term, but in cross-sectional flow, the well model is interpreted as a line-source or -sink term, and distributing the total flow into each layer is necessary. There are two different rate allocation methods: the mobility allocation method and the potential allocation method (Nolen and Berry, 1972; Aziz and Settari, 1979). The mobility allocation method assures that the difference of potential between the wellbore and the gridblock is the same for all blocks communicating with the given well. The rate is therefore allocated to each layer according to the ratios of mobility. The potential method accounts for the fact that the potential difference between the wellbore and the gridblock containing the well may differ in each layer so that the potential difference is taken into account and the flow rate entering into each layer is according to the ratios of both mobility and potential. In a layered reservoir, the fluid flowing in vertical direction depends on the degree of communication with

adjacent layers. If the adjacent layers are well-communicating, the fluid easily flows vertically; the resistance of fluid flow is low and as a result, the potential difference between will be small. Conversely, if the adjacent layers have poor communication, the fluid will hardly flow vertically; the resistance to flow is high and so is the potential difference. Accordingly, the potential difference is not always the same for all layers and the mobility allocation method is not suitable then. We have adopted the potential allocation method in the simulator, and the corresponding allocation and solution schemes are given in Table 1.1.

Finite-difference schemes

The simulation space domain is a rectangular prism. Most variables, including pressure, concentrations, adsorption levels, saturations, capillary pressures, phase properties such as composition, density, viscosity, and interfacial tension, relative permeabilities, and permeability reduction factors are calculated and stored at gridblock centers. Some auxiliary variables, such as transmissibilities and phase velocities, are evaluated at the faces between gridblocks. To achieve second-order time accuracy, we use a Crank-Nicolson-type scheme to evaluate the accumulation terms in the basic governing equations. A third-order, TVD high-resolution scheme is used to approximate the first-order spatial derivatives of convection and diffusion terms. Applying the finite-difference approximations to both time and spatial derivatives in the governing differential equations, we obtain a system of finite-difference equations. The numerical scheme is consistent and stable. With the fully implicit formulation, besides the flux-limiter functions, the derivatives of these functions with respect to the related neighboring gridpoint variables also must be evaluated. Some other finite-difference schemes and flux limiters, such as the one- and two-point upstream schemes, Leonard's scheme (1979), and Van Leer's limiter (1979), are also available in the simulator. The limiter functions and their derivatives are given corresponding to the different schemes with flow directions either in or against the coordinate directions and for nonuniform grids. A second-order central-difference scheme is used to approximate the second-order spatial derivative of diffusion terms.

Solution schemes

At each gridpoint, we have a total number of n_c finite-difference residual equations consisting of n_c-1 component conservation equations and one pressure equation. This means that the total number of independent or primary variables is n_c . Besides the reference-phase pressure and saturation, we choose some relevant phase concentrations as other primary variables. The remaining phase saturations, concentrations, pressures, and physical properties are secondary variables and depend on the primary variables. They can be obtained using saturation constraints, phase-equilibrium relations, capillary-pressure relations, and all other constitutive relations. The nonlinear system of residual equations can be linearized and solved using a Newton iteration. The Jacobian matrix for the Newton iteration is formed by differentiating the nonlinear system of residual equations with respect to the primary variables. The Jacobian matrix and the residual equations are updated at the end of each iteration, and the iteration continues until the relative changes in the primary variables between two successive approximations are small enough to satisfy given tolerance criteria. For a three-dimensional simulation problem of n_c components using $N_x N_y N_z$ gridblocks, the total number of equations is $n_c N_x N_y N_z$. The Jacobian matrix is constructed such that the primary variable indexes are the faster-changing indexes in the solution vector. With the high-order scheme, a total of 25 gridpoints may be used in the finite-difference equations (Fig. 1.1). The matrix structure of simulating a three-dimensional, two-component problem using the high-order scheme and $5 \times 5 \times 3$ gridblocks is shown in Fig. 1.2. The solution of the linear system of equations represents the most costly aspect of a fully implicit numerical simulator. Using an efficient solver can greatly improve the efficiency of the simulator. Both direct and iterative solvers can be employed to solve the system of equations, although iterative solvers are preferred for multidimensional problems, which have Jacobian matrices with large bandwidths.

Simulation Results and Analyses

We showed test results of simulating tracer convection-diffusion, waterflood, and polymerflood problems in one-dimensional and two-dimensional areal cases in last year's report. The first purpose of these tests was to verify both the mathematical formulations and the finite-difference schemes and to ensure the correctness of the program coding. The second purpose was to compare the accuracy and stability of our high-resolution scheme and fully implicit formulation with other finite-difference schemes and the IMPES formulation. For the same purposes, we have conducted test cases for two-dimensional, cross-sectional and three-dimensional problems. We will show and analyze results of simulating a three-dimensional tracer convection-diffusion, a three-dimensional polymerflood with horizontal wells, and a two-dimensional, cross-sectional polymerflood, which is also used to test our well model and compare the two rate allocation methods: mobility allocation and potential allocation.

Three-dimensional convection-diffusion problem

The simulation domain is a cube with an edge of 5 ft and a porosity of 0.2. The permeabilities in each direction are the same, 200 md. The injected fluid with tracer has properties identical to those of the resident fluid in the domain. A 5x5x5 uniform grid was used with an injection well at (1,1,1) and a production well at (5,5,5) (Fig. 1.3a). Injection rate was 0.2 ft³/day and the total injection time was 375 days, which gave a total injection of 3 pore volumes. One test had a longitudinal dispersivity of 0.1 ft and the other, 1 ft, which gives Peclet numbers of 5 and 50, respectively. The transverse dispersivity was 0 for all tests.

To establish the validity of the three-dimensional formulation of the conservation equations, simulations were conducted using the UTCHEM5.3 and the fully implicit simulator with the TVD high-order scheme and the same timestep size of 0.5 days, corresponding to a Courant number of 0.5. Tracer production histories are plotted in Fig. 1.4. Good agreement between the two simulator results was obtained for both Peclet numbers. We then increased the timestep size to compare the stability of the IMPES formulation and fully implicit formulation. Figure 1.5 gives the results of the IMPES simulator and shows that the simulator produced unstable results at a timestep size of 0.6 days (Courant number of 0.6) for a Peclet number of 5 and at 1.1 days (Courant number of 1.1) for a Peclet number of 50. Figure 1.6 shows the results of the fully implicit simulator. Contrary to the IMPES simulator results, the stability is preserved even at a timestep size of 10 days (Courant number of 10), and there are no significant differences between the results using the timestep sizes of 0.5, 5, and 10 days (Courant numbers of 0.5, 5, and 10) because of the high-order time accuracy.

In last year's report, we gave two-dimensional simulation results of the fully implicit simulator to show the TVD flux-limiter effects on the high-order scheme. Results are given here to show the same effects for three-dimensional problems. We tested the same three-dimensional convection-diffusion problem with a Peclet number of 50 using the high-order scheme without flux limiting and a Courant number of 5. Figure 1.7 gives the normalized tracer concentration at the cubic center and clearly shows the numerical oscillations created by the scheme. These oscillations become even more severe at higher Peclet numbers as demonstrated in Fig. 1.8 for a Peclet number of 500 for the same problem. The lower-order space discretization with one- and two-point upstream schemes are available in the simulator. These are the conventional finite-difference schemes employed by most fully implicit simulators. Figures 1.7 and 1.8 also give the results of the one-point upstream scheme and show the scheme creates more numerical smearing than the high-order scheme.

The grid shown in Fig. 1.9 is used to verify our nonuniform grid formulation. We define an expansion ratio R , the ratio of the adjacent gridblock size, to measure the grid nonuniformity. Figure 1.10 shows the tracer production history results of our fully implicit high-order scheme.

The results of using the uniform grid are almost identical to those of using the nonuniform grid with an expansion ratio of 10. A timestep size with an average Courant number of 0.5 was used for both grids. For the IMPES method, because of its Courant stability restriction, the smaller gridblocks cause stability problems when using grids of larger expansion ratio. Figure 1.11 demonstrates that for the same problem, the IMPES method becomes unstable at an expansion ratio of 1.85 with the same timestep size used by the fully implicit method.

Three-dimensional polymerflood with horizontal well

The simulation domain is 165 ft in the x direction, 165 ft in the y direction, and 25 ft in the z direction with a porosity of 0.25. The permeabilities in each direction are 200 md. A 5x5x5 uniform grid was used. A horizontal injector was placed from (1,1,3) to (5,1,3) and a vertical producer from (3,5,1) to (3,5,5) (Fig. 1.3b). The reservoir has an initial oil saturation of 0.8 and is then flooded by polymer. The mobilities of aqueous and oleic phases are characterized by S^2/μ_a and $(1-S)^2/\mu_o$, where S is the aqueous phase saturation and μ_a and μ_o are the aqueous and oleic phase viscosities, respectively. μ_o equals 2 cp and μ_a is calculated by $(1+10C_{4a})$ cp, where C_{4a} is the polymer concentration in the aqueous phase. 0.1 wt% polymer was injected continuously for 90.75 days with an injection rate of 1,875 ft³/day, which gave a total injection of 1 pore volume.

The results of oil recovery, water cut, and effluent normalized polymer concentration were obtained using the UTCHEM5.3 and the fully implicit simulator with the TVD high-order scheme. At a timestep size of 0.363 days (Courant number of 0.1), the two simulators gave almost same results (Fig. 1.12). At a larger timestep size of 4.0 days (Courant number of 1.1), the results of the IMPES simulator became unstable, characterized by oscillations and lower oil recovery (Fig. 1.13), while the results of the fully implicit simulator show nearly no change (Fig. 1.14) in all recovery curves at larger timestep sizes of 3.63 and 7.26 days (Courant numbers of 1.0 and 2.0).

Two-dimensional, cross-sectional polymerflood

The simulation domain is 10 ft in the x direction, 1 ft in the y direction, and 5 ft in the z direction with a porosity of 0.2. The permeabilities in each direction are the same, 200 md. A 10x1x5 uniform grid was used. An injector was placed from (1,1,1) to (1,1,5) and a producer goes from (5,1,1) to (5,1,5) (Fig. 1.3c). Initial reservoir conditions and fluid and polymer properties are the same as those of the three-dimensional case. The longitudinal dispersivity is 0.1 ft (Peclet number of 100) and the transverse dispersivity is 0. Capillary pressure endpoint is 3.16 psi(darcy)^{1/2}, corresponding to a Rapoport and Leas number (the ratio of viscous to capillary forces) of 5. 0.1 wt% polymer was injected continuously for 1 day with an injection rate of 10 ft³/day, which gave a total injection of 1 pore volume.

The results of oil recovery, water cut, and effluent normalized polymer concentration were obtained using the UTCHEM5.3 and the fully implicit simulator with the TVD high-order scheme. At a timestep size of 0.001 days (Courant number of 0.01), the agreement between the results of the two simulators is good (Fig. 1.15). At a timestep size of 0.01 days (Courant number of 0.1), the results of the IMPES simulator show some differences in polymer concentration curves (Fig. 1.14) and water-cut curves (Fig. 1.17) compared with the results at a Courant number of 0.01, and become unstable at a timestep size of 0.05 days (Courant number of 0.5), as characterized by oscillations in all recovery curves. For the fully implicit simulator, the results show nearly no changes in all recovery curves (Figs. 1.18 and 1.19) at larger timestep sizes.

To test our well model and to compare the mobility rate allocation method with the potential rate allocation method, we used the same two-dimensional, cross-sectional polymerflood test case except the production well was completed only at the top layer (Fig. 1.3c) to induce the vertical pressure difference and vertical flow. We simulated the case using UTCHEM5.3 for the mobility

rate allocation method and the fully implicit simulator for the potential rate allocation method. A small timestep size of 0.001 days (Courant number of 0.01) was used for UTCHEM simulation to avoid numerical effects.

We first used a vertical permeability of 200 md, which is equal to the horizontal permeability, assuming the degree of communication with adjacent layers is relatively good in this case. Figure 1.20 shows the polymer concentration and oil production histories, and Figs. 1.21 and 1.22 show the water saturation and polymer concentration distributions at 0.5 pore volumes injected. There is little difference using the two rate allocation methods for this case. We next used a vertical permeability of 2 md, which is 0.01 times the horizontal permeability and consider this a poor communicating case. Figure 1.23 indicates apparent differences in the polymer concentration and oil production histories using the two rate allocation methods. These differences can also be found in the water saturation and polymer concentration distributions (Figs. 1.24 and 1.25), where the mobility method gives a more uniform displacement than the potential method.

Summary, Conclusions, and Future Work

The development of a fully implicit, compositional, chemical flooding simulator is in progress. Higher time accuracy and higher-resolution are achieved using a Crank-Nicolson scheme for time-derivative approximation and a third-order discretization scheme with a total variation diminishing (TVD) flux limiter for computing interface concentrations, transmissibilities, and mobilities. Numerical stability is obtained by solving the pressure and the component conservation equations simultaneously. The simulator now can handle three-dimensional problems. We have shown results of simulating a three-dimensional tracer convection-diffusion, a three-dimensional polymerflood with horizontal wells, and a two-dimensional, cross-sectional polymerflood. Three-dimensional formulations and program coding were verified by the good agreement with the results of same test problems simulated using UTCHEM5.3 at small timestep sizes. With both using the TVD high-order scheme, the fully implicit simulator can take much larger timesteps than the IMPES simulator. Using the fully implicit simulator, numerical smearing effects of the lower-order schemes can be effectively reduced by the high-order scheme, and the numerical oscillation effects of the high-order scheme can be effectively reduced by the TVD flux limiter. A potential rate allocation method is adopted for multicell well models, which is more suitable when high flow resistance exists along the direction of multicell wells.

We are now implementing phase-behavior properties into the fully implicit simulator and will later test our implicit method on surfactant flood problems. We will continue testing our solution schemes by using different solvers and timestepping algorithms.

TASK 2. OPTIMIZATION OF SURFACTANT FLOODING

Introduction

The main objective of Task 2 is to learn how to increase the cost effectiveness of surfactant flooding. Systematic and realistic reservoir simulation is the only method to optimize the design of surfactant floods. These simulations have to take into account the reservoir description in addition to process parameters.

Last year we reported on the stochastic simulations of surfactant/polymer flooding under different reservoir conditions such as vertical-to-horizontal permeability, different permeability realizations, and various geostatistical parameters such as correlation length and reservoir heterogeneity. We studied the improved injectivity by using a horizontal injector instead of vertical.

During the past year, we continued to further learn how to optimize surfactant floods by investigating the direction of the horizontal well, i.e., parallel to the x or y direction, and the impact of vertical drainholes. For the first time, we investigated the impact of distributed residual oil saturation on surfactant/polymer oil recovery. This was done in three different reservoirs with entirely different reservoir descriptions.

Another means of increasing the cost effectiveness of surfactant flooding is to lower the amount of injected chemicals required to recover a given amount of oil. We investigated the effectiveness of low-tension polymerflooding (LTPF) under different reservoir descriptions and with various process parameters to reduce the amount of surfactant required. The impact of surfactant adsorption with competition from polymer was investigated in connection with LTPF.

Subtask 2.1 Stochastic Simulation of Surfactant Flooding

In last year's report (Pope and Sepehrmoori, 1994), we reported on the stochastic simulations of surfactant/polymer flooding in a midcontinent U.S. sandstone-type oil reservoir. We studied and reported on different reservoir conditions such as vertical-to-horizontal permeability ratio, different permeability field realizations, and various geostatistical parameters such as correlation length and reservoir heterogeneity. We studied the improved injectivity by using a horizontal injector instead of a vertical well. To further optimize the surfactant/polymer flood, we investigated the horizontal wellbore orientation and vertical drainholes. To study the impact of the distribution of residual oil saturation, an important reservoir property, on surfactant flooding, we generated several distributions based on the permeability and repeated the simulations. To investigate the potential for LTPF, we performed simulations with reduced surfactant concentration.

The simulation results for this subtask are referred to as simulations in Reservoir I described below.

Subtask 2.2 Evaluation of Surfactant Flooding using Horizontal Wells

In this subtask, we have investigated the potential of surfactant flooding with horizontal wells using a different reservoir description than described above. Several production strategies were considered, i.e., vertical injector and producer wells, vertical injector and horizontal producer, horizontal injector and vertical producer, and horizontal injector and producer wells. Consistent with our past results, the combination of horizontal injector and vertical producer appeared to have economic merit. The locations of both wells were also studied with respect to reservoir permeability.

The results of this subtask are referred to as simulations in Reservoir II.

Subtask 2.3 Evaluation of Low Tension Polymerflooding

Kalpakci *et al.* (1993) have proposed a new approach to cost-effective surfactant flooding termed low-tension polymerflood (LTPF). Coinjection of low concentration of surfactant (about 0.3 vol.%) and polymer (about 750 ppm) followed by polymer drive (about 500 to 750 ppm) appears, under some conditions, to lower chemical consumption. In LTPF, the time the chemical slug is injected is longer; however, the time scale for oil recovery is not excessively extended. This approach has the potential of reducing the front-end and total chemical costs. The total amount of chemicals injected is greatly dependent on the choice of the surfactant and polymer used, reservoir description, and operating constraints. There are a number of laboratory studies on the interactions between polymer and surfactant during LTPF (Austad *et al.*, 1993; Austad and Taugbol, 1993). Correct choice and amount of polymer propagated with and ahead of the surfactant bank have the potential to reduce the surfactant adsorption.

We have made both modeling and simulation efforts to include the experimental observation that surfactant retention is reduced in the presence of polymer during chemical flooding. The Langmuir-type surfactant adsorption model in UTCHEM is modified to account for the presence of polymer. The adsorbed surfactant concentration is reduced as a function of polymer concentration (Wu, 1996).

The potential of LTPF was studied in all three reservoirs considered here.

Reservoir Description

To study the effect of location of the horizontal wellbore, vertical drainholes, permeability-distributed residual oil saturation, competitive surfactant/polymer adsorption, and the sensitivity of each of these to reservoir description, we performed simulations in three different reservoirs with significantly different properties and initial conditions. A brief description of each reservoir and simulation data is given below.

Reservoir I

The permeability field was generated stochastically with a Dykstra-Parsons coefficient of 0.8 and a geometric mean of 50 md. Vertical-to-horizontal permeability ratio was 0.1. A quarter-symmetry element of a 40-acre five-spot pattern was considered. The simulated area was 660 ft in both x and y directions with the thickness of 140 ft. The simulation grid was 11x11x5. The porosity was uniform and equal to 0.136. The horizontal injector well was linked to the vertical injection well and placed in the high-permeability layer 2 along the y axis with a constant injection pressure of 1,250 psia (Fig. 2.1). The vertical producer operated with a constant pressure of 250 psia. Tables 2.1 and 2.2 give the input parameters and the injection scheme. More detail on the reservoir description and physical properties can be found in the last annual report (Pope and Sepehrnoori, 1994). The reservoir was first waterflooded with a low initial water saturation of 0.2, and the simulation ended when a water cut of 98% was reached. After waterflooding, 0.25 pore volumes of 2.5 vol.% surfactant were injected. The surfactant slug contained 1,000 ppm polymer and was followed by another 0.5 pore volumes of 1,000 ppm polymer and finally by chase water injection for 3.25 pore volumes.

Reservoir II

The permeability and porosity were different for each gridblock but similar to a layered description. Porosity was in the range of 0.06 to 0.24. Permeability in the horizontal direction ranged between 14 md for the low-permeability layer at the bottom (layer 8) to 700 md for the highest-permeability layer (layer 4). Permeability for the other layers was on the order of 30 to 80 md. The vertical-to-horizontal permeability ratio was 0.2. Some of the key input parameters are listed in Table 2.3. The simulation grid was 13x7x8 in the x, y, and z directions as shown in Fig. 2.2.

In each simulation discussed here, we first waterflooded the reservoir for one year followed by a dilute slug of surfactant/polymer termed low-tension polymerflood (LTPF). We investigated the significance of the well orientation and well location. The simulation results indicated that the combination of a horizontal injector and a vertical producer gives the highest oil recovery and only slightly less than when both wells are horizontal. The horizontal injector was located in the 10th gridblock in the 7th layer and extended from gridblock 2 through 7 in the y direction. Vertical producer was perforated in layers 1 through 8 and located in (1,1). The wells operated at either constant injection pressure of 6,206 psia or constant injection rate of 25,409 B/D and constant production pressure of 2,175 psia. The salinity was kept constant at 0.627 meq/ml and slightly above optimum salinity of 0.575 meq/ml and in the type III phase environment. Surfactant was injected at a concentration of 0.005 volume fraction for 0.4 pore volumes along with 250 ppm (0.025 wt %) polymer followed by a 0.2 pore volumes of 250 ppm polymer drive,

and followed by a water postflush. These are very small amounts of chemical and would be reasonable only if the efficiency is very high.

Reservoir III

The reservoir description in this example is heterogeneous with properties favorable for chemical flooding, i.e., high permeability and porosity as given in Table 2.4. The two-dimensional vertical cross-sectional simulation grid is 26 in the horizontal x direction and 8 in the vertical z direction. To mimic conditions before the start of tertiary oil recovery, the reservoir was first waterflooded until a water cut of 0.94 was reached. The initial waterflood simulations were performed with the reservoir initialized uniformly at residual water saturation of 0.147.

After waterflooding, 0.4 PV of 0.5 vol.% surfactant was injected at a constant rate of 2,000 B/D. The surfactant slug contained 500 ppm for 0.3 PV and 250 ppm for 0.1 PV of polymer. The chemical slug was then followed by chase water for 1.45 PV. The simulation included a temperature gradient, since the initial reservoir temperature was 158°F and the injected water temperature was 122°F. The effect of temperature on phase behavior was accounted for by changing both the height of binodal curve (HBNT parameters in Table 2.4) and the effective salinity (β parameter in Table 2.4). This is a new feature of UTCHEM. We have also considered the heat gain from the overburden and underburden rocks. The salinity was constant and in the type II(-) phase environment at the initial temperature of 158 °F but because of the imposed temperature gradient, the effective salinity changed during the chemical flood.

Horizontal Wells with Vertical Drainholes

To further optimize the surfactant/polymer flood in this stochastic permeability field, we placed the horizontal injection wellbore along the x direction as shown in Fig. 2.3 (Reservoir I). Figures 2.4 and 2.5 compare the results with the horizontal wellbore along the y direction reported last year. The results indicated that placing the horizontal wellbore along the x direction lowered the injectivity and increased the project life from 18.7 years to 38.3 years. However, the sweep efficiency increased since the ultimate oil recovery showed an increase of 15.4% for the wellbore along the x direction (Fig. 2.5). The cumulative oil recovery was about the same at the end of the polymer drive for the two cases and the difference became greater after chase water injection (Fig. 2.5). Analysis of the permeability field suggests that the favorable mobility ratio due to polymer solution was responsible for the efficient displacement of the oil out of the originally poorly swept region. At the end of the polymer drive, the zones of high permeability located in the opposite corners along the y direction were unswept. When these zones were swept with the wellbore along the x direction during the chase water, trapping was minimized and the oil recovery increased from 42.0% to 72.4%.

With the horizontal injection wellbore along the x direction, higher oil recovery was obtained because the initial 0.75 PV polymer drive effectively swept the zones of the reservoirs of low permeability that trapped the oil at the end of the initial waterflood. Injectivity, however, was low and vertical drainholes were considered in order to improve the injectivity by increasing the contact area with the reservoir. Figure 2.3 shows the location of the wells. Cumulative oil recovery for the cases with and without vertical drainholes is plotted in Fig. 2.6 versus time and Fig. 2.7 versus PV injected. The results show a significant increase in both injectivity and sweep efficiency. The project life decreased from 38.3 years to 32.0 years and the cumulative oil produced increased from 72.4 % to 77.6%.

Residual Oil Saturation Dependence on Permeability

The waterflood residual oil saturation (S_{orw}) was uniform in all simulations reported here and last year. To study the significance of distributed versus uniform waterflood residual oil

saturation on chemical flooding, S_{orw} was varied as a function of permeability using several permeability - S_{orw} relationships in the three different reservoir descriptions above. We attempted to include more properties that are known to be rock-dependent, such as the waterflood residual oil saturation and relative permeability curves, in these simulations. Some physical properties such as capillary pressure and capillary desaturation curves in UTCHEM are already computed as a function of rock permeability. But this is the first time that we have studied surfactant/polymer flooding in several permeability fields including the one generated stochastically with permeability-dependent residual oil saturations.

Reservoir I

The waterflood residual oil saturation (S_{orw}) was uniform and equal to 0.25 in the simulations reported last year and in the previous section. To investigate the effect of both the magnitude and nonuniform residual oil saturation on the surfactant/polymer flooding using stochastic permeability distributions, (1) the S_{orw} was increased from 0.25 (Case 1) to 0.30 (Case 2) and (2) two sets of permeability-dependent S_{orw} distributions were also investigated as follows:

$$\text{Case 3: } S_{orw} = \exp(-1.1859127 k^{0.04})$$

$$\text{Case 4: } S_{orw} = \exp(-0.941164 k^{0.1})$$

A volume-weighted S_{orw} of 0.25 was also preserved in these distributions. The horizontal injector wellbore was along the y direction and in the second layer. The producer was vertical and a constant pressure drop of 1,000 psi was applied (see Tables 2.1 and 2.2). Figure 2.8 shows the S_{orw} values plotted as a function of permeability. Figures 2.9 and 2.10 show the oil-phase capillary desaturation curve (CDC) of the lowest and highest permeability gridblocks for Cases 3 and 4. The CDC curves corresponding to a waterflood residual oil saturation of 0.25 are also shown. As shown in these figures, S_{orw} ranges from about 19% to about 32% in Case 3 (Fig. 2.9), and from about 12% to about 44% in Case 4 (Fig. 2.10).

Figures 2.11 and 2.12 show the cumulative oil produced as a function of time and pore volumes injected for the cases studied. The results indicate that the oil recovery is more sensitive to the amount of targeted oil than how it is distributed. Figures 2.13 through 2.20 show cross sections of oil concentration profiles for Cases 1 through 4 at two different times. Prior to surfactant injection, the reservoir was waterflooded with 2.81 pore volumes of water. The water cut at the initiation of surfactant/polymer flood is about 98%. Figures 2.11 and 2.12 show that the cumulative oil recovery is the highest for Case 2, i.e., when a constant S_{orw} of 0.3 is used. This can be attributed to the fact that because of the higher S_{orw} in Case 2 compared to Case 1 (25%) or Cases 3 and 4, where a volume-weighted average S_{orw} of 25% was also preserved, less oil was recovered during waterflooding in Case 2. Hence, the chemical flood target oil volume is largest in Case 2. Even though Cases 3 and 4 have the same volume-weighted average S_{orw} (on a reservoir-wide basis) as Case 1 (constant S_{orw} of 25%), observe that the cumulative oil recovery for Case 3 is higher than that of Case 1, while the recovery for Case 4 is higher than that of Case 3. This is also an indication that as the range in the S_{orw} distribution increases (as in Case 4 compared to Case 3), less oil can be recovered through waterflooding, and hence a higher chemical flood target oil volume. Figures 2.13 through 2.20 show that the volumetric sweep is rather poor and that the surfactant/polymer flood followed by water drive in Cases 1 through 4 contacted about the same regions of the reservoir. Hence, if a larger surfactant/polymer slug were to be used in Cases 3 and 4, the cumulative oil recovery could potentially be higher if there is adequate surfactant to contact the lower permeability regions where the waterflood residual oil saturation is higher.

Reservoir II

A constant waterflood residual oil saturation (S_{orw}) of 0.25 in all the gridblocks was initially used. In the following simulations, the impact of S_{orw} was investigated. First, the S_{orw}

was uniformly increased from 0.25 to 0.30. Since residual oil saturation (S_{orw}) is correlated with permeability, subsequent simulations were conducted using an empirical correlation to assign S_{orw} to each gridblock. The distributions studied were

$$S_{orw} = \exp(-0.88222 k^{0.125})$$

$$S_{orw} = \exp(-1.1048 k^{0.0625})$$

$$S_{orw} = \exp(-0.5665 k^{0.25})$$

In these distributions, a volume-weighted S_{orw} of 0.25 was preserved. Figure 2.21 shows the S_{orw} values plotted as a function of permeability using the above correlations. Note the varied distribution of S_{orw} investigated using each of the above correlations. Figures 2.22 through 2.24 show the oil-phase capillary desaturation curves of the lowest- and highest-permeability gridblocks for each distribution, respectively. S_{orw} ranges from about 13% to about 33% in the first distribution, from about 19% to about 29% in the second distribution, and from about 5% to about 40% in the third distribution.

Figures 2.25 through 2.27 show the results of these simulations. A major, but surprising, conclusion is that the chemical flood performance of this reservoir is quite insensitive to the waterflood residual oil saturation. This insensitivity can be attributed to the early initiation of the chemical flood (only one year after waterflooding). At the initiation of chemical flooding, the initial oil saturation in the waterflooded gridblocks was still very much above the residual saturation.

We repeated three of the above cases, namely the case with S_{orw} of 0.25, the case with S_{orw} of 0.30, and the case where S_{orw} is a function of permeability ($S_{orw} = \exp[-0.88222 k^{0.125}]$), under tertiary conditions. The reservoir was first waterflooded for 1 pore volume (about 7 years) prior to the commencement of chemical flood. Figures 28 and 29 show the cumulative oil production for the three cases during the chemical flood project life. Since the chemical flood target oil volume was greatest when an S_{orw} of 0.30 was used, it also yielded the highest cumulative oil production. The distributed S_{orw} case gave the lowest tertiary oil production even though the volume weighted S_{orw} was also equal to 0.25. This is partly caused by the correlation used to produce the S_{orw} distribution; a higher permeability reservoir will yield lower residual oil saturation. Also, because of the presence of a very-high-permeability layer in this reservoir, it was observed that the displacement was dominated by channeling effects. Hence, the sweep was very poor and the contacted gridblocks were mostly higher-permeability gridblocks contributing to the channeling phenomenon. Consequently, the chemical flood target oil volume in these gridblocks was the least compared to the other two cases.

Reservoir III

Initially, the S_{orw} was uniformly increased from 0.25 (Case 1) to 0.30 (Case 2). Since it is very plausible that higher-permeability regions or gridblocks have lower S_{orw} , simple empirical correlations relating S_{orw} to reservoir permeability were used to assign the waterflood residual oil saturation to each gridblock. The distributions studied were

$$\text{Case 3: } S_{orw} = \exp(-0.016187 k^{0.5})$$

$$\text{Case 4: } S_{orw} = \exp(-0.001753 k^{0.75})$$

$$\text{Case 5: } S_{orw} = \exp(-0.233604 k^{0.2})$$

Since a constant S_{orw} of 0.25 was used in the original calculations, a volume-weighted S_{orw} of 0.25 was also preserved in these distributions. Figure 30 shows the S_{orw} values plotted as

a function of permeability. Figures 2.31 through 2.33 show the oil phase capillary desaturation curve (CDC) of the lowest- and highest-permeability gridblocks for each distribution (Cases 3 through 5), respectively. The CDC corresponding to a waterflood residual oil saturation of 0.25 are also shown in these figures. As shown in these figures, S_{orw} ranges from about 18% to about 30% in Case 3 (Fig. 2.31), from about 14% to about 32% in Case 4 (Fig. 2.32), and from about 22% to about 27% in Case 5 (Fig. 2.33).

Figures 2.34 through 2.36 show the results of these simulations. Figures 2.37 and 2.38 show the oil concentration profiles at 0.5 and 1.8 pore volumes injected, respectively. Figure 2.34 shows that except for Case 2 where S_{orw} was held constant at 0.30, the permeability-dependent S_{orw} cases (Cases 3 through 5) yielded about the same chemical flood cumulative oil recoveries as Case 1. In Case 2, when S_{orw} was held constant at 0.30 during the waterflood period prior to initiation of the surfactant/polymer flood, it is obvious that the least amount of oil was recovered during the waterflood (about 65.76% of OOIP) compared to the other cases with either constant S_{orw} of 0.25 (Case 1, 71.04% of OOIP) or variable S_{orw} but preserving a volume-weighted S_{orw} of 0.25 (Cases 3 to 5). Consequently, the chemical flood target oil volume for Case 2 is the largest, thus resulting in highest chemical flood cumulative oil recovery.

Waterflood oil recovery for Cases 3 through 5 are 69.84%, 69.09%, and 70.59% of OOIP, respectively. Accordingly, Fig. 2.34 shows that Case 4 yielded the second highest chemical flood cumulative oil recovery, followed by Case 3. For all practical purposes, the cumulative oil recoveries for Cases 3 through 5 can be considered quite similar to that of Case 1. This is actually quite misleading, because they give the impression that the surfactant/polymer flood oil recovery is quite insensitive to the S_{orw} distributions investigated. On the contrary, Fig. 2.37 shows that the chemical flood oil bank response is the strongest and sharpest when the range of residual oil saturation in the reservoir is the largest, such as in Case 4. This effect is also demonstrated by Figs. 2.35 and 2.36. Figure 2.38 shows that at the end of the waterdrive (1.8 pore volumes injected), the oil concentration in the lower-permeability regions that have not been contacted by the surfactant is higher in Cases 3 to 5 than in Case 1. On the other hand, the oil concentration in the uncontacted (by surfactant) higher-permeability regions are lower in Cases 3 through 5 compared that in Case 1. Hence, this apparent insensitivity of the ultimate oil recovery to the S_{orw} distributions used in our study can be attributed to the canceling effects noted earlier. Finally, if a larger surfactant slug were injected, there is a greater potential to increase the oil recovery from Cases 3 to 5 compared to Case 1 because of the presence of higher target oil volume.

Low-Tension Polymerflooding

We have studied the polymer/surfactant interactions such as surfactant adsorption in the presence of polymer, effect of polymer preflush, effect of amount of injected surfactant and polymer, and effect of surfactant properties on LTPF. Here, however, we only give the results of competitive adsorption and polymer preflooding.

Reservoir I

To explore the potential of low-tension polymerflooding (LTPF) as an alternative to the traditional surfactant/polymer flooding in this stochastic permeability field in an effort to increase the cost effectiveness of surfactant flooding, we altered the amount of chemical injected to mimic the conditions of low-tension polymer flooding (Kalpakci *et al.*, 1993). The surfactant concentration was reduced from 0.25 of the base case simulations discussed above to 0.005 vol. fraction and the slug size was increased from 0.25 to 0.40 PV. Therefore, the total amount of surfactant injected was reduced from 0.05 to 0.002 vol. fraction x PV. This is a very small amount of surfactant and a lower concentration of surfactant than that used historically in chemical flooding. However, the results of Kalpakci *et al.* (1993), Austad *et al.* (1993), and others in recent

years indicate that the very best of the synthetic ethoxy and propoxy sulfate and sulfonate surfactants can still be effective under these dilute conditions. This is thought to be in part due to the very low surfactant adsorption in the presence of polymer. The polymer concentration was 1,000 ppm in both the 0.4 PV surfactant slug and 0.5 PV polymer drive. The polymer drive was then followed by 2.1 PV chase water. To eliminate the effect of injectivity in these runs in order to better understand only the impact of the small amount of injected chemicals, the simulations discussed here were performed at a constant rate of 2,244 B/D. The residual oil saturations were distributed according to the permeability field as Case 3 in the previous section. We have also studied the polymer/surfactant interactions such as surfactant adsorption in the presence of polymer and effect of polymer preflush on LTPF. The results are shown in Figs. 2.39 through 2.44. The base case refers to the simulations where the interaction between surfactant and polymer is neglected (without competitive adsorption). As shown in Fig. 2.39, the oil recovery increased from 41% to 47% because of the higher concentration of active surfactant (Fig. 2.41). The decrease in the adsorbed surfactant concentration because of the presence of polymer is shown in Fig. 2.42.

To investigate the effect of polymer preflooding in conjunction with the competitive adsorption, we simulated a case where 0.1 PV polymer with 1,000 ppm concentration was injected ahead of the surfactant/polymer slug. The results in Fig. 2.43 indicate that there is an increase of 4% from injection of additional polymer. However, an incremental increase due to competitive adsorption is about the same (5%) as the case without polymer preflooding. The impact of polymer concentration on the adsorbed surfactant concentrations is shown in Fig. 2.44.

Reservoir II

Figures 2.45 through 2.47 show the results. The simulation results for the case without polymer seems attractive in terms of oil recovery (52% of OOIP). However, it is well-known that polymers are needed for the mobility control and integrity of the chemical slug. The competitive adsorption has very little effect on the oil recovery for this case. Figure 2.47 shows the effect of polymer in reducing the adsorbed surfactant concentration from 0.043 to 0.01 mg/g rock. The insensitivity to the level of adsorbed surfactant in this case is due to a very low surfactant adsorption in the base case. To further investigate this, the maximum surfactant adsorption corresponding to the injected concentration of 0.005 vol. fraction was increased from 0.10 to 0.42 mg/g rock and the above simulations were repeated. The results are shown in Figs. 2.48 to 2.50 with higher sensitivity to the surfactant adsorption. The surfactant adsorption isotherm is shown in Fig. 2.51.

Reservoir III

The oil recovery in this high-permeability reservoir is about 57% for the base-case LTPF with very small amount of injected surfactant (Fig. 2.52). Note that we have not included the polymer/surfactant interactions in the base-case simulation. Profiles of oil concentration at several times are shown in Fig. 2.53. Figure 2.54 shows the profiles of surfactant concentration overlaid by the temperature contours at several PV injected, which indicate that the temperature front is ahead of the chemical slug for most part of the flood (0.7 PV). Figure 2.55 shows the profiles of the surfactant concentration overlaid by the polymer concentration contours. The results show that there is always polymer present ahead of the surfactant slug. Maximum adsorption concentrations corresponding to the injected concentration were 0.36 mg/g rock for surfactant and 33 μ g/g rock for polymer.

To investigate the impact of competitive polymer/surfactant adsorption, we repeated the base-case simulation with competition from polymer included in the surfactant adsorption calculations. The sensitivity of LTPF oil recovery to surfactant adsorption with competition from polymer is shown in Fig. 2.52. The oil recovery is increased from 56% to 77% because of the reduced surfactant retention (Fig. 2.56). These results might be too optimistic and are shown here

to only illustrate the trend. Actual results will depend on the specific adsorption isotherms for the reservoir formation, surfactant and polymer solutions, and many other factors. Even for this favorable illustration, the predicted oil recovery would be less when the three-dimensional effects are taken into account. More realistic results and the economic impact of LTPF will be the subject of the future reports.

To ensure that enough polymer concentration is propagated ahead of the surfactant slug to fully benefit from the competitive adsorption, the base case was repeated but a 0.2 PV polymer solution with 250 ppm concentration was injected prior to the injection of surfactant/polymer slug (referred to as polymer preflooding in the figures). Figure 2.57 shows that the oil production response is quicker, as expected because of a better mobility control, in the case with polymer preflooding compared to the base case. The ultimate oil recovery, however, is about the same with or without the additional polymer injected ahead of the chemical slug. To explore whether the polymer ahead of the surfactant slug had any additional improvement due to polymer/surfactant interactions, a simulation run was performed with competitive adsorption calculation included. The oil recovery was increased from 54% to 74% with an incremental oil recovery of 20% (Fig. 2.57) compared to 22% for the cases without the polymer preflow (Fig. 2.52). Therefore, the only advantage of polymer injection prior to chemical slug in this reservoir under the conditions studied is the earlier oil recovery response (Fig. 2.58), and the ultimate recovery is fairly insensitive with or without competitive adsorption. Figures 2.59 and 2.60 show the effluent surfactant concentration overlaid by the polymer concentration contours at several PV injected for the case with polymer preflooding are shown in Fig. 2.61. The results indicate that high concentrations of polymer propagated ahead of polymer during the entire flood.

Summary, Conclusions, and Future Work

Our simulation study in the stochastic permeability field showed that the horizontal wellbores exhibited higher injectivity and the improvements are more pronounced during the injection of high-viscosity polymer solution. The orientation of the horizontal well, i.e., wellbore parallel to x or y direction, was an important design parameter in optimizing the surfactant/polymer flood due to the permeability distribution. The use of vertical drainholes linked to the horizontal injector proved to be effective only when the permeability around the injector was low or the vertical permeability was too low for sufficient crossflow. The combination of vertical producer and horizontal injector does appear to have economic merit for the several reservoirs investigated here.

To better characterize the reservoir, we included permeability dependent residual oil saturation, which is a very fundamental part of reservoir characterization and has been neglected in most studies. To do this correctly, the effect of rock permeability on relative permeability and capillary pressure was also included. The simulation results indicated that the tertiary oil recovery was sensitive, as expected, to the magnitude of the waterflood residual oil saturation in the cases studied here with stochastically distributed either relatively low permeability of Reservoir I or high permeability of Reservoir III. The other not very obvious result is that the ultimate chemical oil recovery was fairly insensitive to how the target oil is distributed. For many years petroleum engineers speculated that the residual oil saturation distribution based on the rock permeability has a significant impact on oil recovery using enhanced oil recovery techniques. The more permeable zones have less oil than the less permeable zones and different from a uniformly assigned saturation to be recovered at the end of waterflooding. However, the simulations performed here consistently showed that the tertiary oil recovery is not very sensitive to how the remaining target oil is distributed as long as an average residual oil saturation is preserved. To draw more concrete conclusions, future simulations need to be done, i.e., with different vertical-to-horizontal permeability ratios, different chemical slug sizes, etc.

We also investigated the potential of low-tension polymerflood for these same reservoirs. The preliminary results indicate that the oil recovery was still good even though a very small amount of surfactant was used. There are some improvements in the performance of the flood when the polymer-surfactant interactions are modeled, i.e., reduced surfactant adsorption because of the presence of polymer. These results might be too optimistic and are shown here only to illustrate the trend. Actual results will depend on the specific adsorption isotherms for the reservoir formation, surfactant and polymer solutions, and many other factors. More realistic results and the economic impact of LTPF will be the subject of future reports.

NOMENCLATURE

a_{4a}	=	Polymer concentration in the aqueous phase
C_{κ}	=	Component κ concentration
$C_{w\kappa l}$	=	Injection concentration of component κ in phase l
f_{pw}	=	Residual equation of wellbore pressure
n_b	=	Total number of gridblocks in the multicell well
n_c	=	Total number of components
n_p	=	Total number of phases
n_t	=	Total number of primary variables
n_w	=	Total number of rate constrained wells
N_x	=	Total number of gridblocks in the x direction
N_y	=	Total number of gridblocks in the y direction
N_z	=	Total number of gridblocks in the z direction
p	=	Pressure
p_w	=	Wellbore pressure
Q	=	Flow rate
S_a	=	Aqueous phase saturation
Δx	=	Gridblock size in the x direction
Δy	=	Gridblock size in the y direction
Δz	=	Gridblock size in the z direction

Greek Symbols

λ	=	Courant number
μ	=	Viscosity
ω	=	Flow coefficient for flow rate allocation

Subscripts and Superscripts

a	=	Aqueous phase
i	=	Gridblock index for the x direction
j	=	Gridblock index for the y direction
k	=	Gridblock index for the z direction
l	=	Phase index
m	=	Index for multicell wells
o	=	Oleic phase
w	=	Well index
κ	=	Component index

REFERENCES

- Austad, T., I. Fjelde, K. Veggeland, and K. Taugbol: "Physicochemical Principles of Low Tension Polymer Flood," *J. Pet. Sci. Eng.* (1994) **10**, 208-219.
- Austad, T. and K. Taugbol: "Polymer Gradient as an Alternative to the Salinity Gradient for Controlling the Effects of Dispersion and Retention in LTPF," paper presented at the 14th IEA Collaborative Project on Enhanced Oil Recovery Workshop and Symposium, Salzburg, Germany, Oct. 17-21, 1993.
- Aziz, K. and A. Settari: *Petroleum Reservoir Simulation*, Applied Science Publishers, London (1979).
- Bhuyan, D., L.W. Lake, and G.A. Pope: "Mathematical Modeling of High-pH Chemical Flooding," paper SPE/DOE 17398 presented at the 1988 SPE/DOE Symposium on Enhanced Oil Recovery, Tulsa, OK, April 17-20.
- Camilleri, D., A. Fil, G.A. Pope, B.A. Rouse, and K. Sepehrnoori: "Improvements in Physical Property Models Used in Micellar/Polymer Flooding," *SPE Reser. Eng.* (1987) **2**, No. 4, 433-440.
- Datta Gupta, A., L.W. Lake, G.A. Pope, K. Sepehrnoori, and M.J. King: "High Resolution Monotonic Schemes for Reservoir Fluid Flow Simulation," *In Situ* (1991) **15**, No. 3, 289-317.
- Datta Gupta, A., G.A. Pope, K. Sepehrnoori, and R.L. Thrasher: "A Symmetric, Positive Definite Formulation of a Three-Dimensional Micellar/Polymer Simulator," *SPE Reser. Eng.* (Nov. 1986) **1**, 622-632.
- Delshad, M., G.A. Pope, and K. Sepehrnoori: "A Compositional Simulator for Modeling Surfactant Enhanced Aquifer Remediation," submitted to *J. Cont. Hydrol.*, 1995.
- Edwards, M.: "Adaptive Grid Refinement with a Higher-Order Scheme," Category A Research, Twelfth Annual Report, Enhanced Oil and Gas Recovery Research Program, Center for Petroleum and Geosystems Engineering, The University of Texas, Austin (March 1995).
- Healy, R. N. and R. L. Reed: "Physicochemical Aspects of Microemulsion Flooding," *Soc. Pet. Eng. J.* (1975) **14**, 87-103.
- Huh, C.: "Interfacial Tension and Solubilizing Ability of a Microemulsion Phase that Coexists with Oil and Brine," *J. Colloid Interface Sci.* (1979) **71**, 408-428.
- Kalpakci, B., T.G. Arf, D.M. Grist, S.B. Hyde, O. Vikane, and S. Espedal: "A Preliminary Evaluation of an LTPF Process for Statfjord Field, Norway," presented at the 7th European IOR Symposium, Moscow, Russia, Oct. 27-29, 1993.
- Kim, H.: "A Simulation Study of Gel Conformance Treatments," Ph.D. dissertation, The University of Texas, Austin, in progress.
- Leonard, B.P.: "A Survey of Finite Differences of Opinion On Numerical Muddling of the Incomprehensible Defective Confusion Equation," Finite Element Methods for Convection Dominated Flows, presented at the Annual Winter Meeting of the ASME, New York (Dec. 1979) 1-17.

- Liang, Z.: "Development of a Dual Porosity Thermal Simulator," Ph.D. dissertation, The University of Texas, Austin, in progress.
- Liang, Z., M.A. Miller, and K. Sepehrnoori: "Implementation of a Dual Porosity Model in UTCHEM," Category A Research, Twelfth Annual Report, Enhanced Oil and Gas Recovery Research Program, Center for Petroleum and Geosystems Engineering, The University of Texas, Austin (March 1995).
- Liu, J., M. Delshad, G.A. Pope, and K. Sepehrnoori: "Application of Higher-Order Flux-Limited Methods in Compositional Simulation," *Transport in Porous Media* (1994) **16**, 1-29.
- Nolen, J.S., and D.W. Berry: "Tests of the Stability and Time-Step Sensitivity of Semi-Implicit Reservoir Simulation Techniques," *Soc. Pet. Eng. J.* (Mar. 1972) **12**, 253-266.
- Parker, J.C., R.J. Lenhard, and T. Kuppusamy: "A Parametric Model for Constitutive Properties Governing Multiphase Flow in Porous Media," *Water Resour. Res.* (1987) **23** (4), 618-624.
- Pope, G.A. and R.C. Nelson: "A Chemical Flooding Compositional Simulator," *Soc. Pet. Eng. J.* (Oct. 1978) **18**, 339-354.
- Pope, G.A. and K. Sepehrnoori: "Development of Cost-Effective Surfactant Flooding Technology," First Annual Report, Sept. 30, 1992-Sept. 29, 1993, Contract No. DE-AC22-92BC14885, U.S. DOE (Aug. 1994).
- Saad, N.: "Field Scale Simulation of Chemical Flooding," Ph.D. dissertation, The University of Texas, Austin (Aug. 1989).
- Saad, N., G.A. Pope, and K. Sepehrnoori: "Application of Higher-Order Methods in Compositional Simulation," *SPE Reser. Eng.* (Nov. 1990) **5**, 623-630.
- van Genuchten, M.T.: "A Closed-Form Equation for Predicting the Hydraulic Conductivity of Unsaturated Soils," *Soil Sci. Soc. Am. J.* (1980) **44**, 892-989.
- Van Leer, B.: "Towards the Ultimate Conservative Difference Scheme: V. A Second Order Scheme to Godunov's Method," *J. Comp. Phys.* (1979) **32**, No. 1, 101-136.
- Wu, W.: "Optimization and Numerical Modeling of Chemical Flooding," Ph.D. dissertation, The University of Texas, Austin, in progress.

Table 1.1: Potential Rate Allocation Method and Solution Scheme for Multicell Well

Total injection rate

$$Q = \sum_{l=1}^{n_p} Q_l$$

Injection rate of component κ

$$Q_\kappa = \sum_{l=1}^{n_p} C_{w\kappa l} Q_l$$

Allocated injection rate of component κ in m^{th} layer

$$Q_{m\kappa} = (Q_\kappa/Q) \sum_{l=1}^{n_p} \omega_{ml} (p_w - p_{ml})$$

Derivatives of allocated injection rate of component κ in m^{th} layer

$$\frac{\partial Q_{m\kappa}}{\partial p_{ml}} = -Q_\kappa/Q \sum_{l=1}^{n_p} \omega_{ml}$$

$$\frac{\partial Q_{m\kappa}}{\partial p_w} = Q_\kappa/Q \sum_{l=1}^{n_p} \omega_{ml}$$

$$\frac{\partial Q_{m\kappa}}{\partial C} = Q_\kappa/Q \sum_{l=1}^{n_p} \frac{\partial \omega_{ml}}{\partial C} (p_w - p_{ml})$$

Residual equation of wellbore pressure and its Jacobian elements

$$f_{p_w} = \sum_{m=1}^{n_b} \sum_{l=1}^{n_p} \omega_{ml} (p_w - p_{ml}) - Q$$

$$\frac{\partial f_{p_w}}{\partial p_{ml}} = - \sum_{l=1}^{n_p} \omega_{ml}$$

$$\frac{\partial f_{p_w}}{\partial p_w} = \sum_{m=1}^{n_b} \sum_{l=1}^{n_p} \omega_{ml}$$

$$\frac{\partial f_{p_w}}{\partial C} = \sum_{m=1}^{n_b} \sum_{l=1}^{n_p} \frac{\partial \omega_{ml}}{\partial C} (p_w - p_{ml})$$

Table 1.1: Potential Rate Allocation Method and Solution Scheme for Multicell Well (cont'd.)

Solution Scheme

System of equations of primary variables

$$\begin{bmatrix} A_{11} & A_{12} \\ A_{21} & A_{22} \end{bmatrix} \begin{bmatrix} u_1 \\ u_2 \end{bmatrix} = \begin{bmatrix} b_1 \\ b_2 \end{bmatrix}$$

with each components defined as

A_{11} main Jacobian matrix with a size of n_t by n_t

b_1 main right-side vector with a size of n_t

A_{12} matrix formed by derivatives of $\frac{\partial Q_{mk}}{\partial p_w}$ with a size of n_t by n_w

A_{21} matrix formed by derivatives of $\frac{\partial f_{p_w}}{\partial p_{ml}}$, and $\frac{\partial f_{p_w}}{\partial C}$ with a size of n_w by n_t

A_{22} matrix formed by derivatives of $\frac{\partial f_{p_w}}{\partial p_w}$ with a size of n_w by n_w

b_2 Vector formed by $-f_{p_w}$ with a size of n_w

u_1 Solution vector of primary variables with a size of n_t

u_2 Solution vector of wellbore pressures with a size of n_w

Rewrite the system of equations

$$\begin{cases} (A_{22} - A_{21}A_{11}^{-1}A_{12})u_2 = b_2 - A_{21}A_{11}^{-1}b_1 \\ A_{11}u_1 = b_1 - A_{12}u_2 \end{cases}$$

Table 1.1: Potential Rate Allocation Method and Solution Scheme for Multicell Well (cont'd.)

Procedure of solving for u_1 and u_2 :

- i Solving for interim solution ξ from a set of system of equations $A_{11}\xi=A_{12}$
- ii Solving for interim solution η from the system of equations $A_{11}\eta=b_1$
- iii Computing $\tilde{A}_{22}=A_{22}-A_{21}\xi$
- iv Computing $\tilde{b}_2=b_2-A_{21}\eta$
- v Solving for solution u_2 from the system of equations $\tilde{A}_{22}u_2=\tilde{b}_2$
- vi Computing $\tilde{b}_1=b_1-A_{12}u_2$
- vii Solving for solution u_1 from the system of equations $A_{11}u_1=\tilde{b}_1$

Table 2.1: Simulation Input Data for Reservoir I

Dimensions of the quarter five-spot	660 ft x 660 ft x 140 ft
Porosity	0.136
Type of permeability distribution	log-normal
Geometric average	50.55 md
Standard deviation of the log permeability	1.609
Arithmetic average	181.8 md
Range of permeability	0.293 md — 4343 md
Correlation length in x, y, and z directions	660 ft x 660 ft x 28 ft
Vertical-to-horizontal permeability ratio	0.1
Residual water saturation	0.14
Residual oil saturation	0.25
Water viscosity	0.74 cp
Oil viscosity	7.78 cp
Endpoint water-oil mobility ratio	1.393
Brine salinity assumed all anions	0.611 meq/ml
Divalent cation concentration of brine	0.1275 meq/ml
Injection pressure	1250 psia
Production pressure	250 psia
Number of gridblocks in the x, y and z directions	11 x 11 x 5
Gridblock sizes in the x, y, and z directions	60 ft x 60 ft x 28 ft
Effective length-to-thickness ratio	1.49
Maximum injection rate per quarter five-spot	500 B/D

Table 2.2: Schedule of Injection Conditions for Reservoir I

	Duration (PV)	Surfactant concentration (vol. frac.)	Polymer concentration (wt%)
Surfactant/polymer	from 0 to 0.25 PV	0.025	0.1
Polymer drive	from 0.25 to 0.75 PV	0	0.1
Chase water	from 0.75 PV to end of simulation	0	0

Table 2.3: Simulation Input Data for Reservoir II

Reservoir dimension, ft	4656.8 x 3376.1x 288.0
Number of gridblocks in the x, y, z directions	13 x 7 x 8
Average gridblock sizes, ft	358.2 x 482.3 x 36
Volume-weighted avg. porosity, fraction	0.1265
Arithmetic average permeability in x direction, md	112
Vertical-to-horizontal permeability ratio for each gridblock	0.2
Average (volume) initial water saturation	0.2313
Salinity expressed in total equivalent anions meq/ml	0.627
Calcium ions , meq/ml	0.133
Residual water saturation	0.125
Residual oil saturation	0.25
Water viscosity, cp (90°C)	0.27
Oil viscosity, cp (90°C)	0.29
Oil formation volume factor (constant), B/STB	1.444
Water formation volume factor, B/STB	1.01
Oil compressibility, psi ⁻¹	1.8279x10 ⁻⁵
Water compressibility, psi ⁻¹	1.52317x10 ⁻⁵
Formation compressibility, psi ⁻¹ (P _{ref} = 4,350 psia)	4.8276x10 ⁻⁶
Constant injection rate, B/D	25,409
Production pressure, psia	2,175
Numerical scheme	TVD third-order method

Table 2.4 : Simulation Input Data for Reservoir III

Pilot size, ft	1,315 x 82.02 x 26
Number of gridblocks in the x,y,z	26 x 1 x 8
Average gridblock sizes, ft	50.5 x 82.02 x 3.25
Average (arithmetic) of porosity, md	0.33
Geometric average of permeability in x direction, md	7,349
Initial pressure, psia	3,771
Average initial water saturation	0.147
Salinity expressed in total equivalent anions meq/ml	0.627
Calcium ions , meq/ml	0.133
Residual water saturation	0.147
Residual oil saturation	0.25
Water viscosity @ 122°F, cp	0.42
Oil viscosity @ 122°F, cp	1.25
Longitudinal dispersivity, ft	16
Transverse dispersivity, ft	0.4
Surfactant/polymer slug size, pv	0.4
Surfactant concentration, vol. fr.	0.005 (0.4 pv)
Polymer concentration and slug size, wt% (pv)	0.05 (0.3 pv) 0.025 (0.1 pv)
Postflood, pv	1.45
Constant total injection rate, B/D	2000
Injected temperature, °F	122
Initial temperature, °F	158
HBNT0	0.00017
HBNT1	0.0017
HBNT2	0.00017
β_T	0.00415
Rock density, lb/ft ³	165.43
Reservoir thermal conductivity, (day-ft-°F) ⁻¹	40
Rock heat capacity, Btu/lb °F	0.2117
Water heat capacity, Btu/lb °F	1.0
Gulfax oil heat capacity, Btu/lb °F	0.5
Surfactant heat capacity	1.0
Overburden and underburden thermal conductivity, (day-ft-°F) ⁻¹	35
Numerical scheme	TVD third-order method

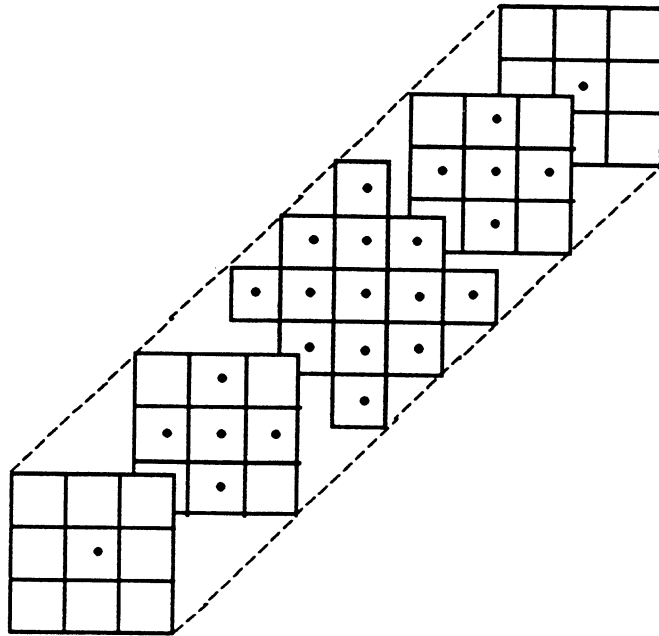


Figure 1.1. Gridpoints used in the high-order finite-difference scheme

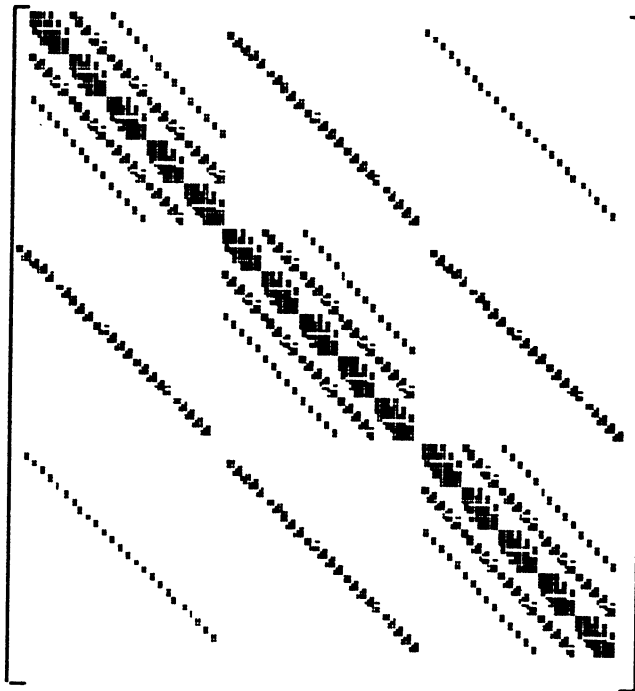
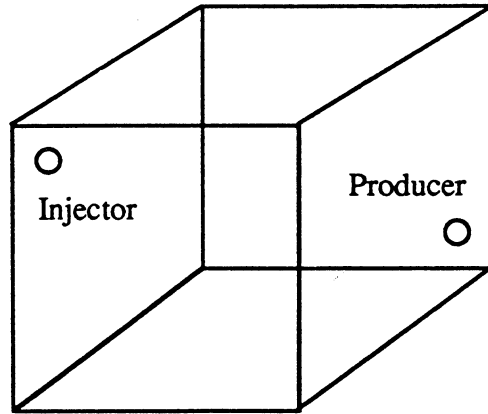
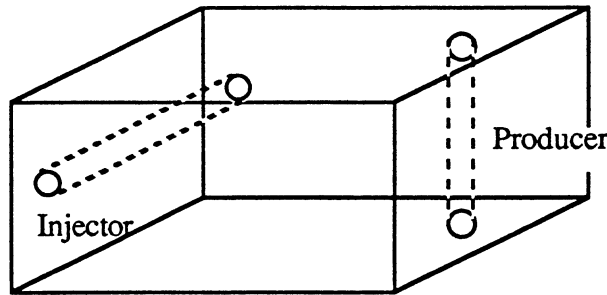


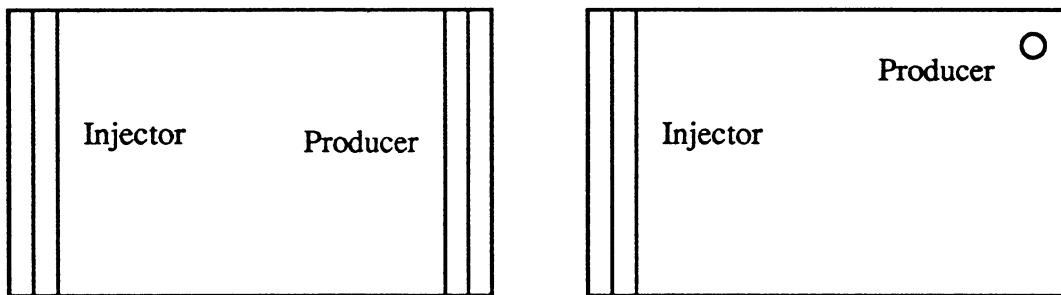
Figure 1.2. Matrix structure for a three-dimensional, two-component problem using the fully implicit high-order method with $5 \times 5 \times 3$ gridblocks.



(a) Well pattern for the three-dimensional tracer convection-diffusion simulation



(b) Well pattern for the three-dimensional polymerflood simulation



(c) Well patterns for the two-dimensional, cross-sectional polymerflood simulation

Figure 1.3. Schematic of well patterns

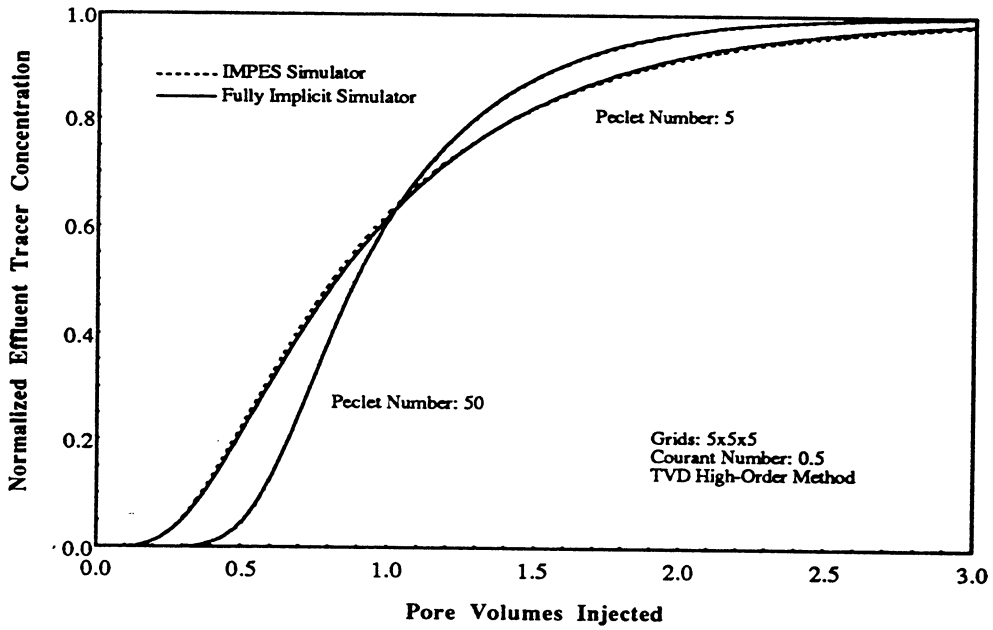


Figure 1.4. Simulation of a three-dimensional tracer convection-diffusion using the IMPES simulator and the fully implicit simulator

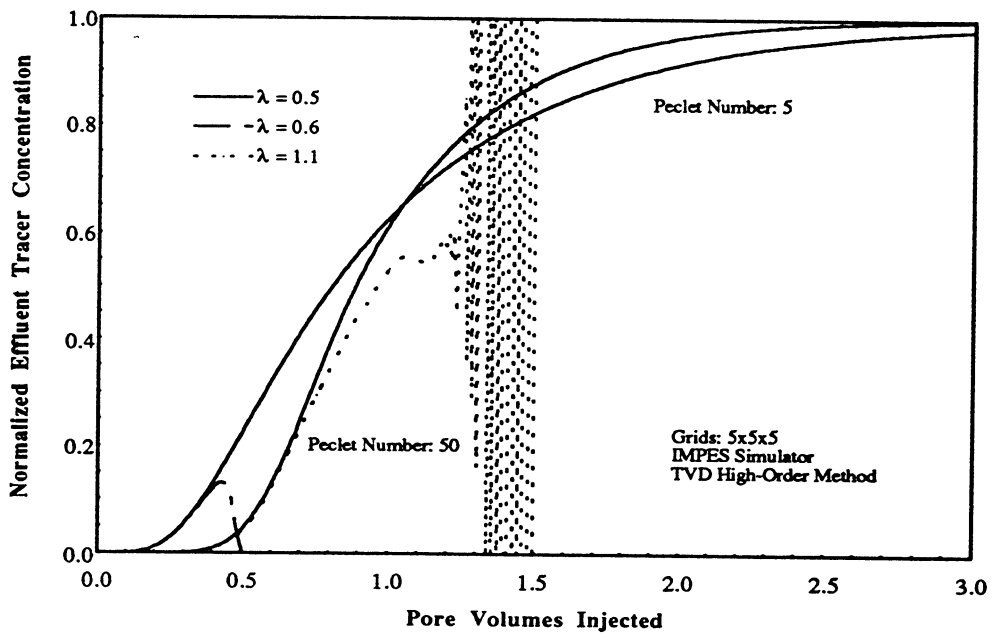


Figure 1.5. Simulation of a three-dimensional tracer convection-diffusion using the IMPES simulator

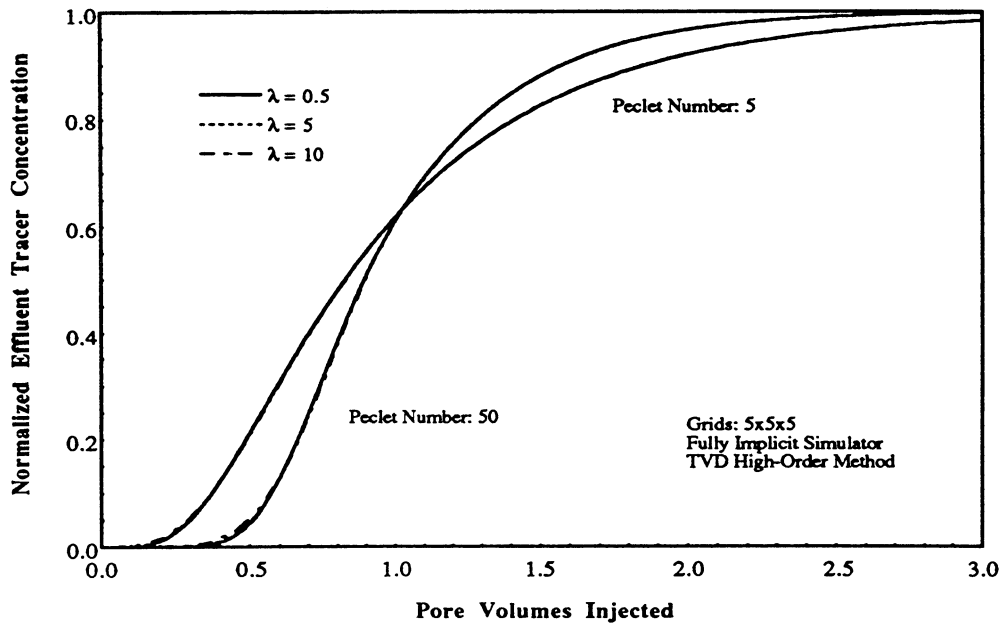


Figure 1.6. Simulation of a three-dimensional tracer convection-diffusion using the fully implicit simulator

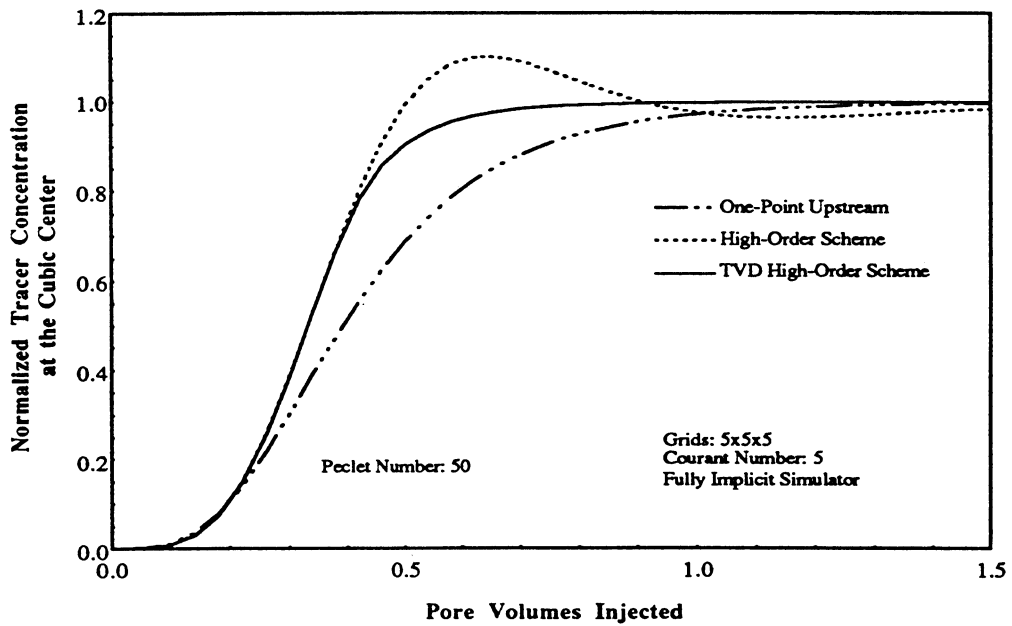


Figure 1.7. Simulation of a three-dimensional tracer convection-diffusion for a Peclet number of 50 using the fully implicit simulator with the high-order scheme without TVD flux-limiting and the low-order scheme

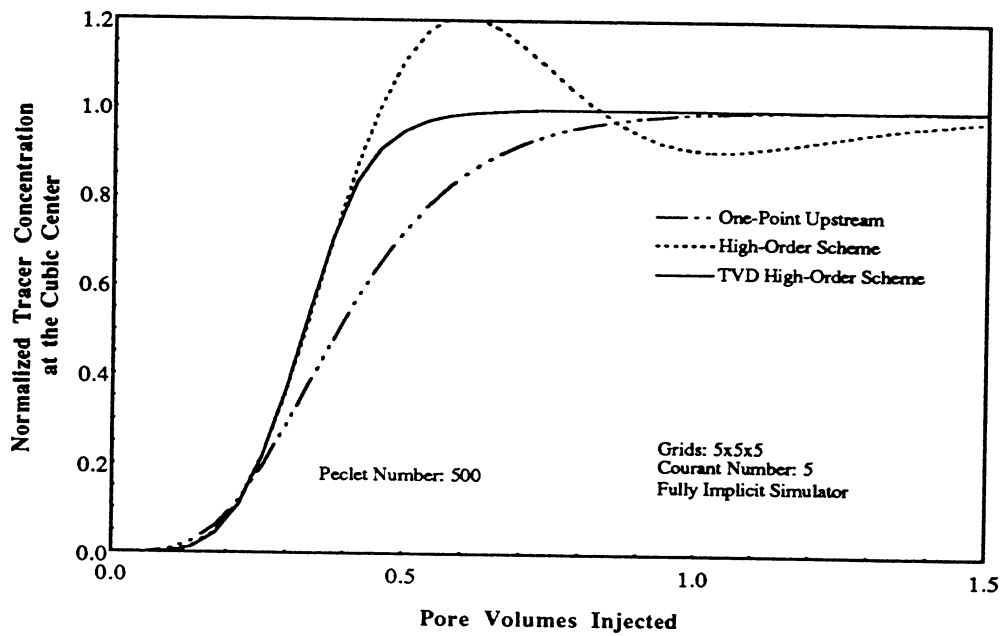
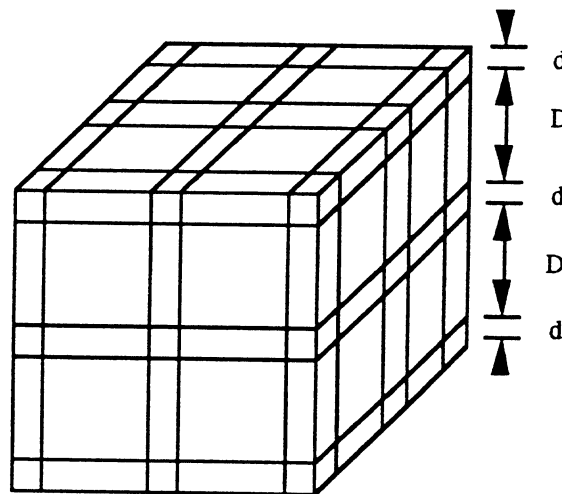


Figure 1.8. Simulation of a three-dimensional tracer convection-diffusion for a Peclet number of 500 using the fully implicit simulator with the high-order scheme without TVD flux-limiting and the low-order scheme



Expansion Ratio: D/d

Figure 1.9. Schematic of nonuniform grids and the expansion ratio.

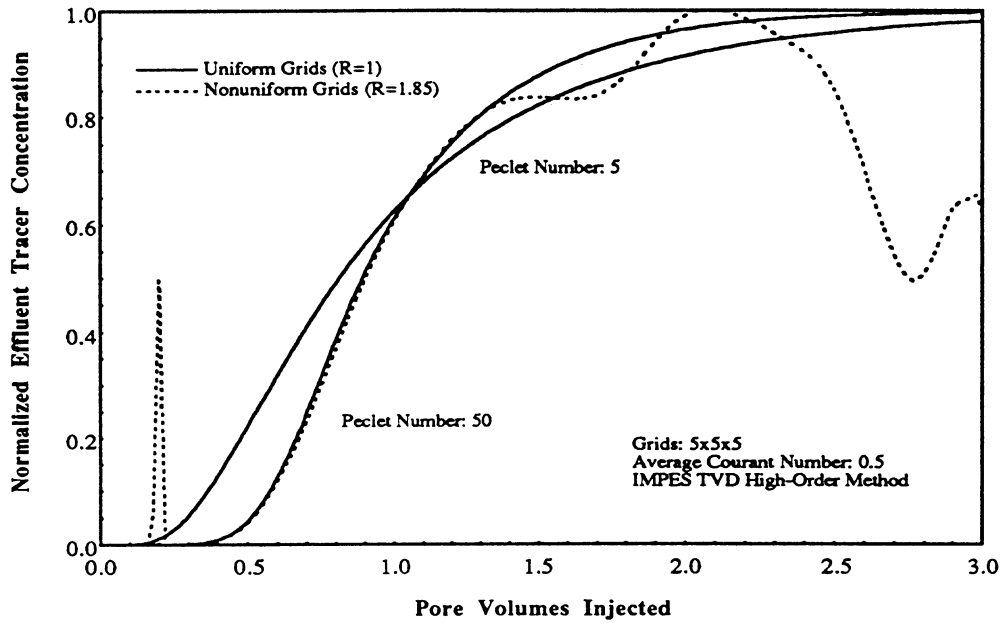


Figure 1.10. Simulation of a three-dimensional tracer convection-diffusion using the IMPES simulator with a nonuniform grids

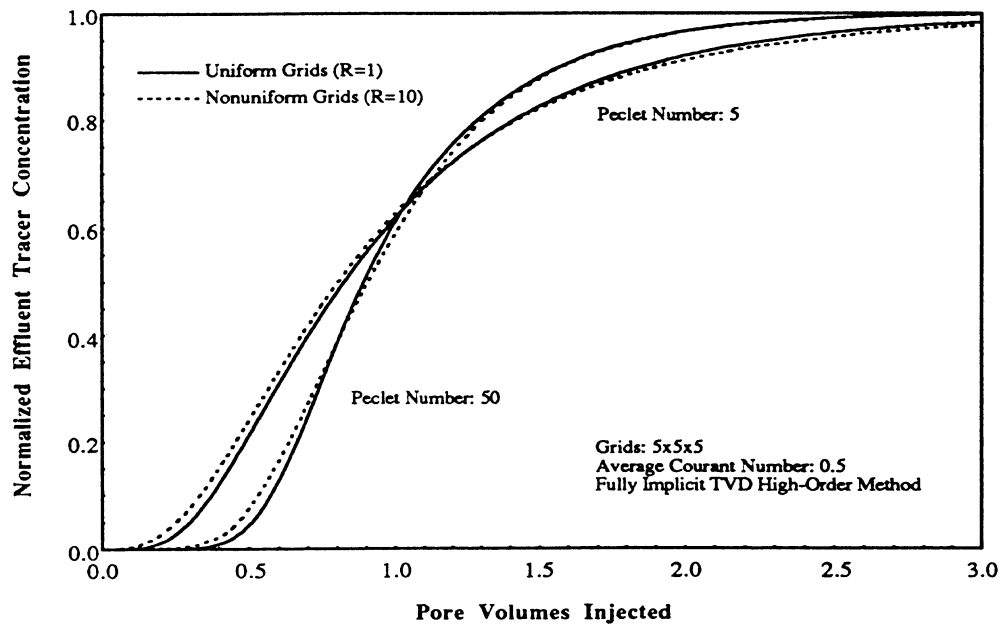


Figure 1.11. Simulation of a three-dimensional tracer convection-diffusion using the IMPES simulator with a nonuniform grids

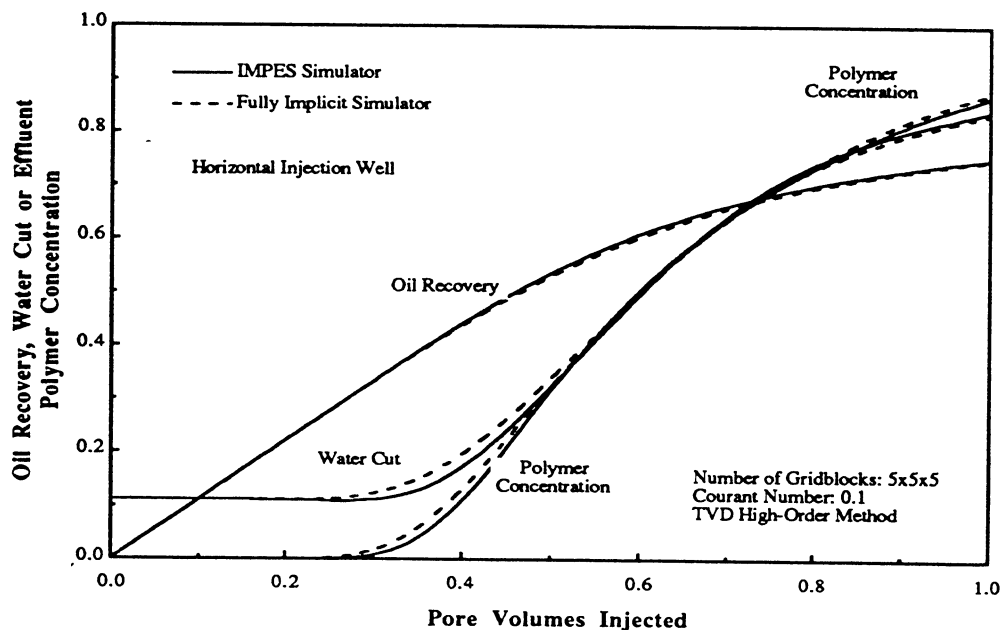


Figure 1.12. Simulation of a three-dimensional polymerflood with horizontal well using the fully implicit simulator and the fully implicit simulator

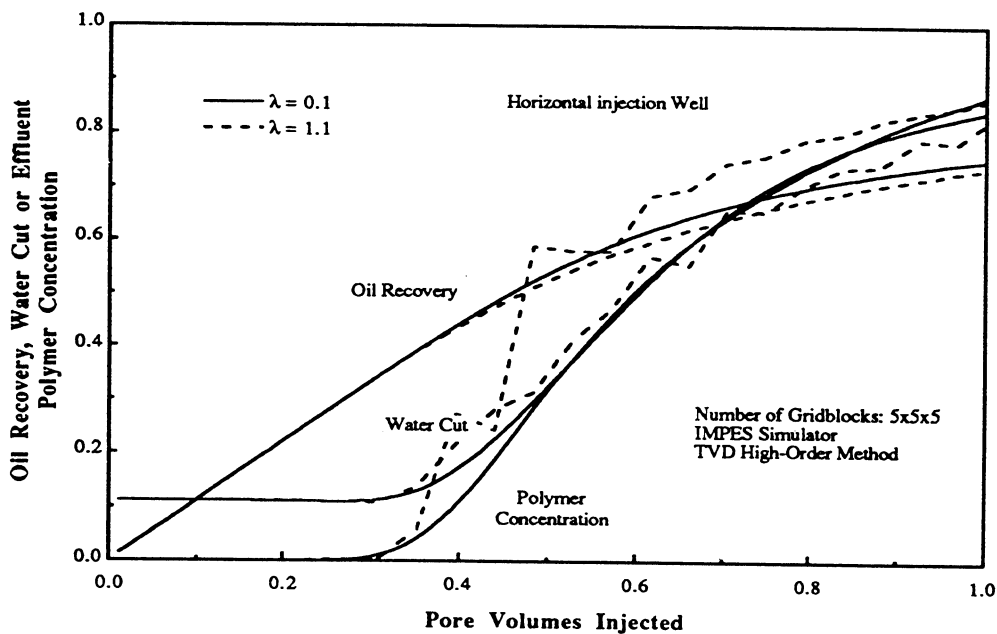


Figure 1.13. Simulation of a three-dimensional polymerflood with horizontal well using the IMPES simulator

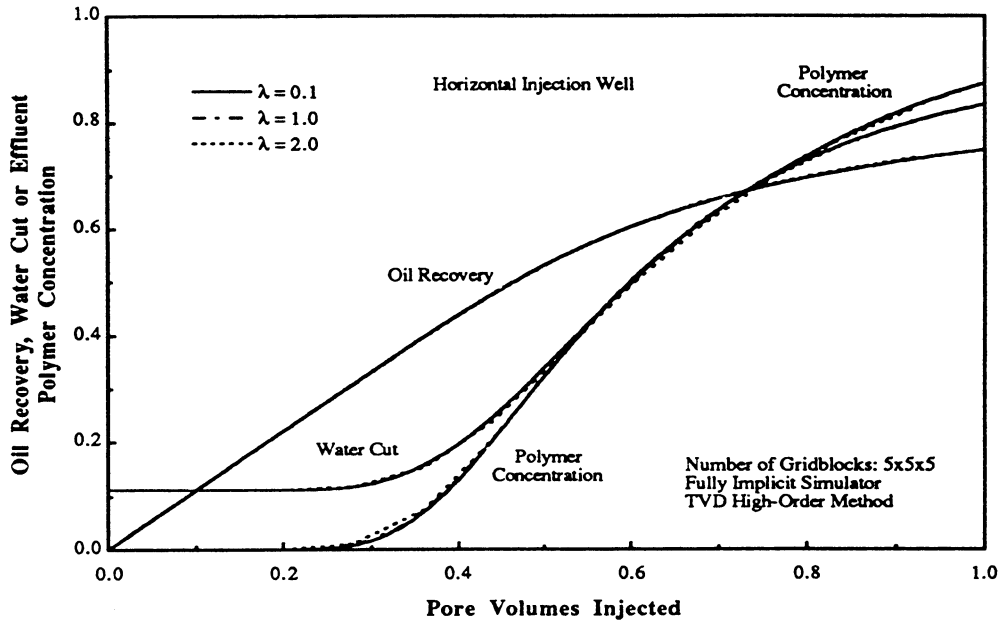


Figure 1.14. Simulation of a three-dimensional polymerflood with horizontal well using the fully implicit simulator

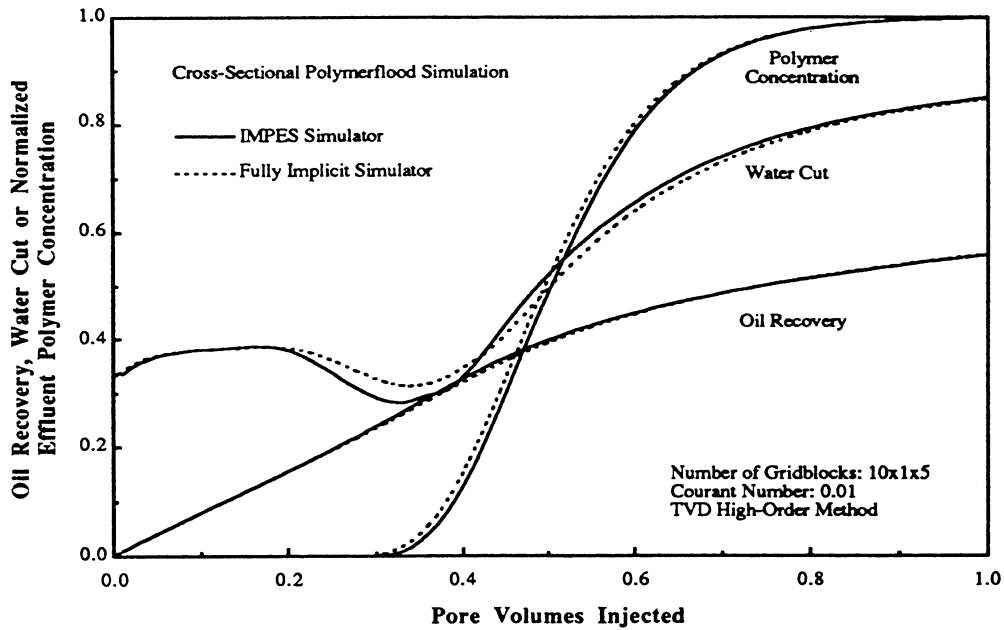


Figure 1.15. Simulation of a two-dimensional, cross-sectional polymerflood using the IMPES simulator and the fully implicit simulator

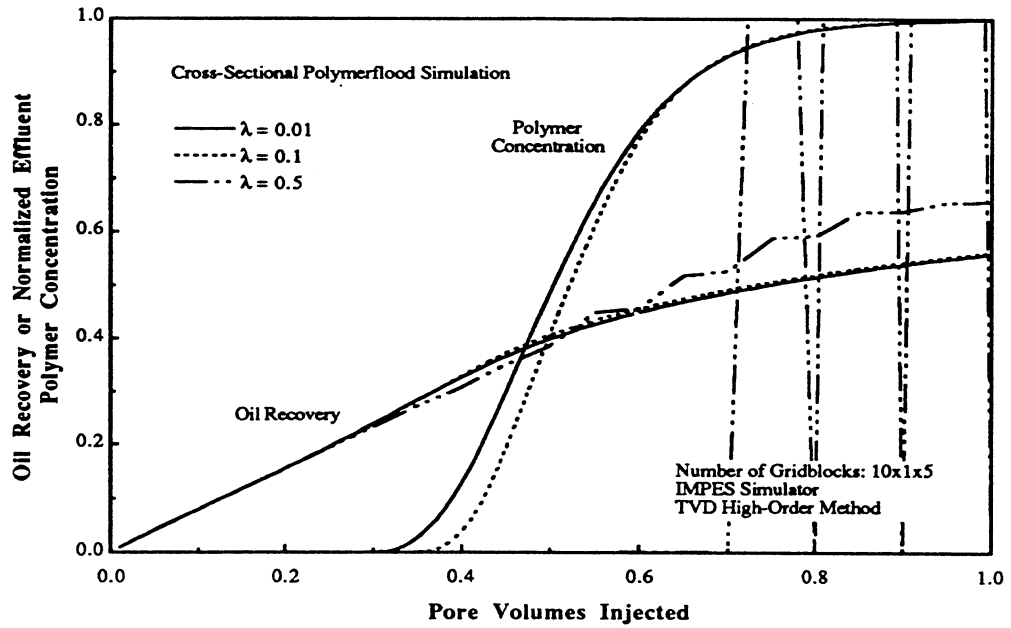


Figure 1.16. Oil recovery and normalized effluent polymer concentration of simulating a two-dimensional, cross-sectional polymerflood using the IMPES simulator

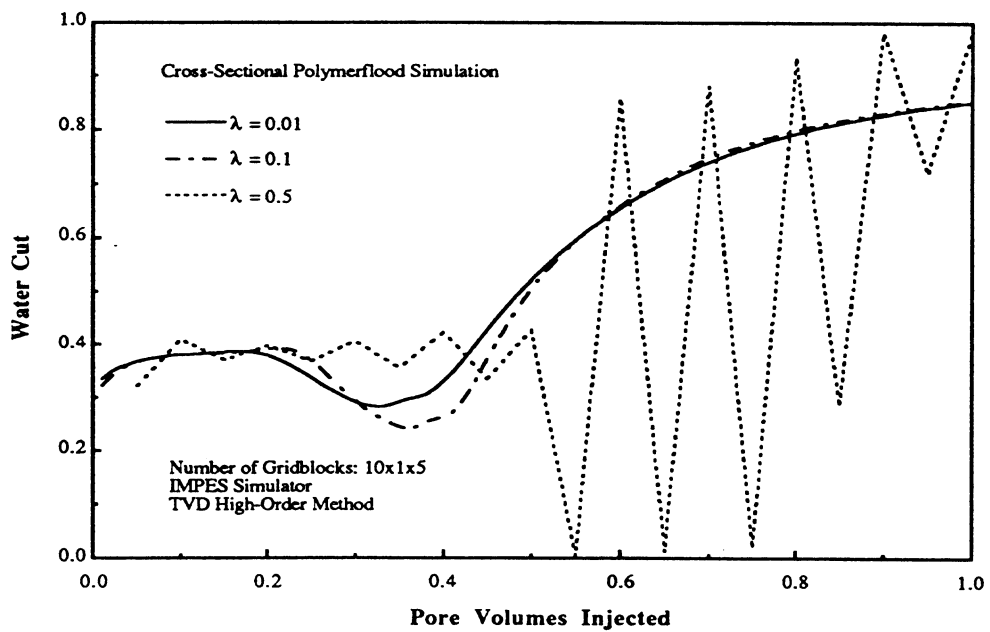


Figure 1.17. Water cut of simulating a two-dimensional, cross-sectional polymerflood using the IMPES simulator

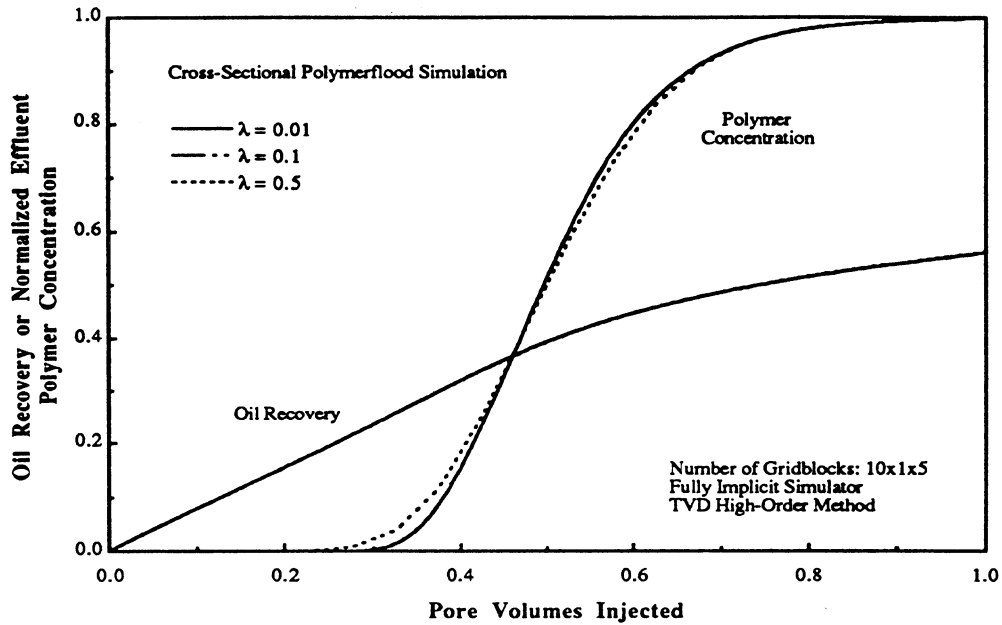


Figure 1.18. Oil recovery and normalized effluent polymer concentration of simulating a two-dimensional, cross-sectional polymerflood using the fully implicit simulator

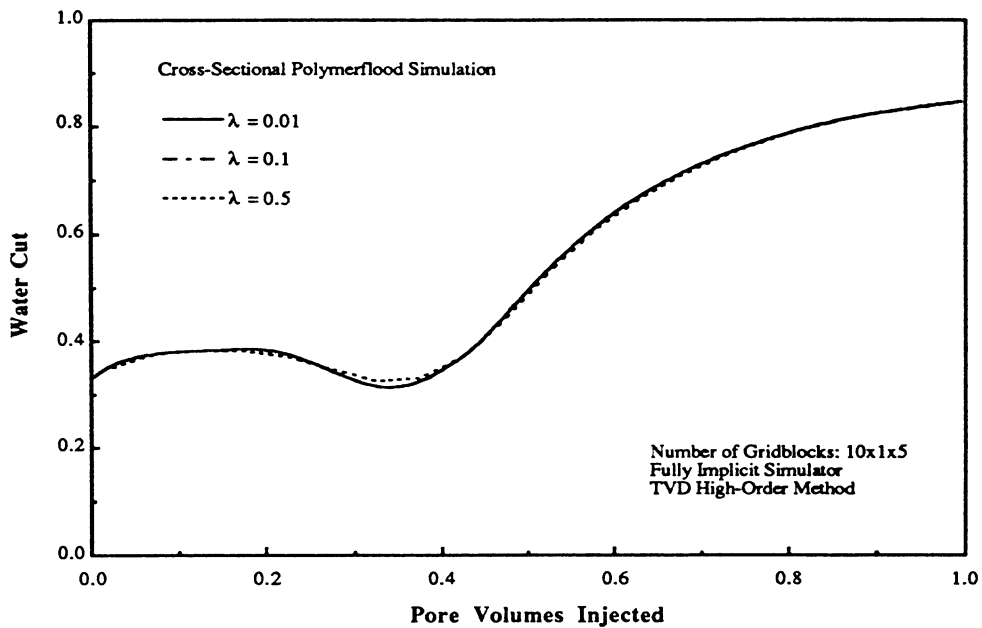


Figure 1.19. Water cut of simulating a two-dimensional, cross-sectional polymerflood using the fully implicit simulator

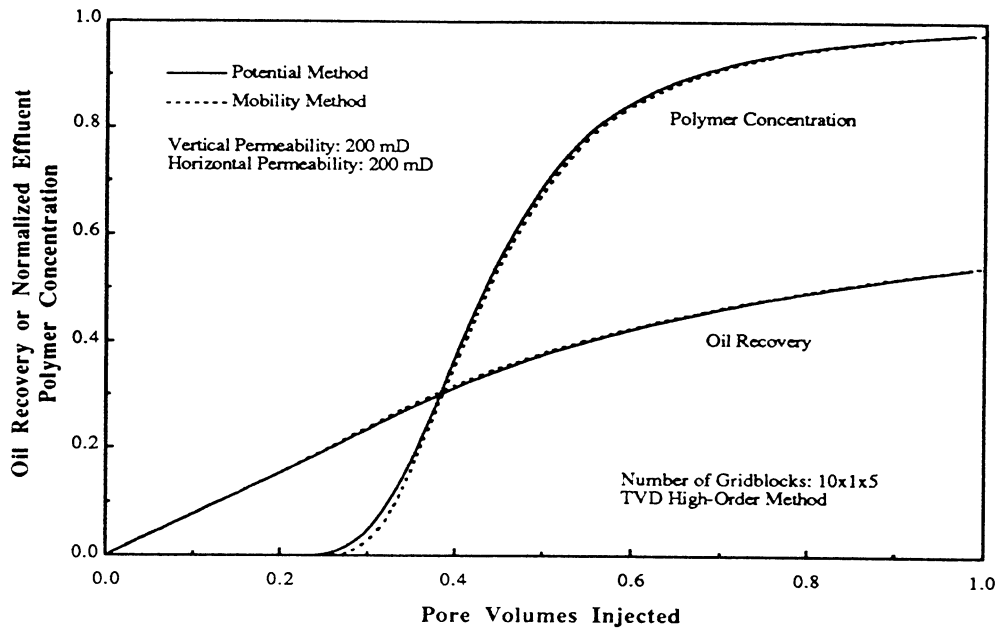


Figure 1.20. Simulation of a two-dimensional, cross-sectional polymerflood with a high vertical permeability

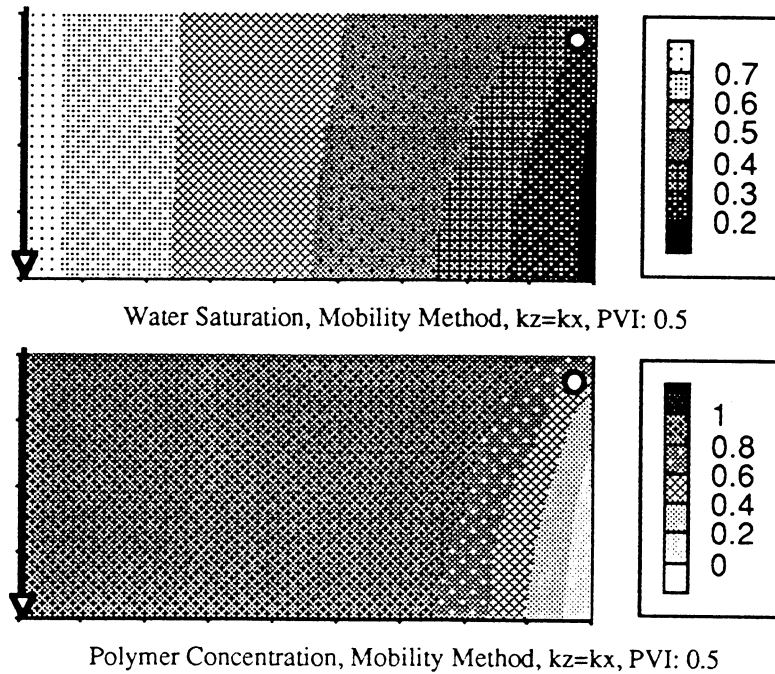


Figure 1.21. Water saturation and polymer concentration distributions with a high vertical permeability using the mobility rate allocation method

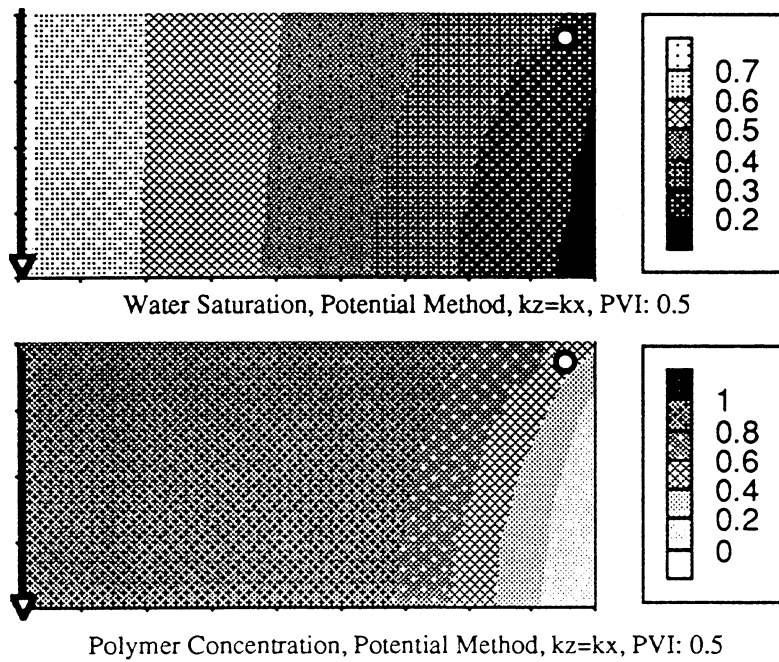


Figure 1.22. Water saturation and polymer concentration distributions with a high vertical permeability using the potential rate allocation method

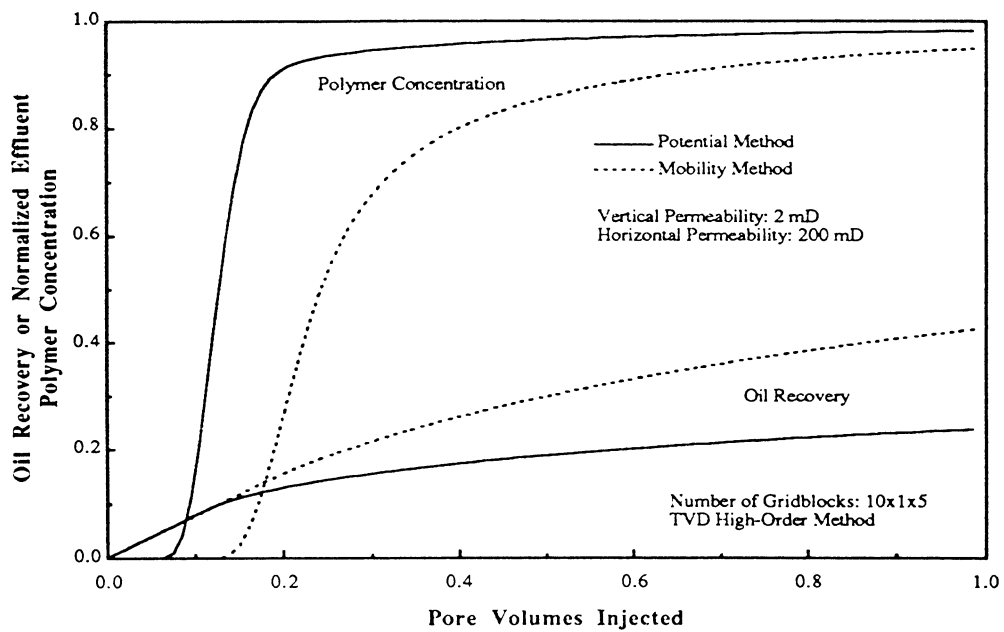
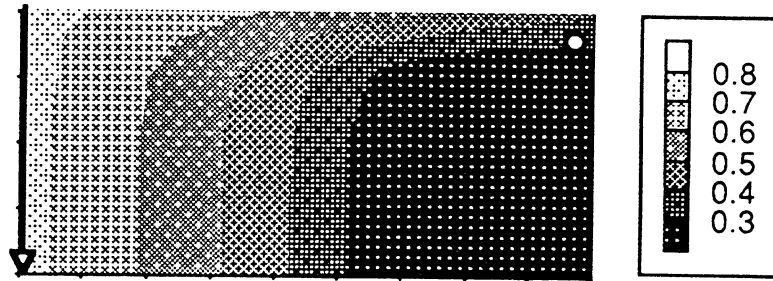
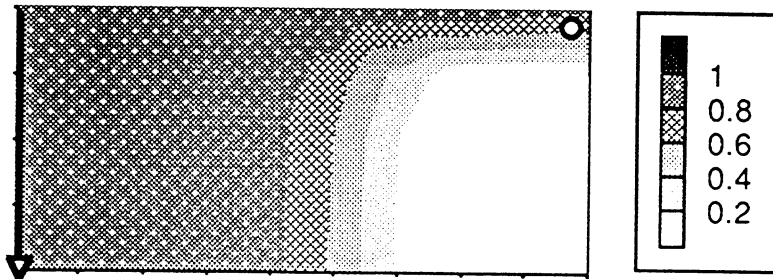


Figure 1.23. Simulation of a two-dimensional, cross-sectional polymerflood with a low vertical permeability

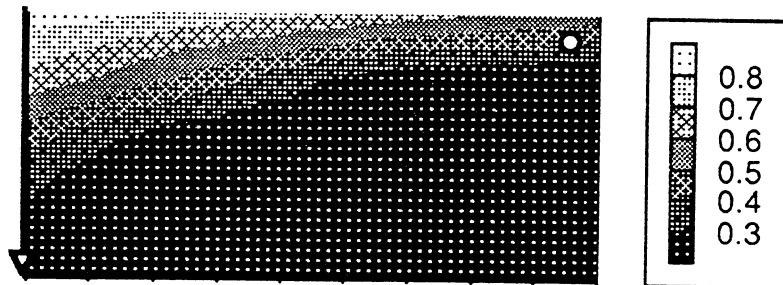


Water Saturation, Mobility Method, $k_z=0.01k_x$, PVI: 0.5

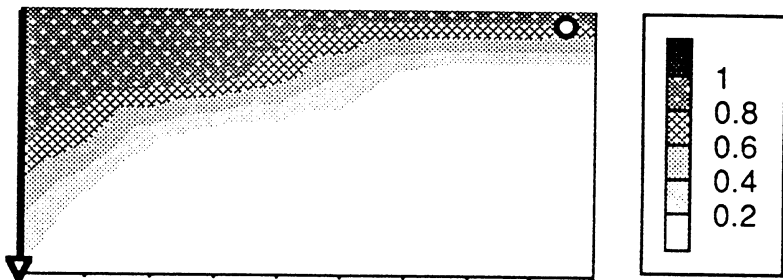


Polymer Concentration, Mobility Method, $k_z=0.01k_x$, PVI: 0.5

Figure 1.24. Water saturation and polymer concentration distributions with a low vertical permeability using the mobility rate allocation method



Water Saturation, Potential Method, $k_z=0.01k_x$, PVI: 0.5



Polymer Concentration, Potential Method, $k_z=0.01k_x$, PVI: 0.5

Figure 1.25. Water saturation and polymer concentration distributions with a low vertical permeability using the potential rate allocation method

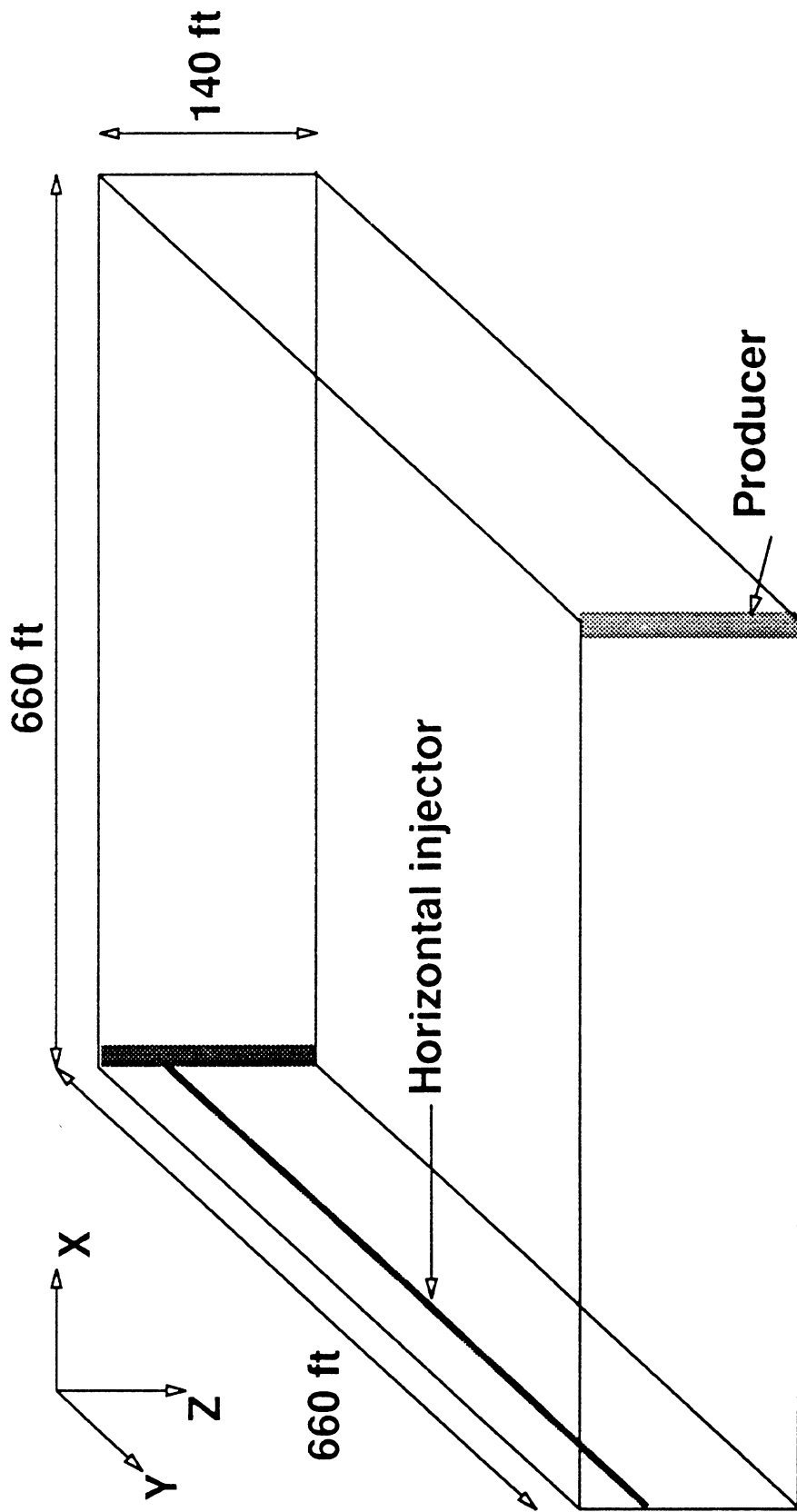


Figure 2.1. Sketch of the quarter five-spot showing the horizontal injection wellbore for Reservoir I

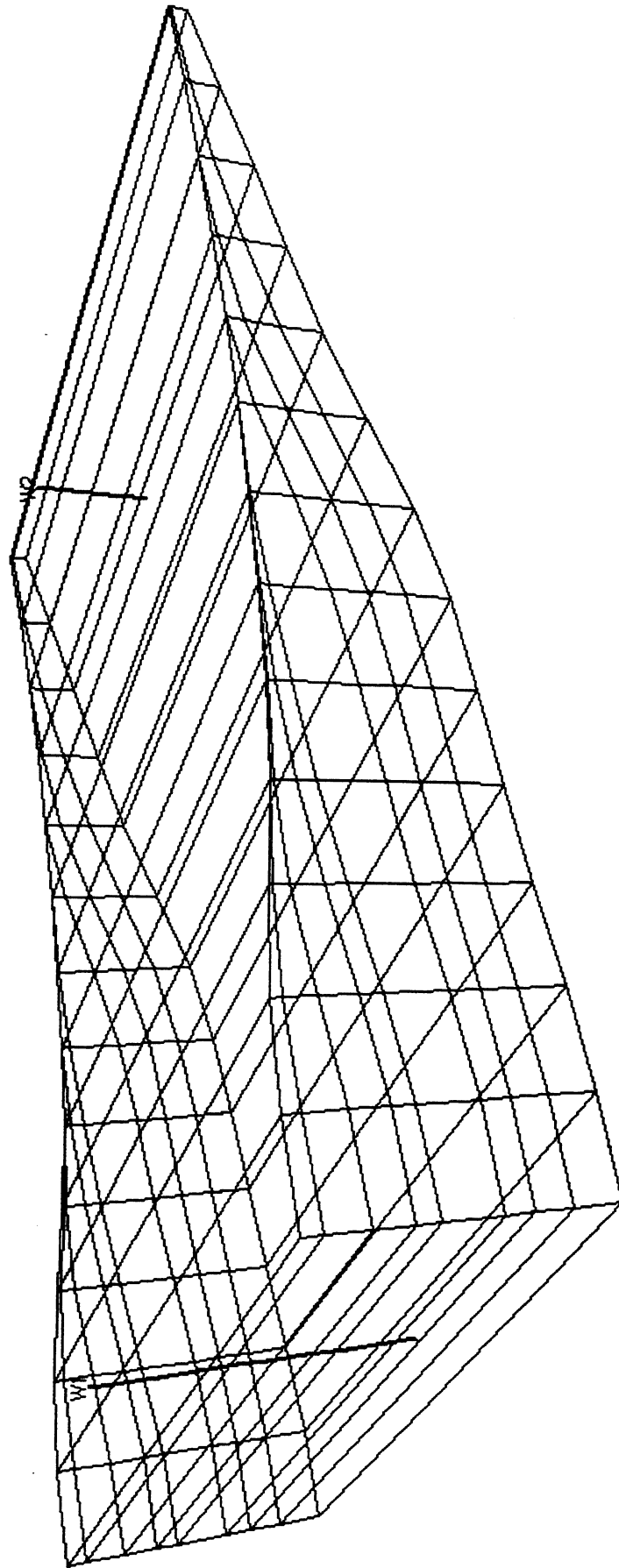


Figure 2.2. Simulation gridblocks for Reservoir II

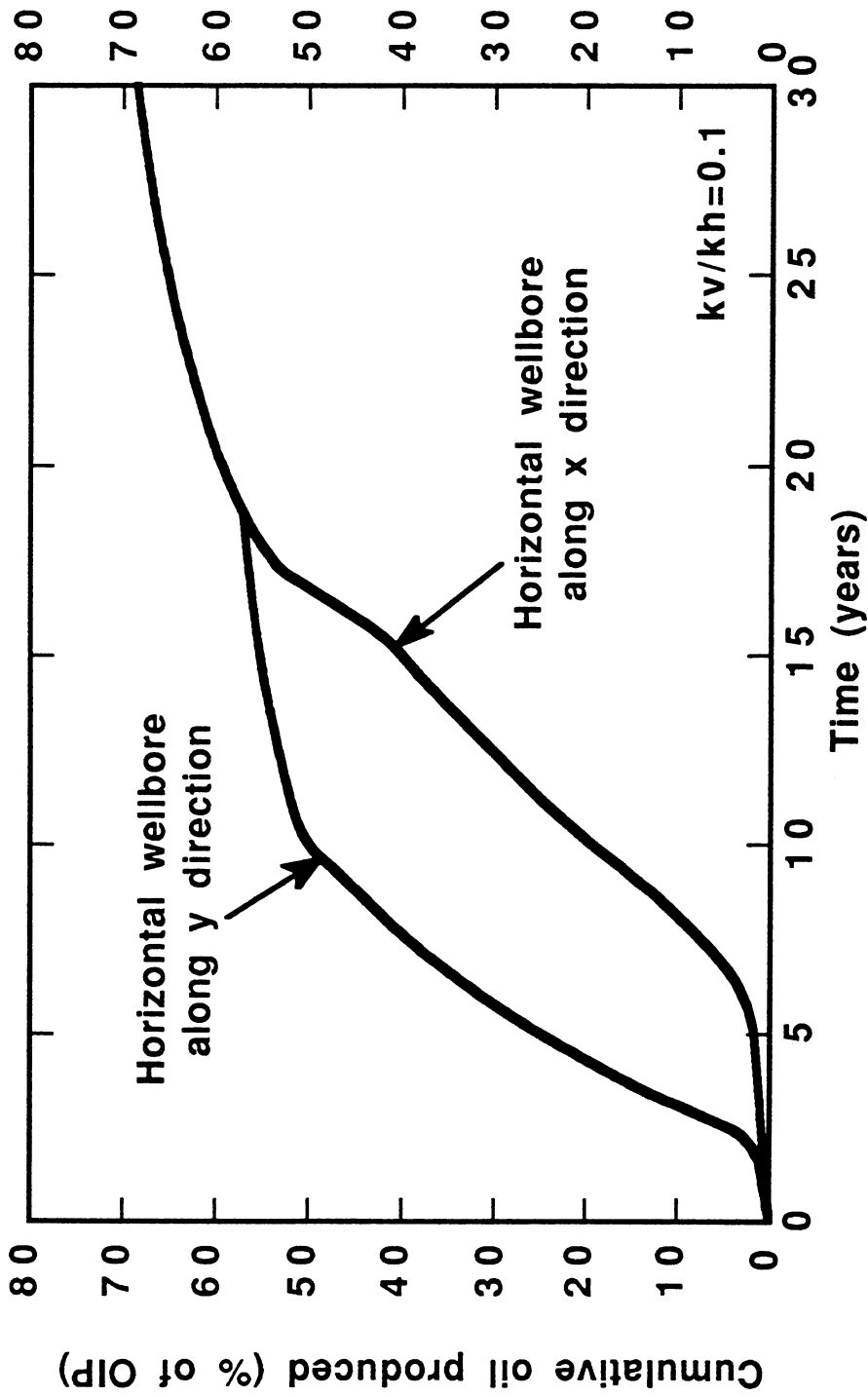


Figure 2.4. Cumulative oil produced versus time for surfactant floods one with the horizontal injection wellbore placed along the x direction and the other placed along the y direction for Reservoir I

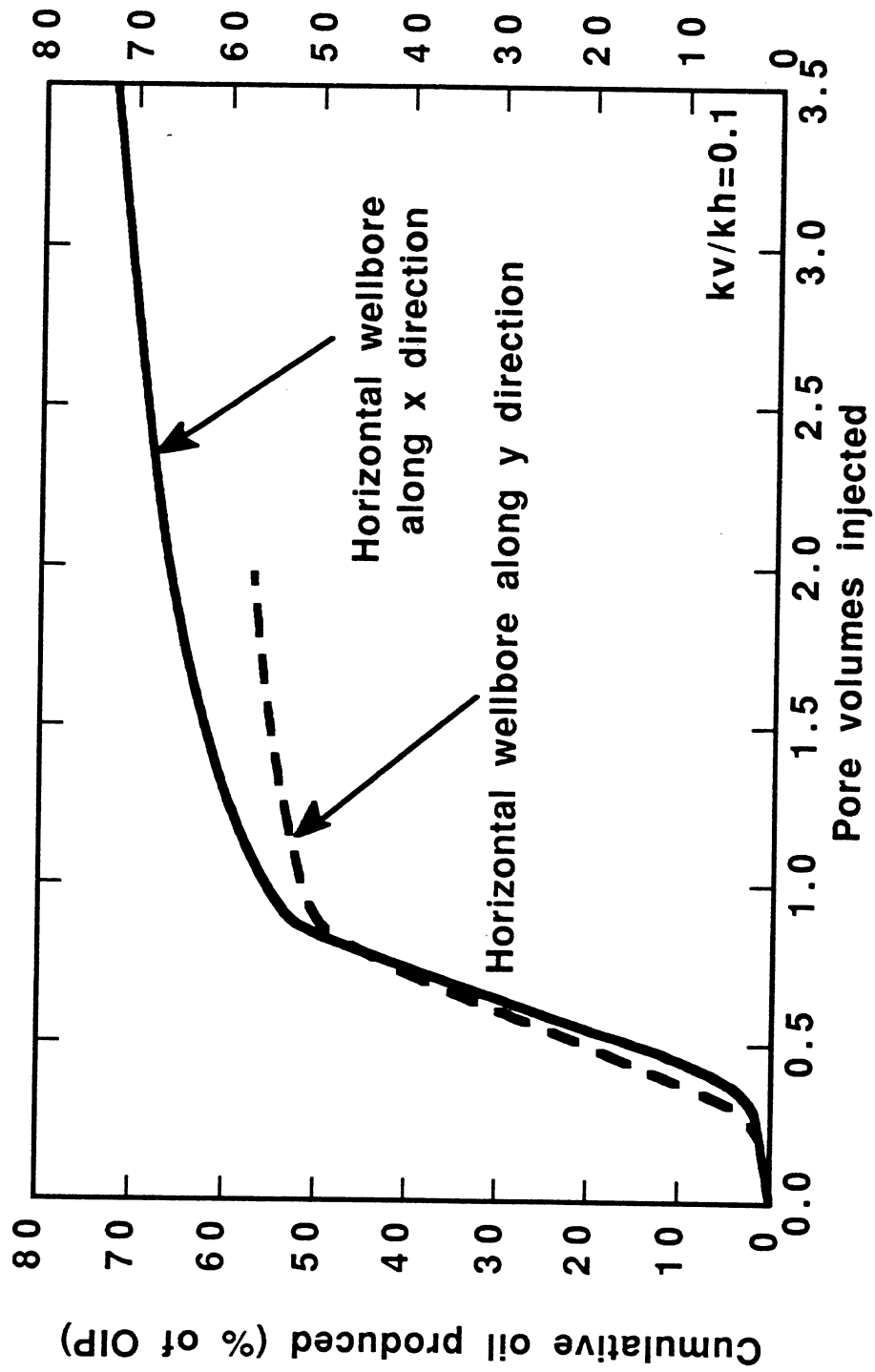


Figure 2.5. Cumulative oil produced versus pore volumes injected for surfactant floods one with the horizontal injection wellbore placed along the x direction and the other placed along the y direction for Reservoir I

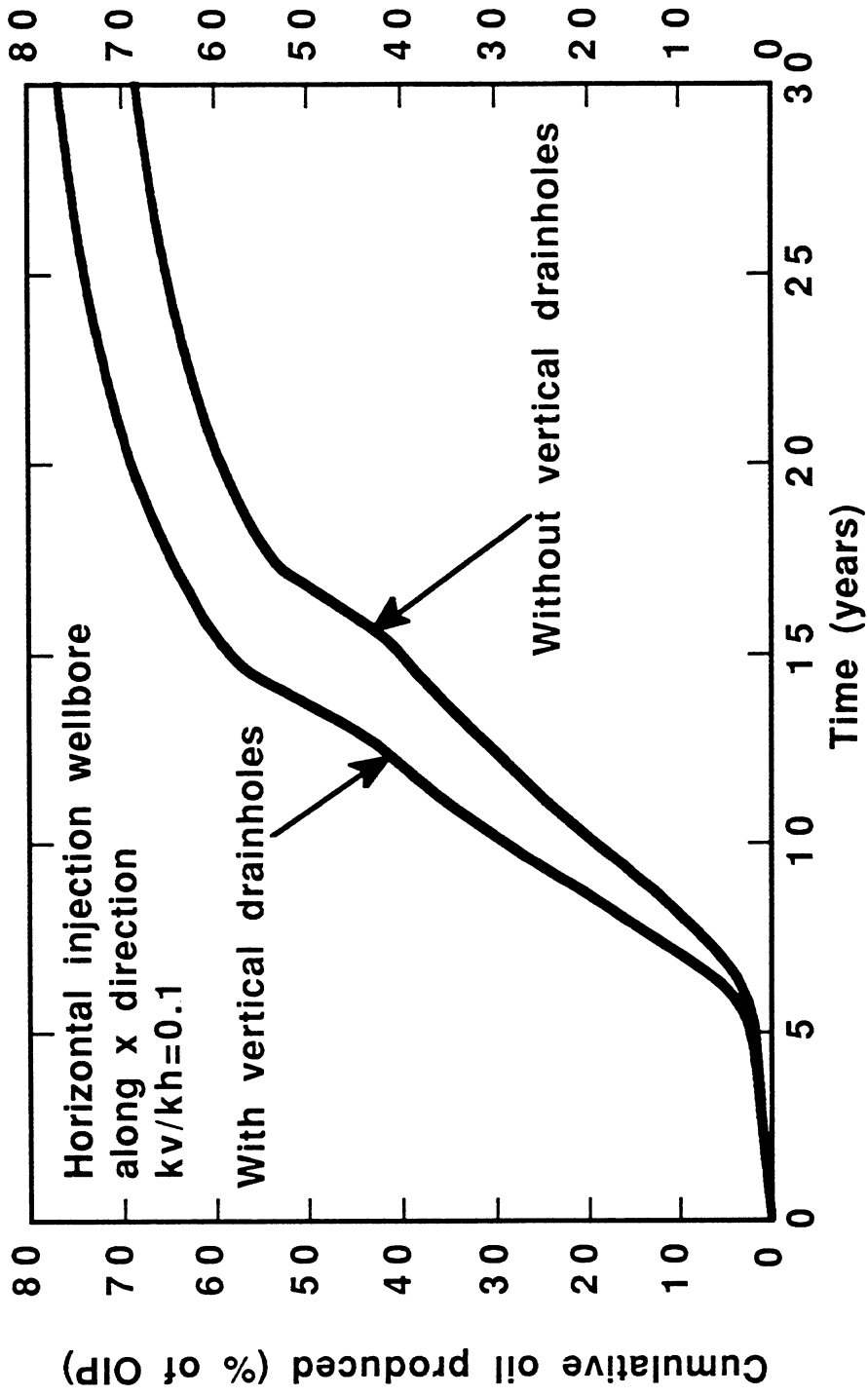


Figure 2.6. Cumulative oil produced versus time for surfactant floods with the horizontal injection wellbore placed along the x direction and with and without drainholes for Reservoir I

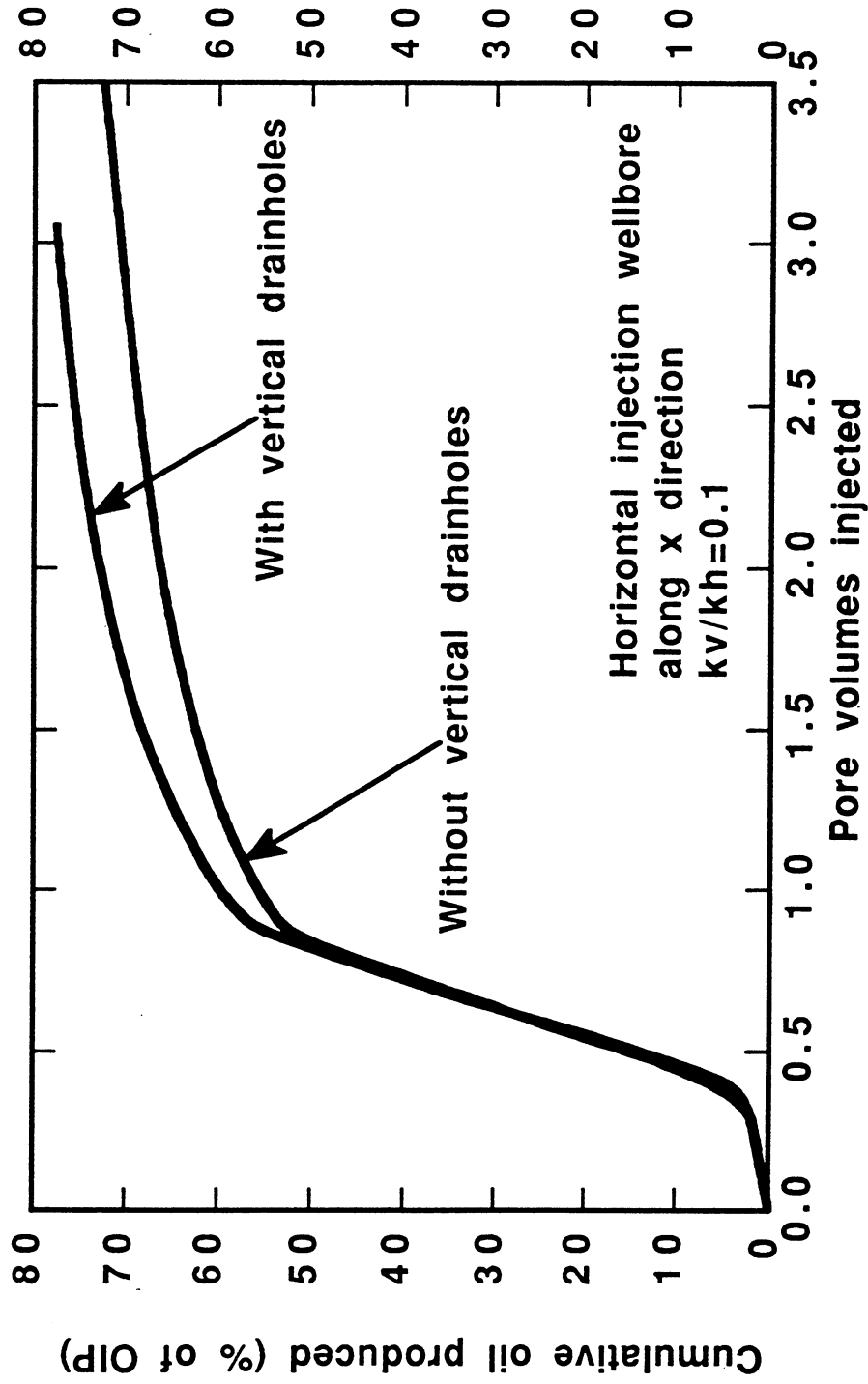


Figure 2.7. Cumulative oil produced versus pore volumes injected for surfactant floods with the horizontal injection wellbore placed along the x direction and with and without drainholes for Reservoir I

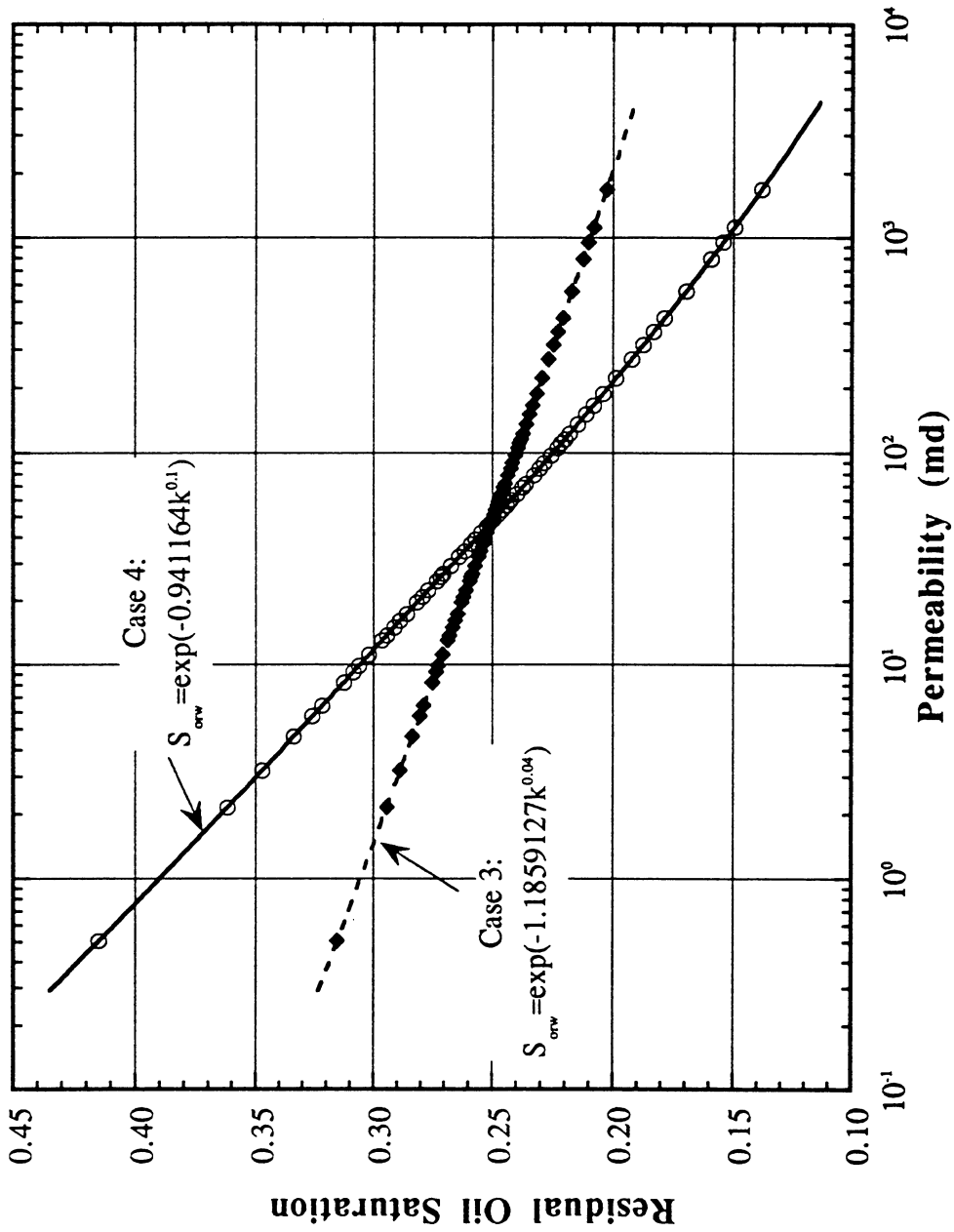


Figure 2.8. Plot of S_{σ_w} as a function of permeability for Reservoir I

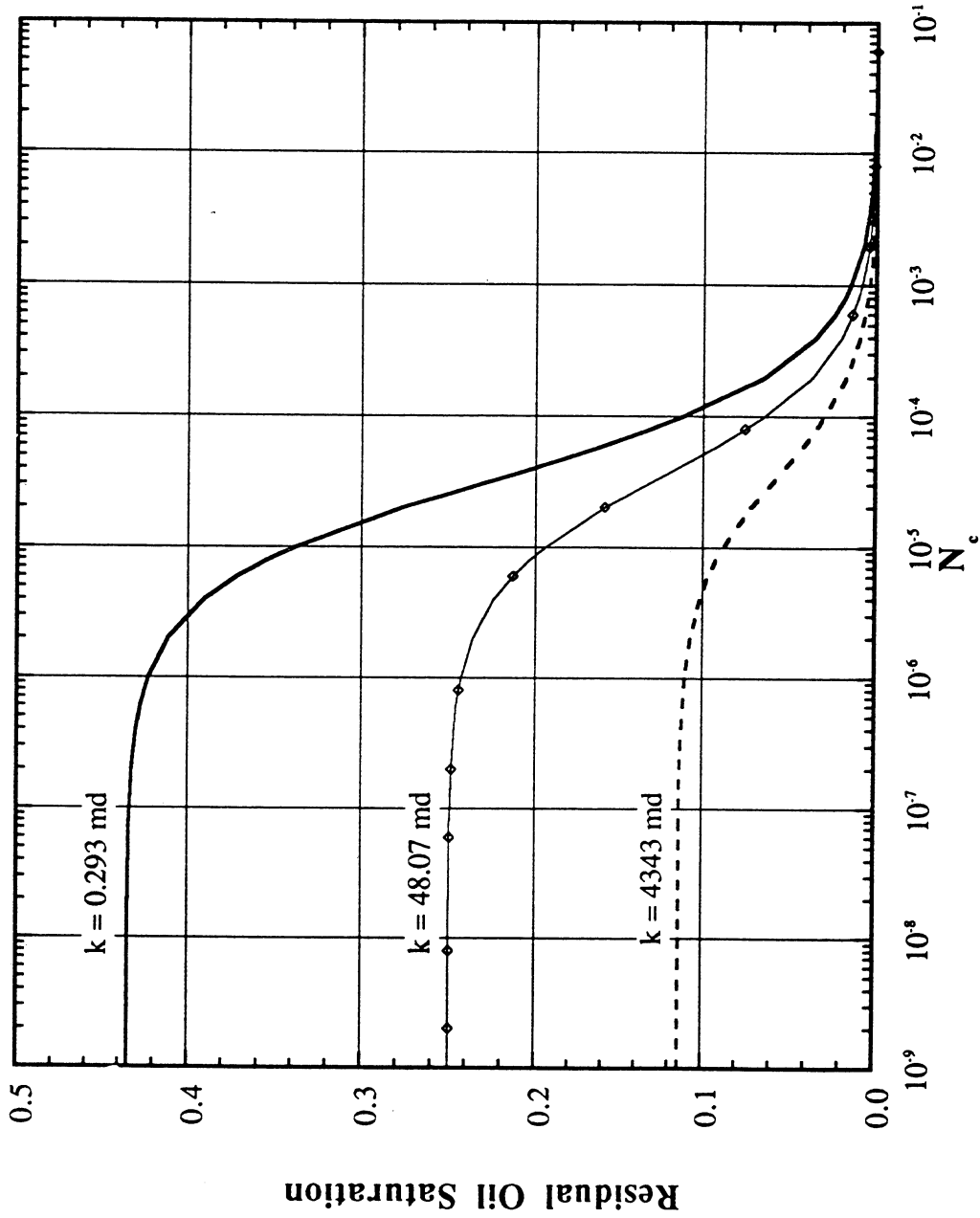


Figure 2.10. Capillary desaturation curves for permeability-dependent S_{orw} (Case 4: $S_{orw} = \exp(-0.941164k^{0.1})$) for Reservoir I

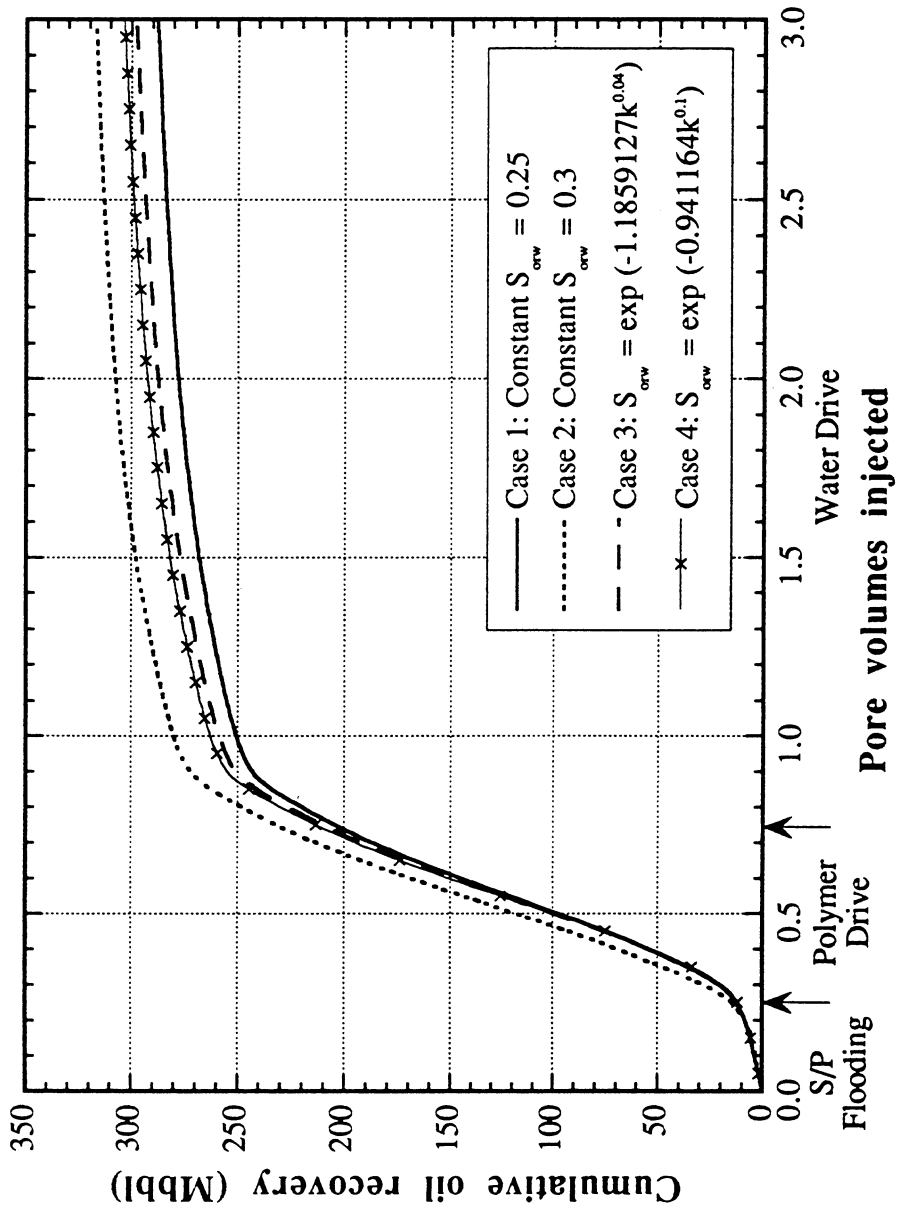


Figure 2.11. Effect of distributed S_{orw} on oil recovery for Reservoir I

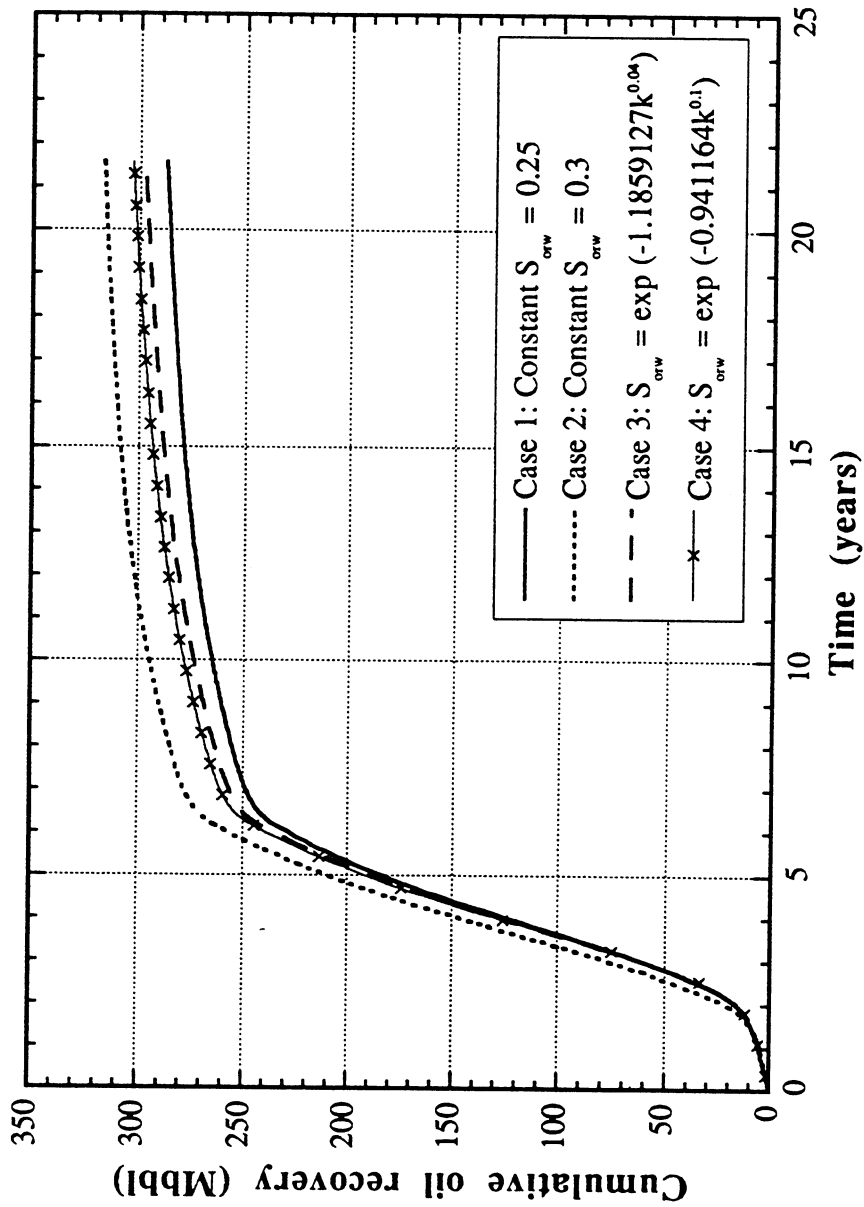


Figure 2.12. Effect of distributed S_{ow} on oil recovery for Reservoir I

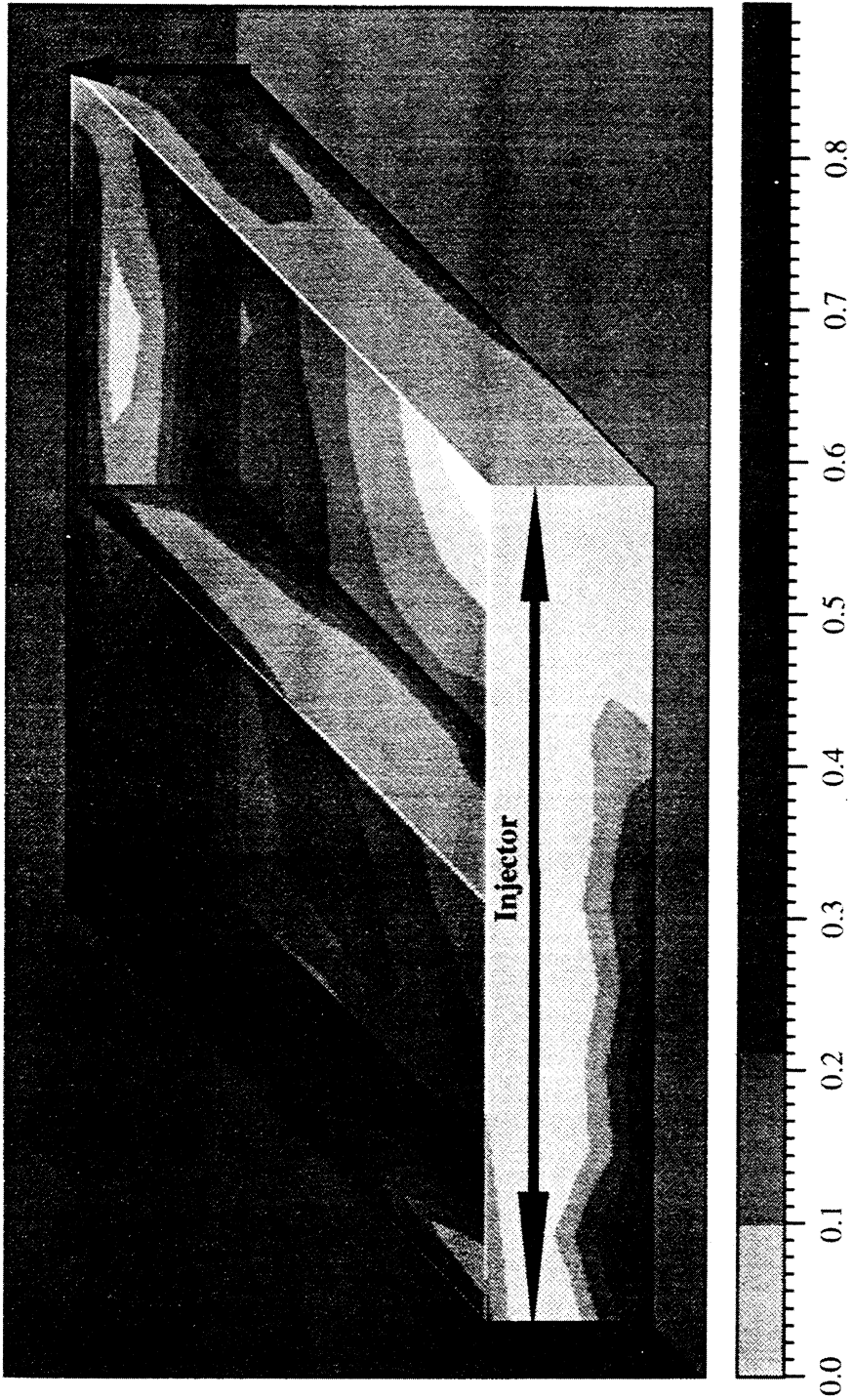


Figure 2.13. Oil concentration distribution at 0.75 pore volumes injected (1,976 days) for Case 1 for Reservoir I

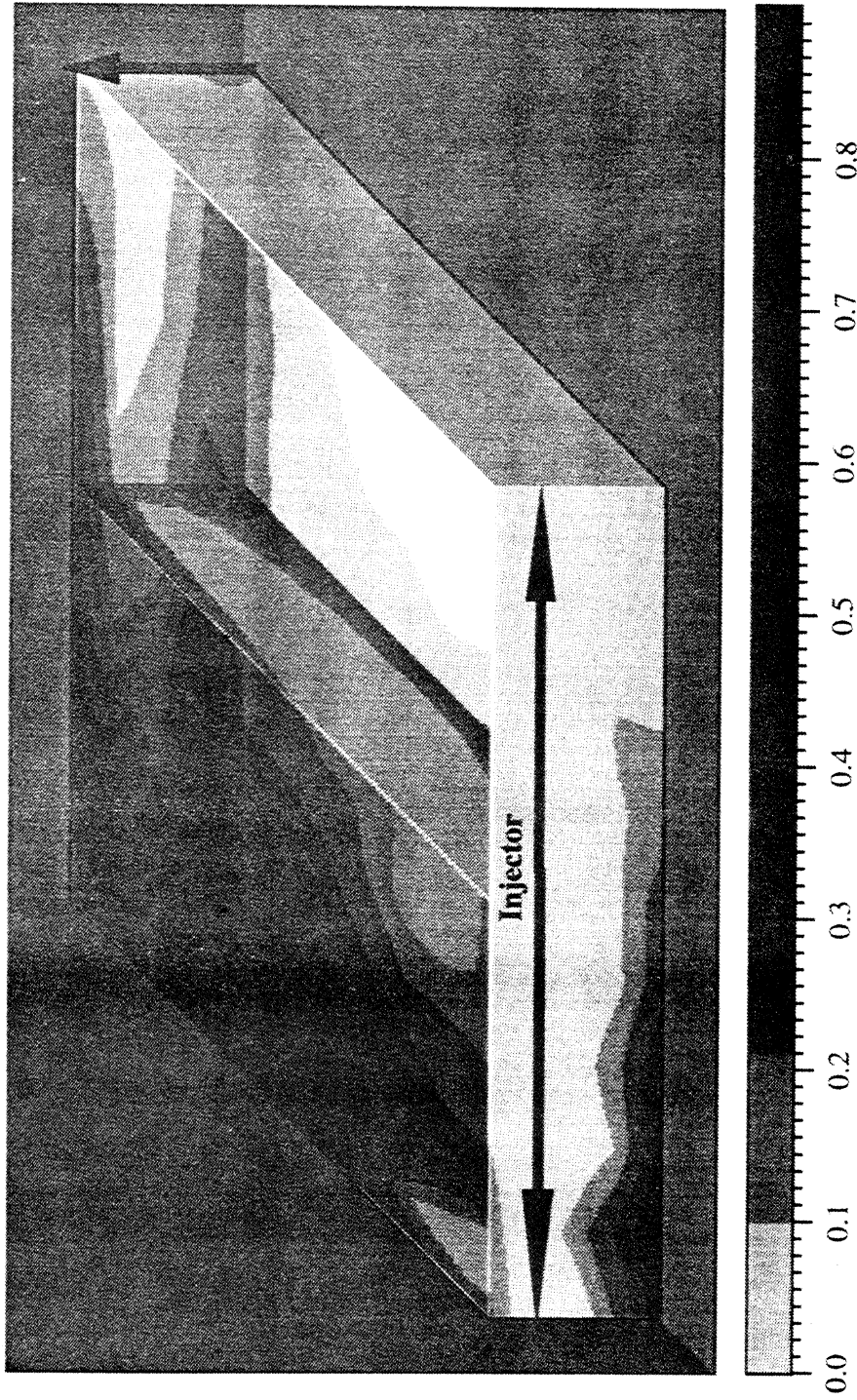


Figure 2.18. Oil concentration distribution at 2.75 pore volumes injected (7,241 days) for Case 2 for Reservoir I

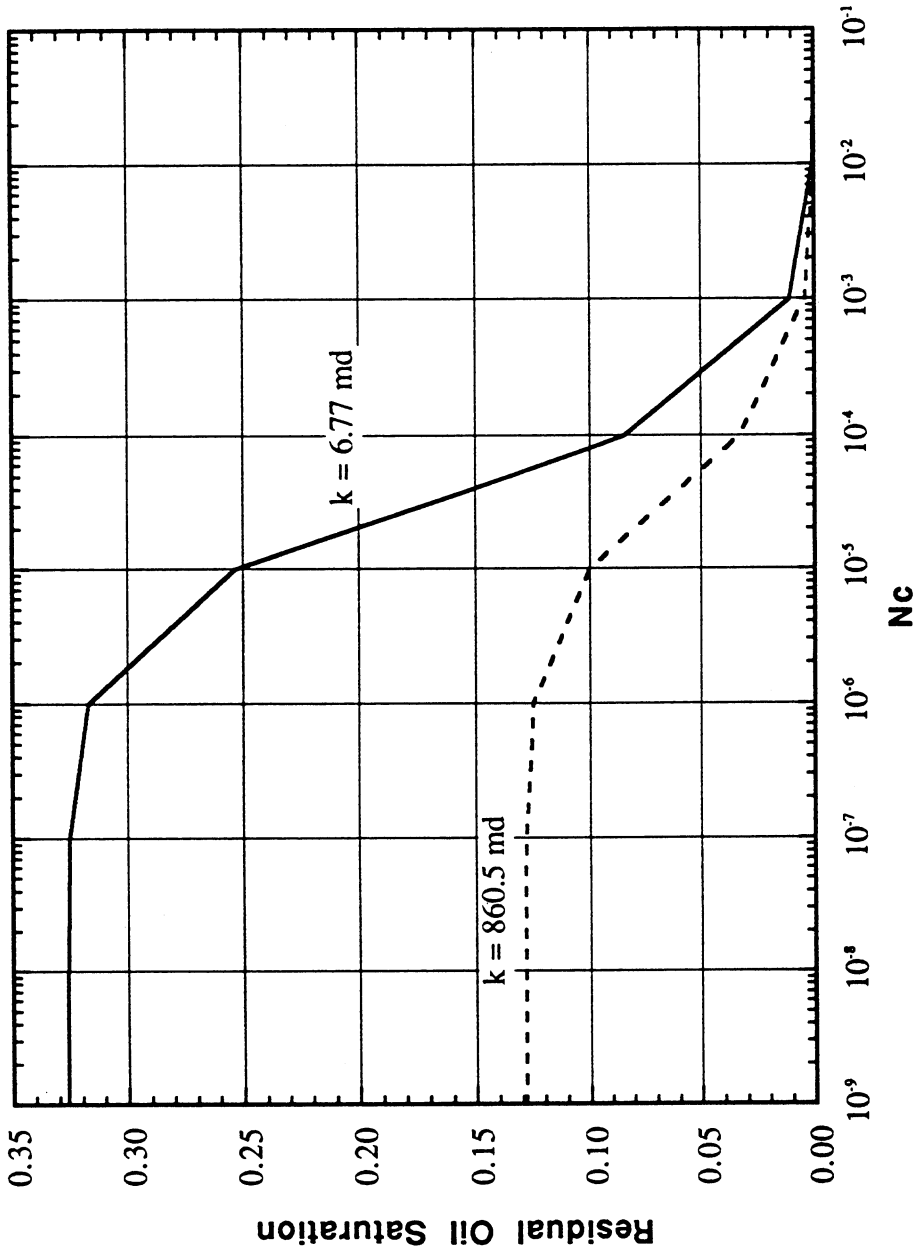


Figure 2.22. Capillary desaturation curve for permeability-dependent S_{orw} ($S_{orw} = \exp(-0.88222k^{0.125})$) for Reservoir II

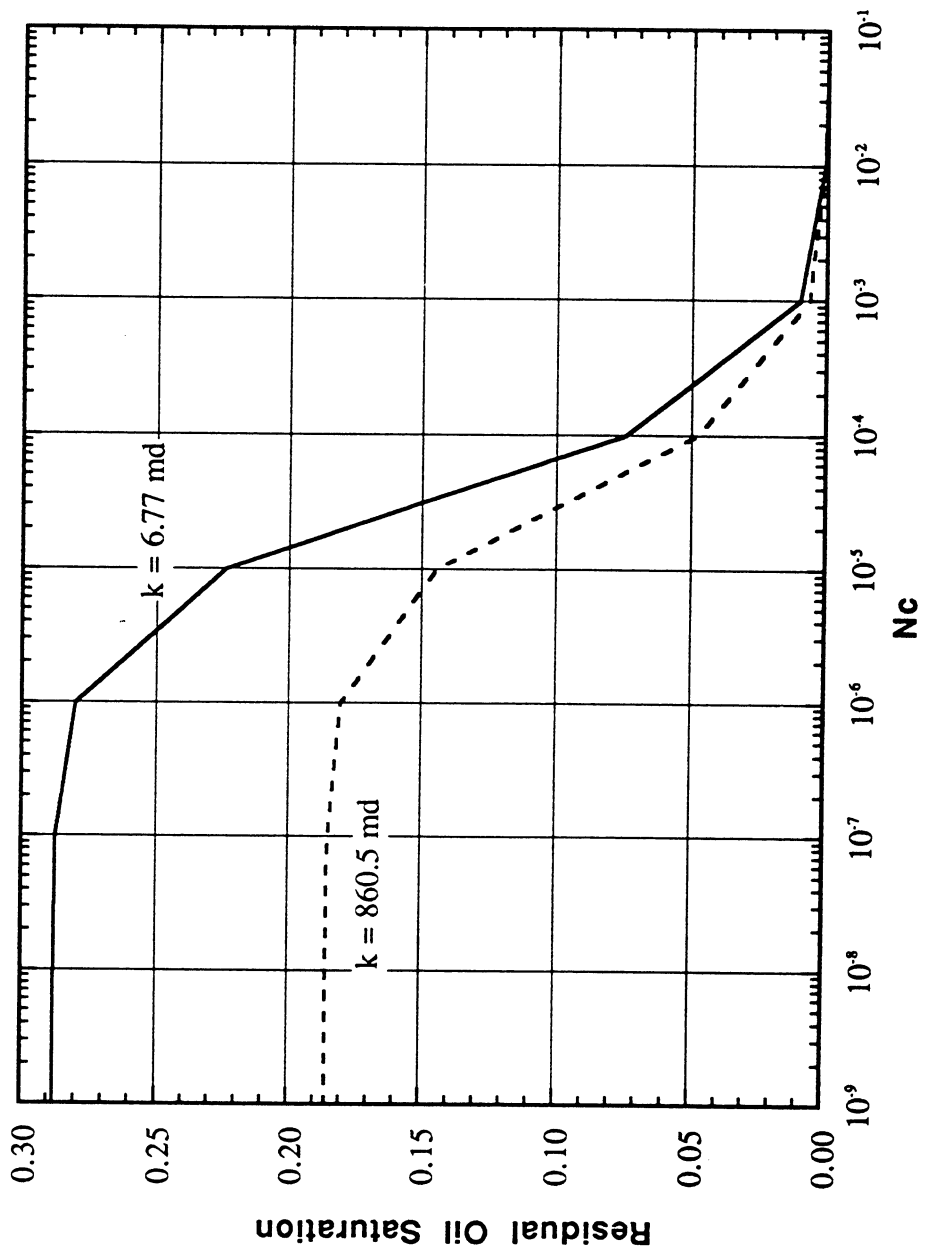


Figure 2.23. Capillary desaturation curve for permeability-dependent S_{orw} ($S_{orw} = \exp(-1.1048k^{0.0625})$) for Reservoir II

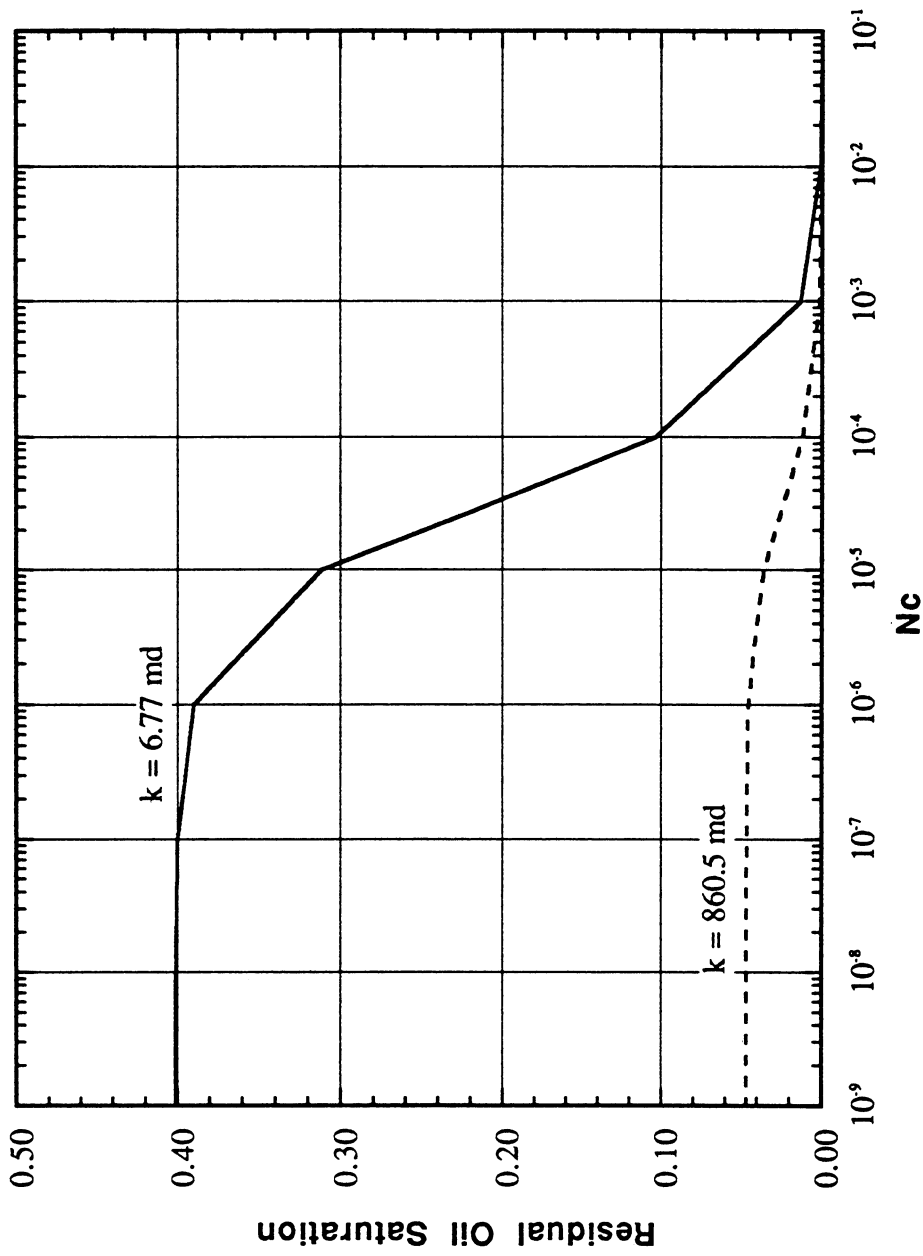


Figure 2.24. Capillary desaturation curve for permeability-dependent S_{orw} ($S_{orw} = \exp(-0.5665k^{0.25})$) for Reservoir II

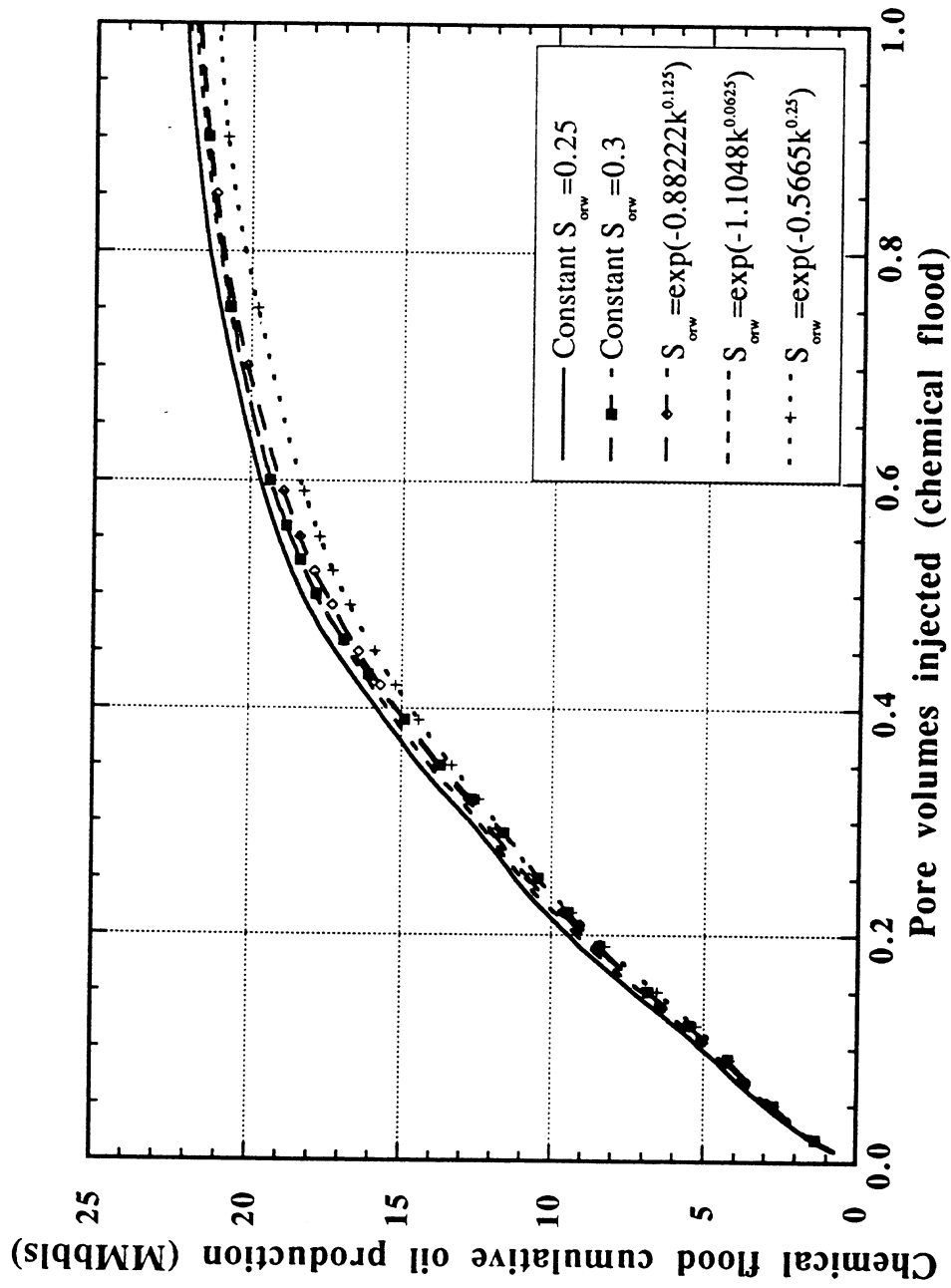


Figure 2.25. Effect of residual oil saturation on chemical flood oil recovery for Reservoir II

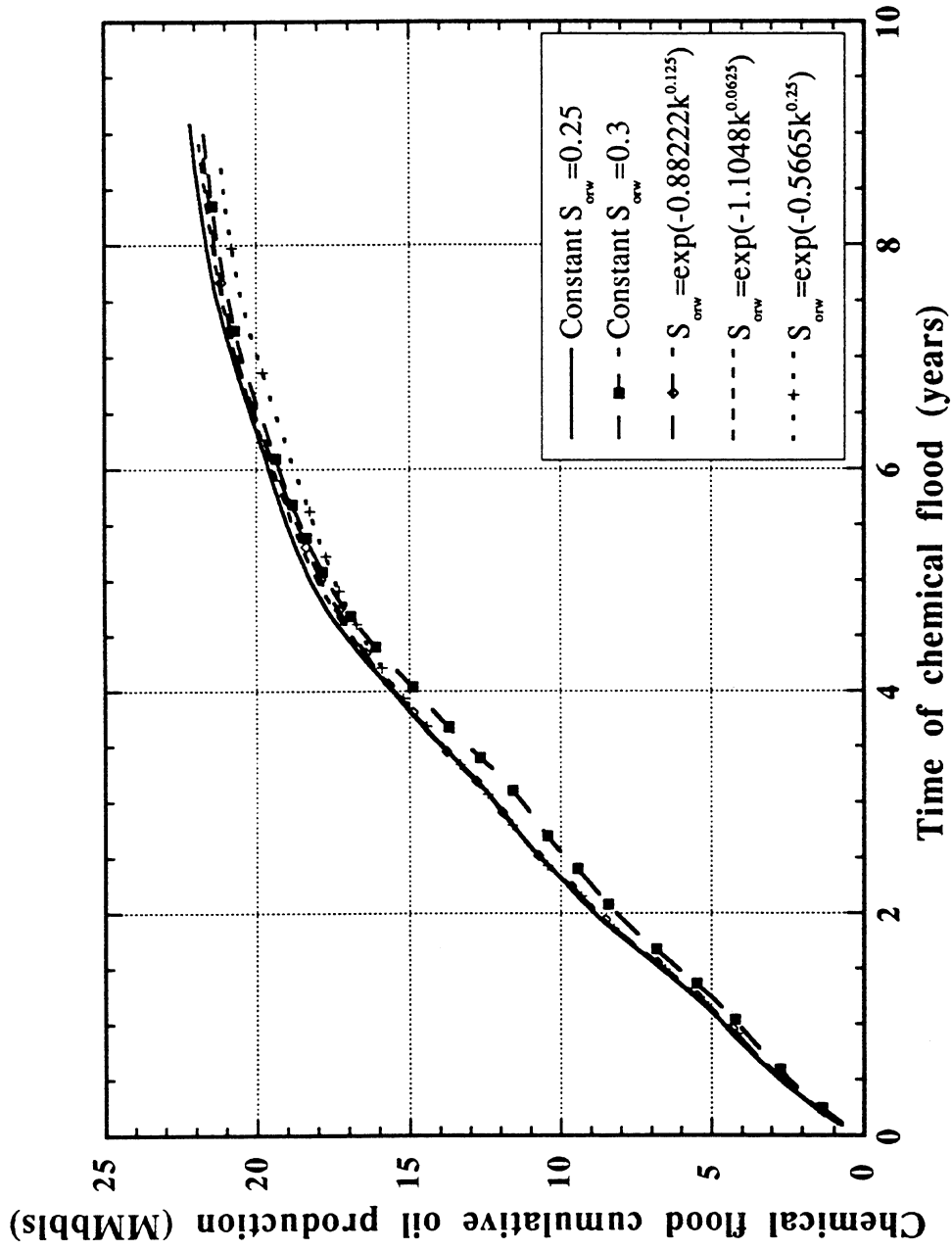


Figure 2.26. Effect of residual oil saturation on chemical flood oil recovery for Reservoir II

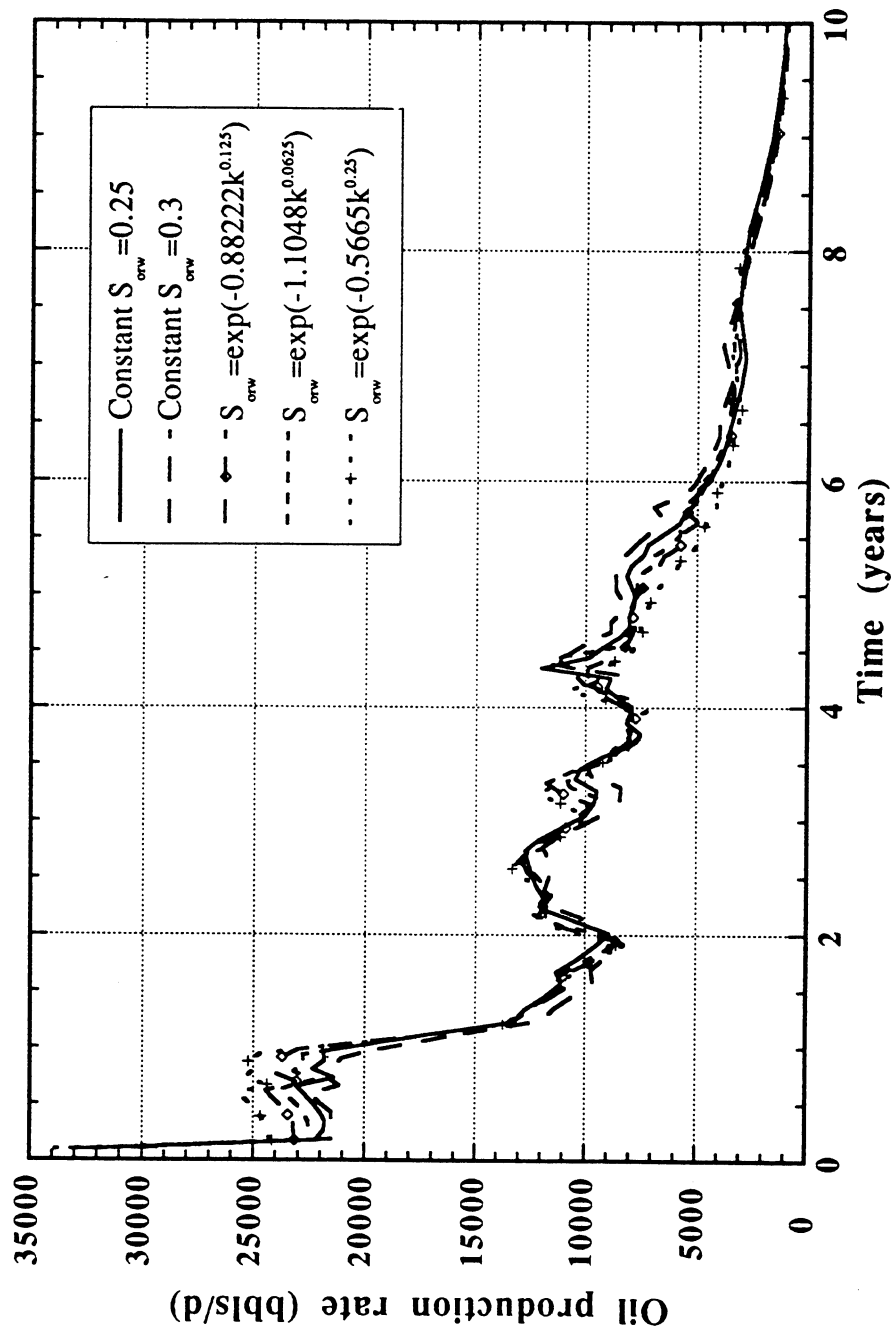


Figure 2.27. Effect of residual oil saturation on oil production rate for Reservoir II

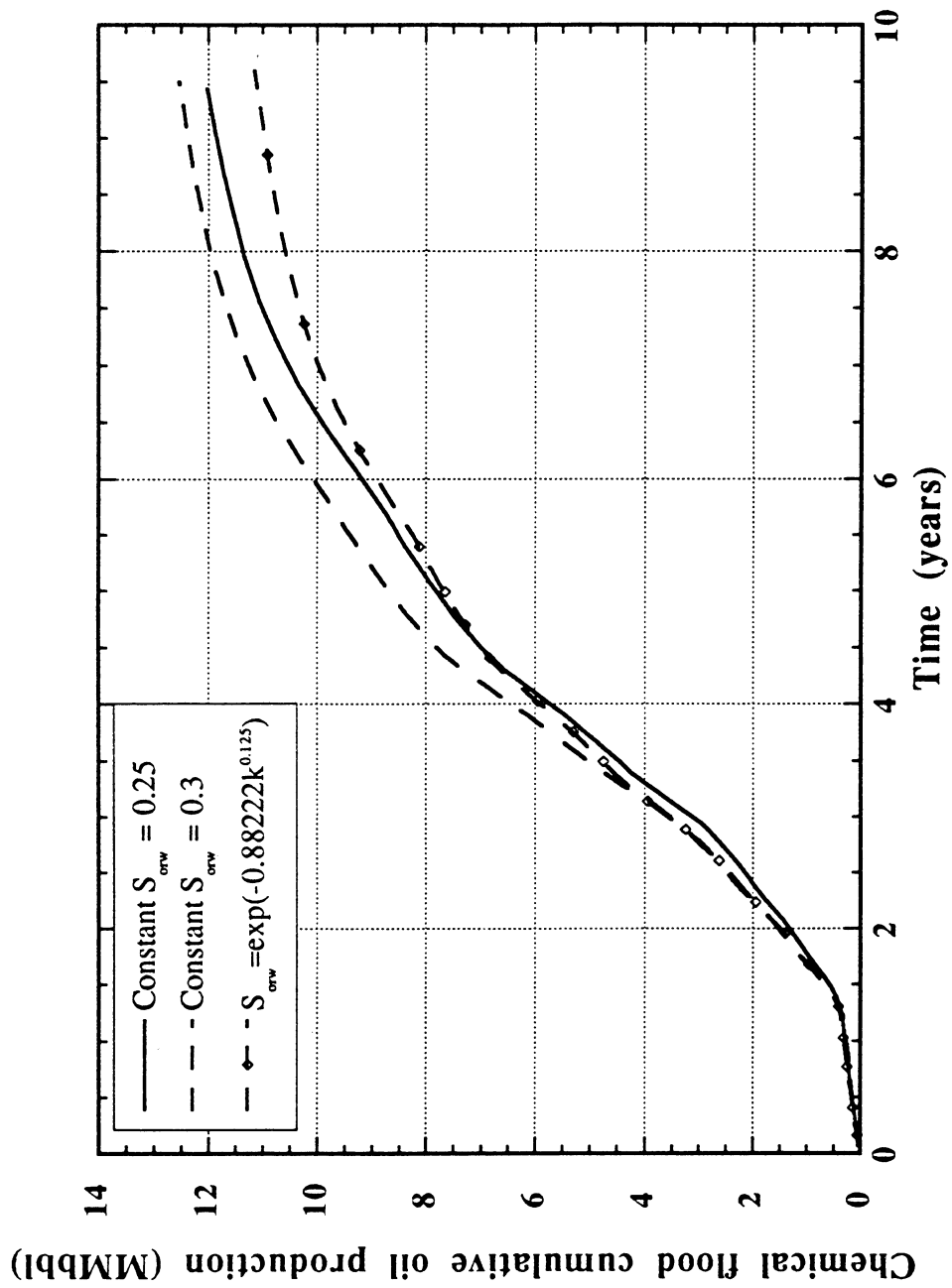


Figure 2.28. Effect of residual saturation on tertiary cumulative oil production for Reservoir II

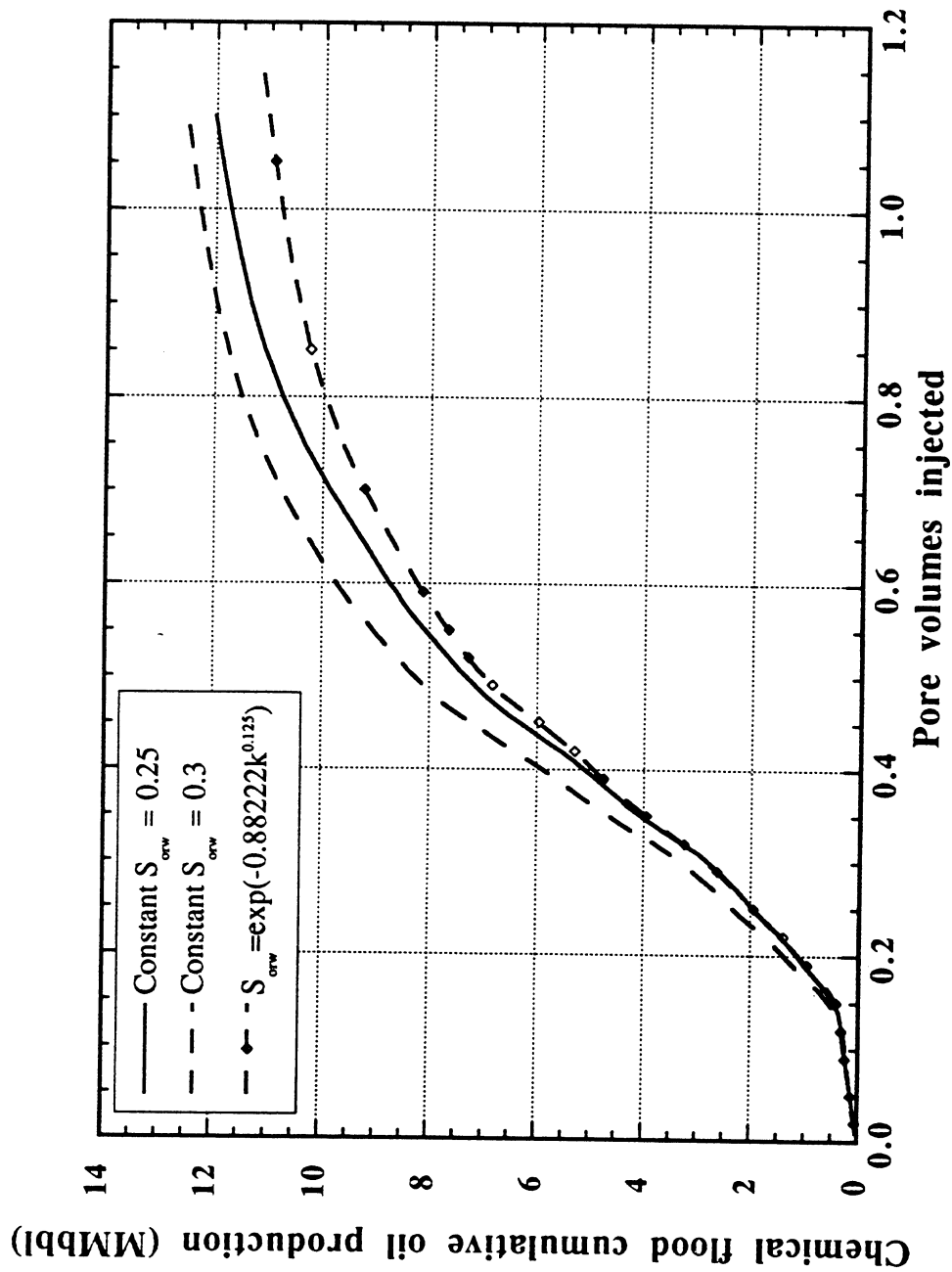


Figure 2.29. Effect of residual saturation on tertiary cumulative oil production for Reservoir II

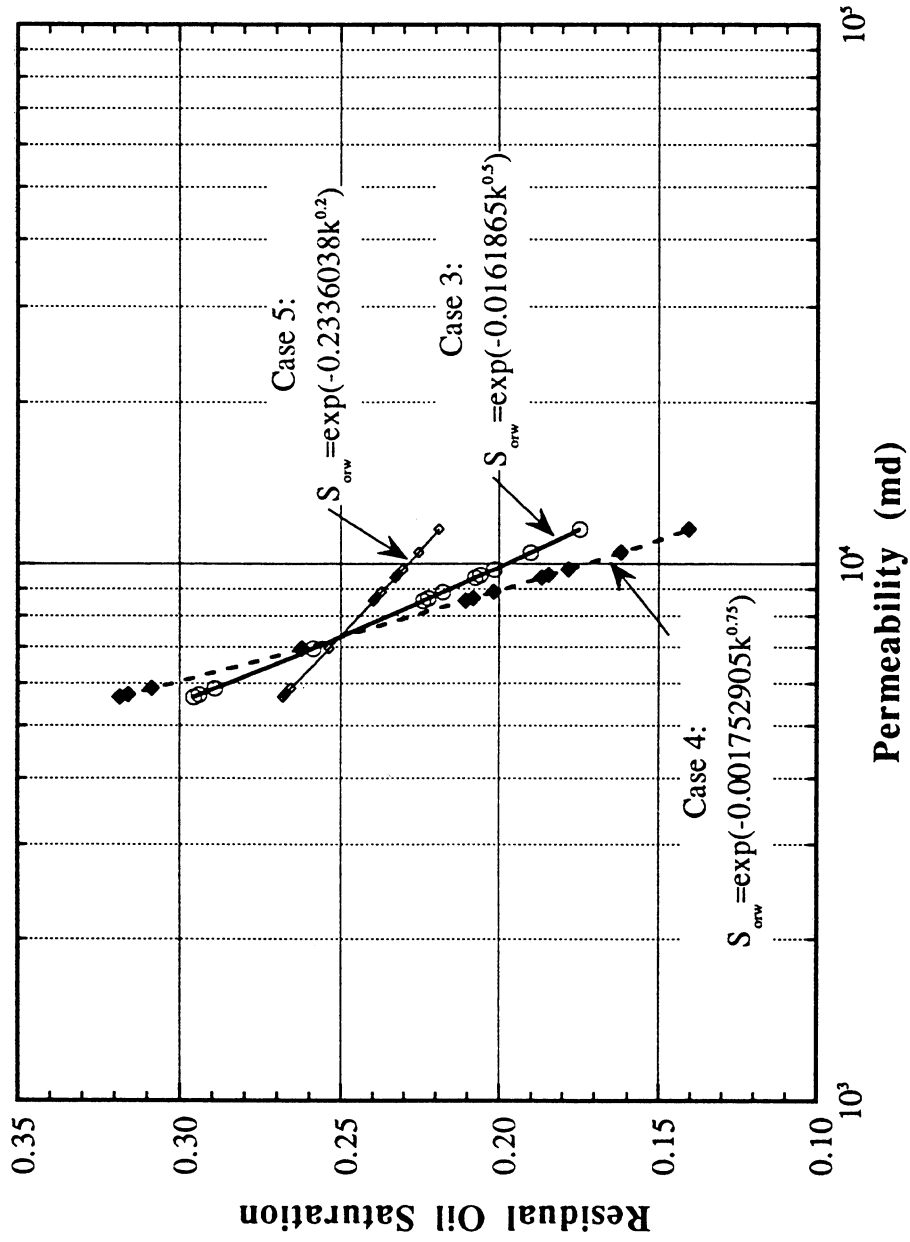


Figure 2.30. Plot of residual oil saturation (S_{orw}) as a function of permeability for Reservoir III

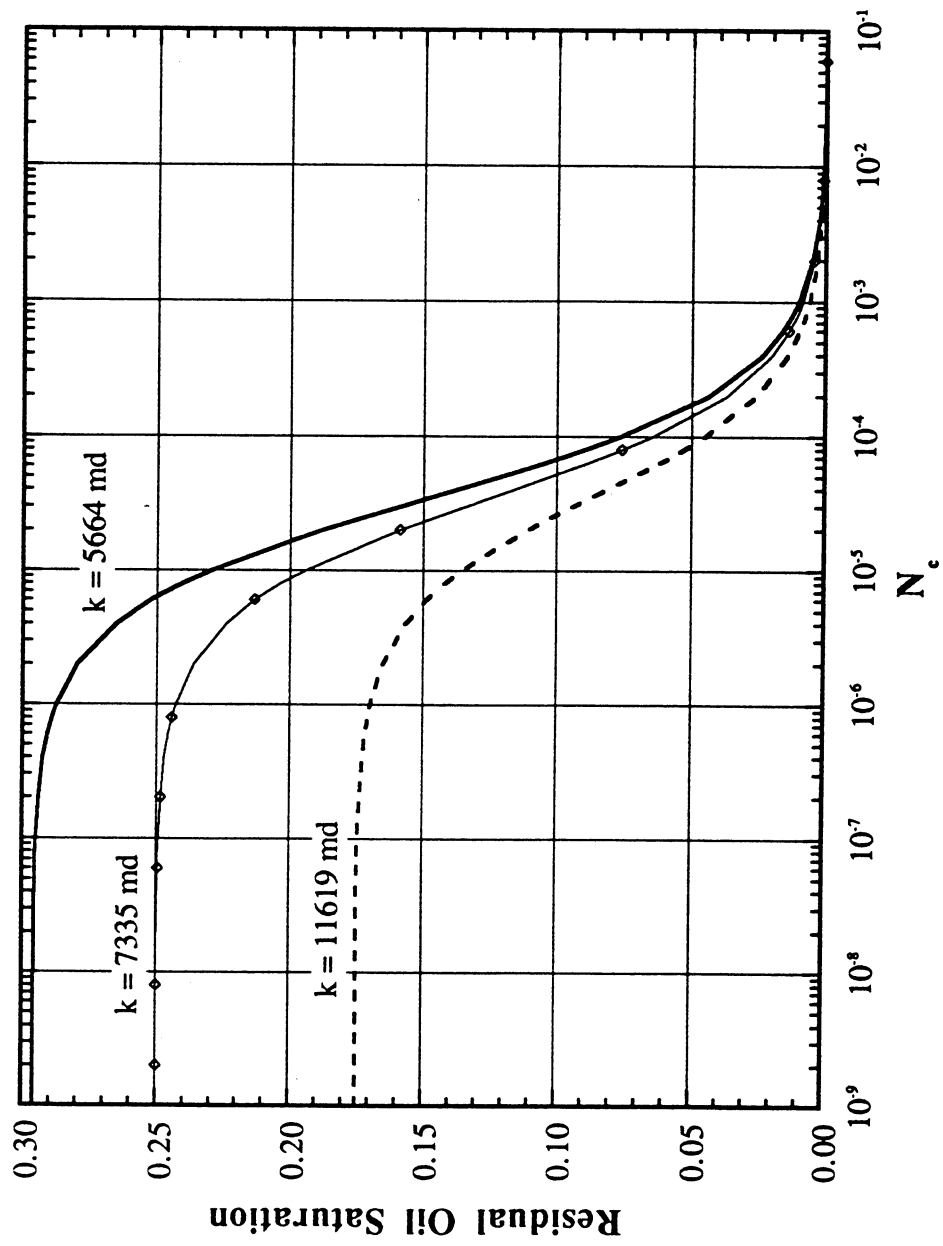


Figure 2.31. CDC for permeability-dependent S_{onw} (Case 3: $S_{onw} = \exp(-0.0161865k^{0.5})$) for Reservoir III

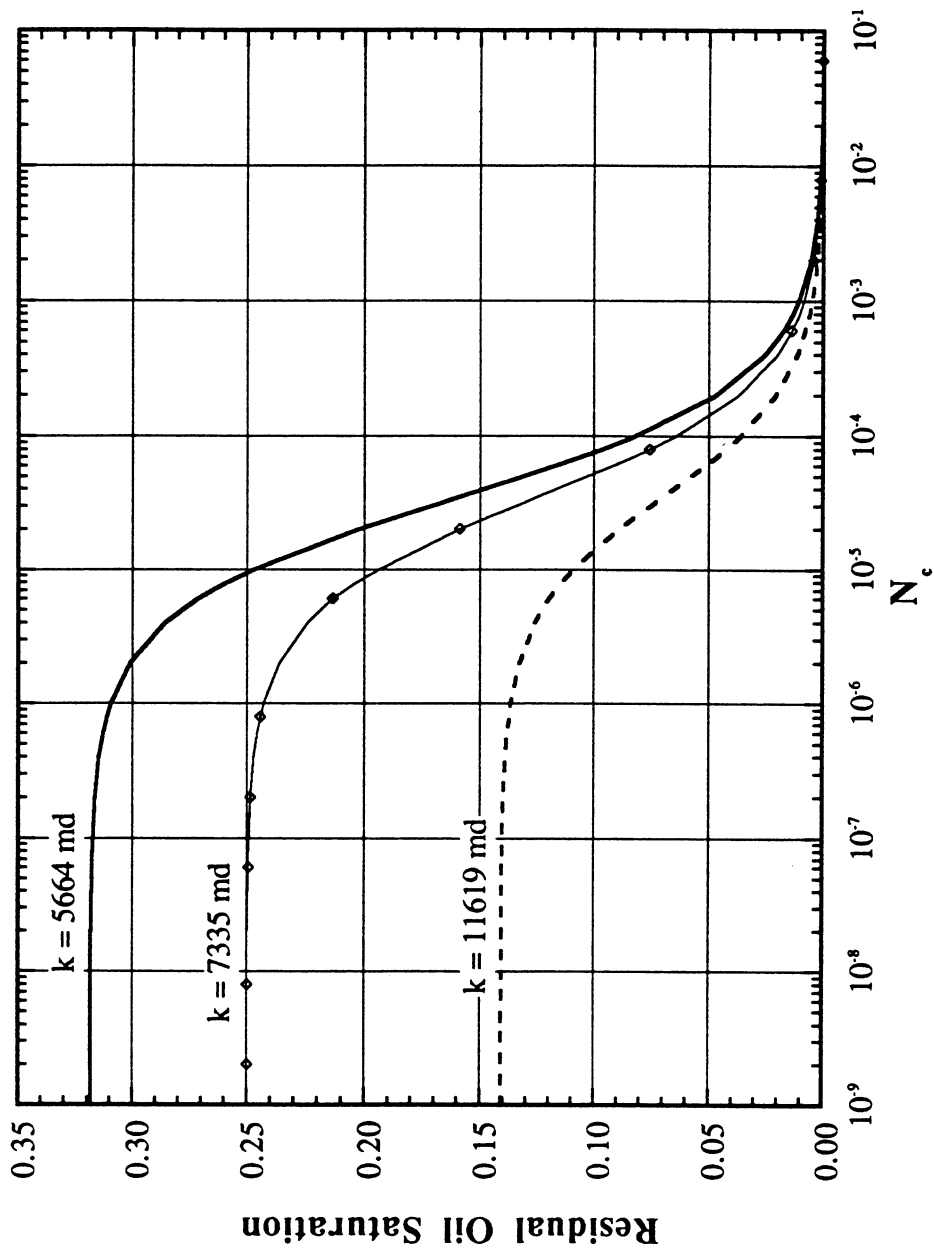


Figure 2.32. CDC for permeability-dependent S_{orw} (Case 4: $S_{orw} = \exp(-0.001752905k^{0.75})$) for Reservoir III

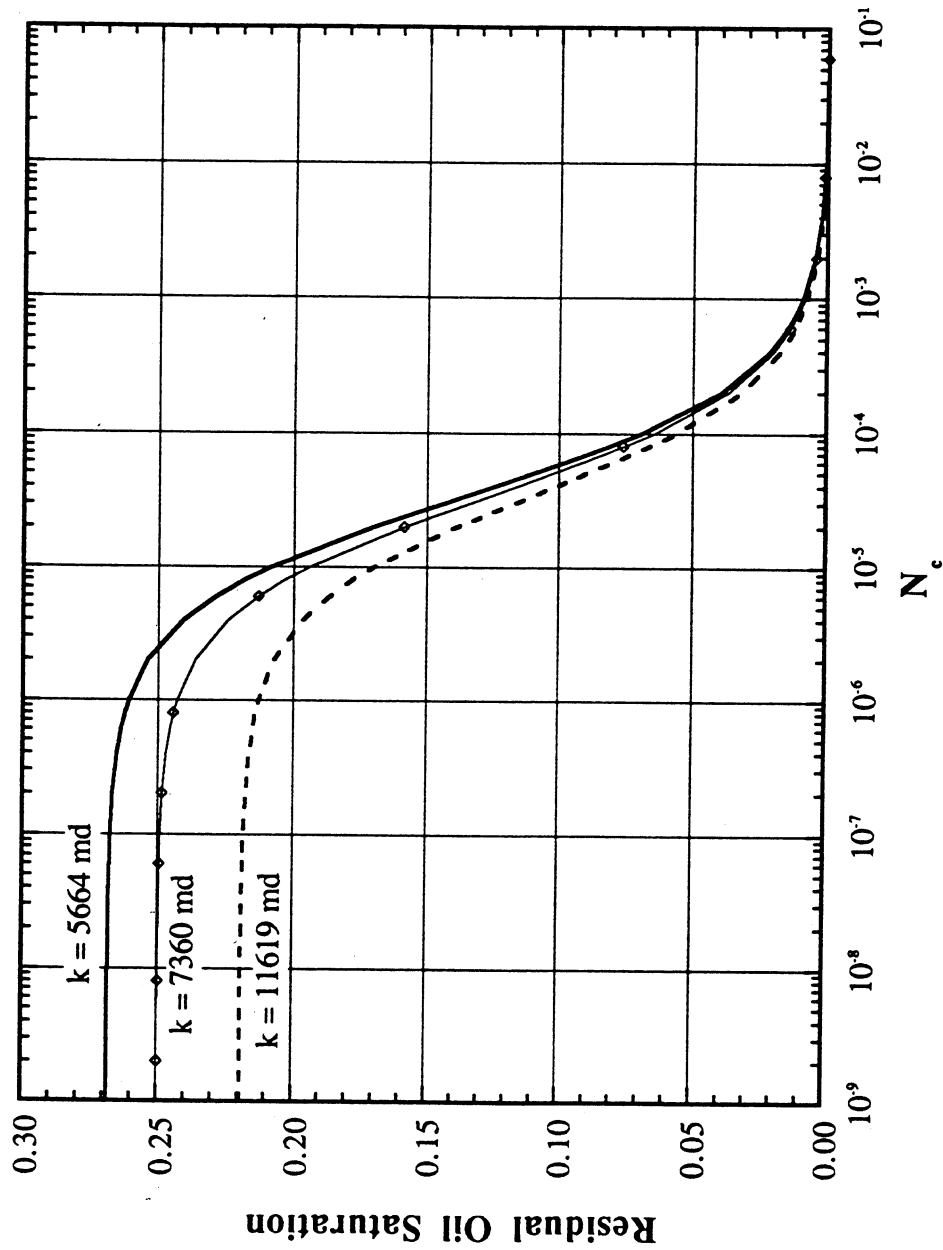


Figure 2.33. CDC for permeability-dependent S_{orw} (Case 5: $S_{orw} = \exp(-0.2336038k^{0.2})$) for Reservoir III

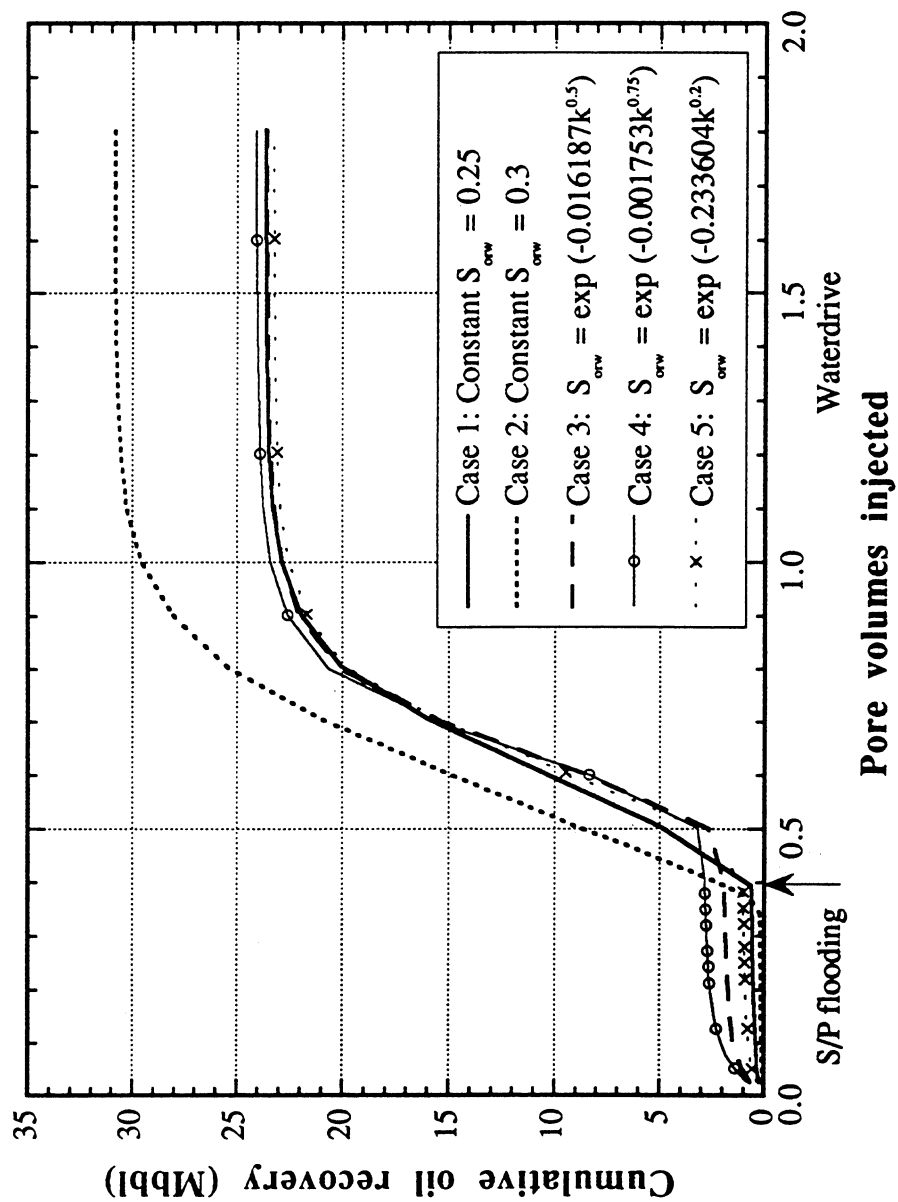


Figure 2.34. Effect of distributed S_{orw} on oil recovery for Reservoir III

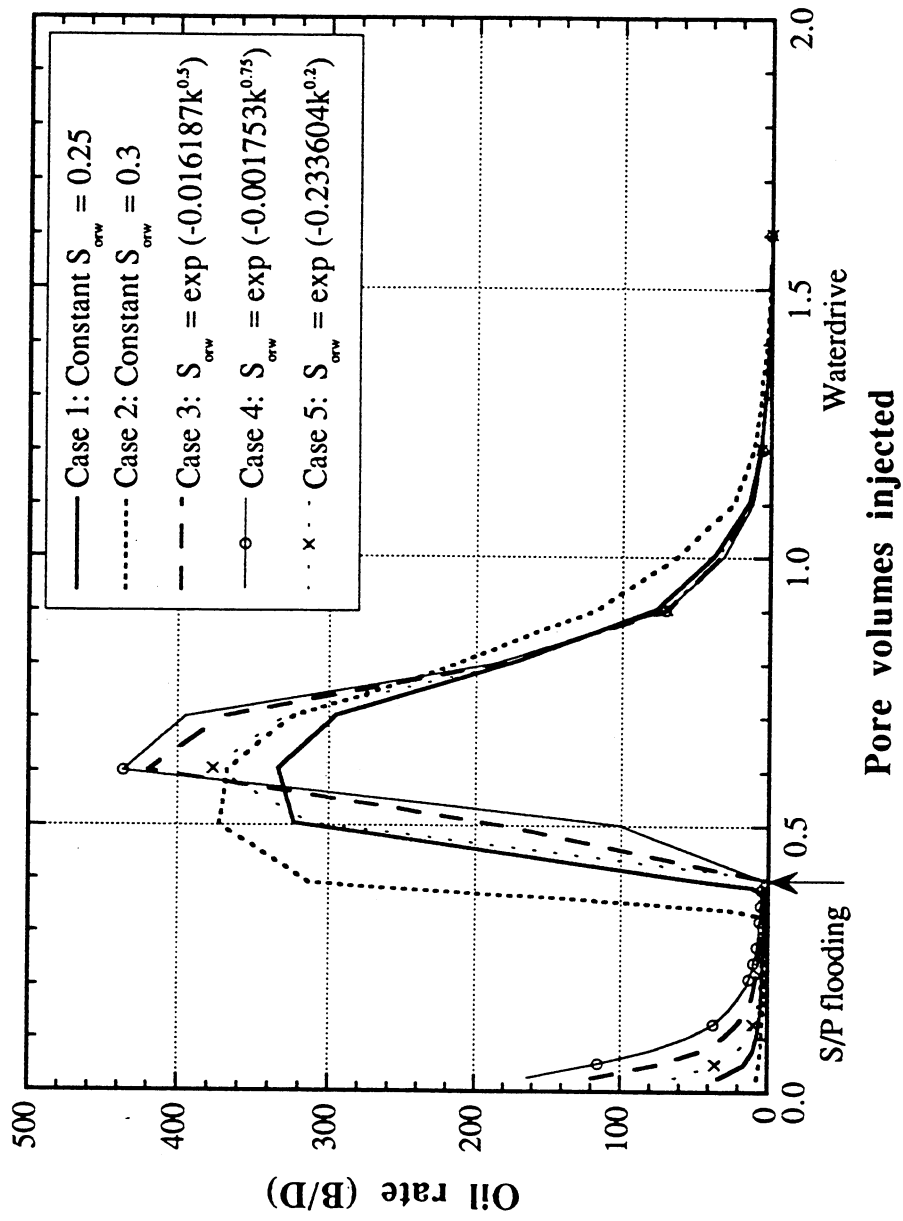


Figure 2.35. Effect of distributed S_{orw} on oil rate for Reservoir III

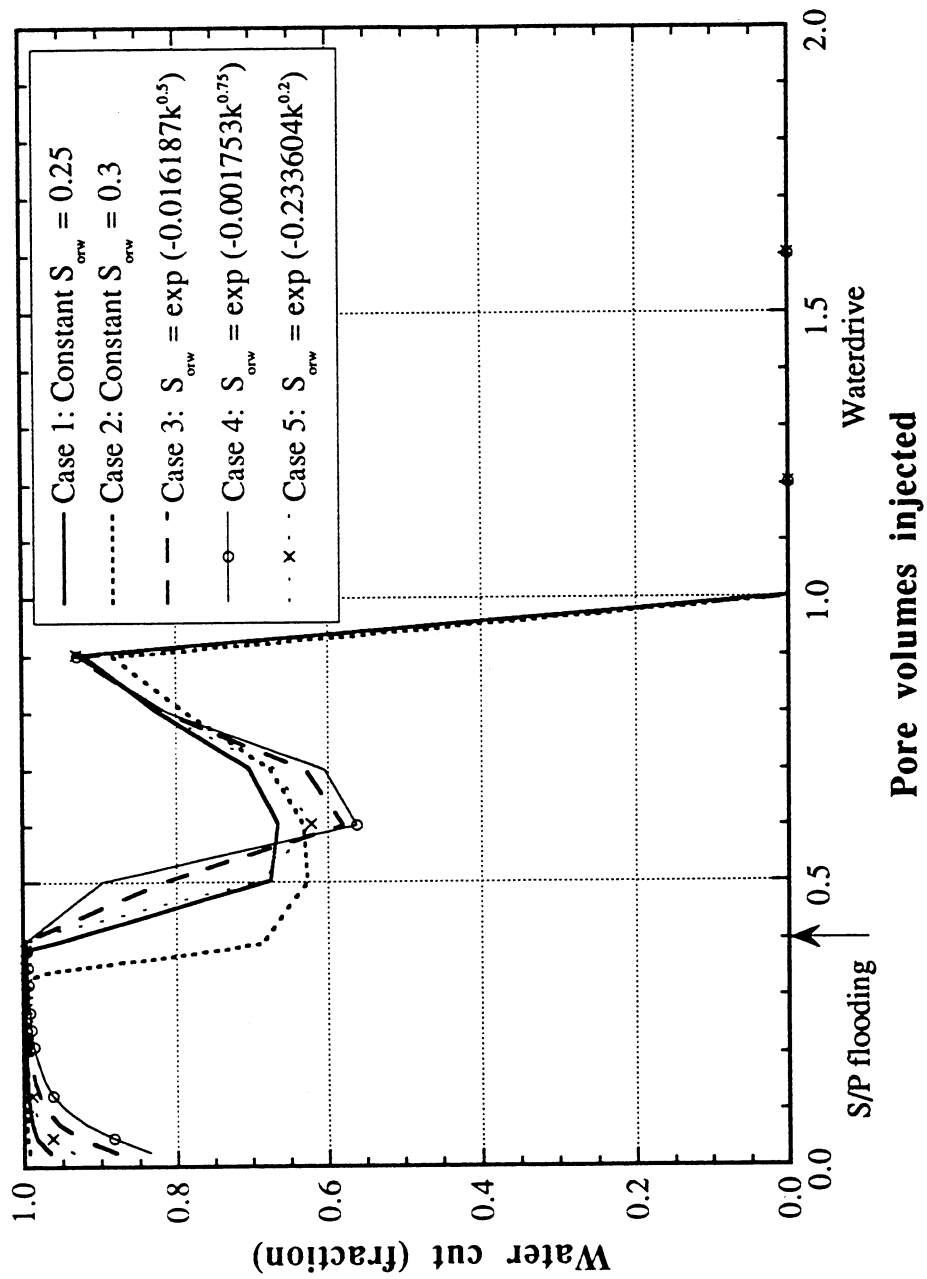


Figure 2.36. Effect of distributed S_{orw} on water cut for Reservoir III

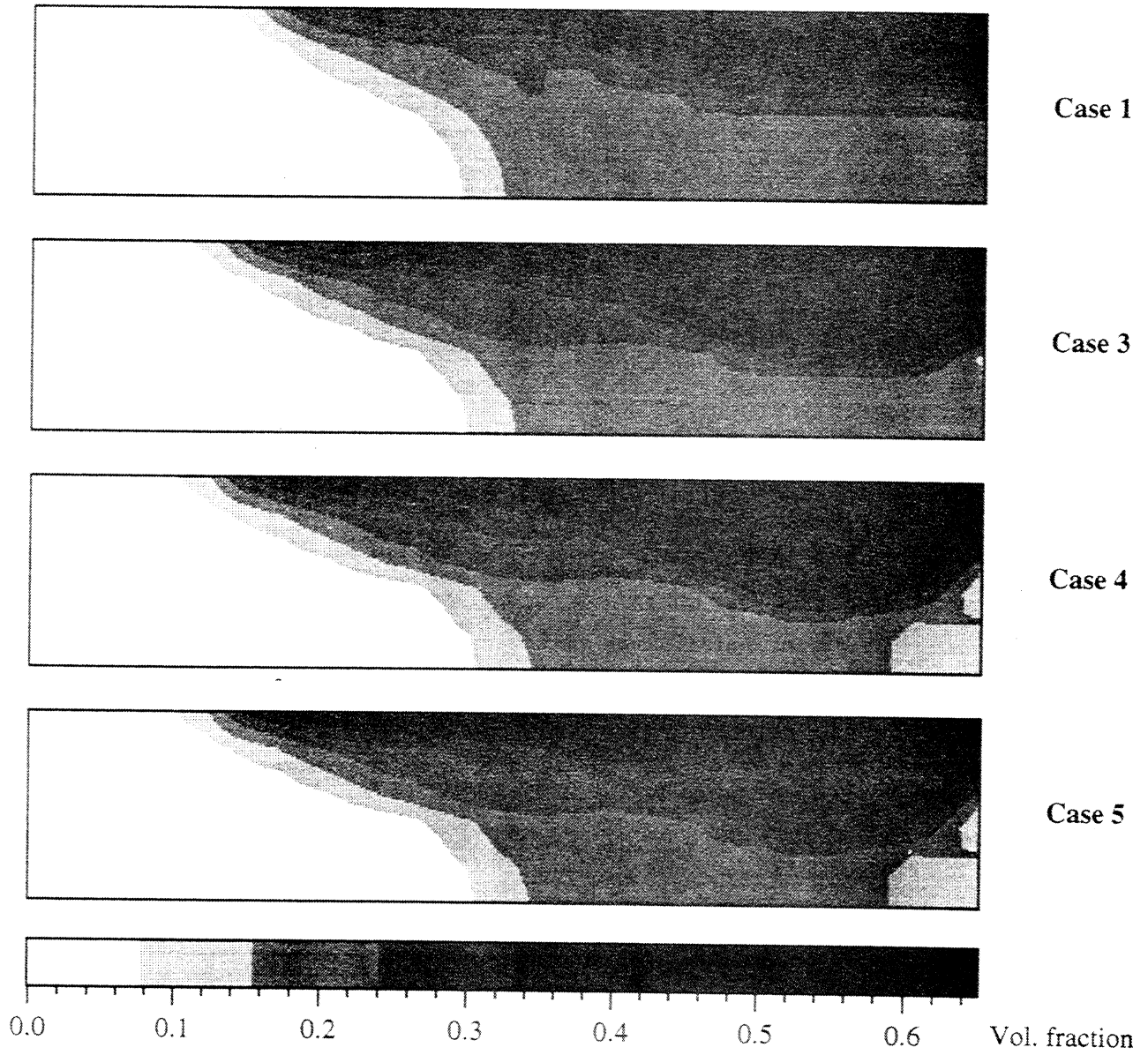


Figure 2.37. Oil concentration distribution at 0.5 PV injected (84 days) for Reservoir III

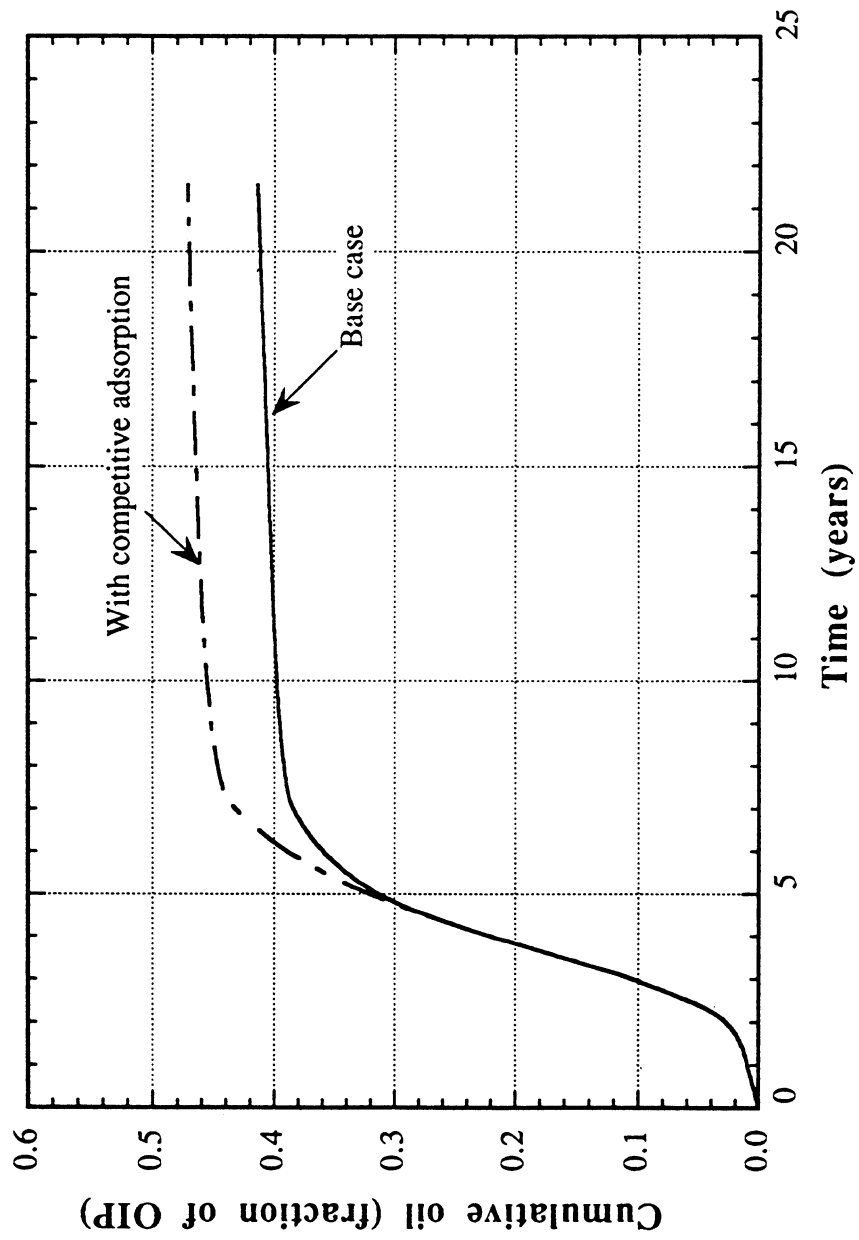


Figure 2.39. Effect of competitive adsorption on oil recovery for Reservoir I

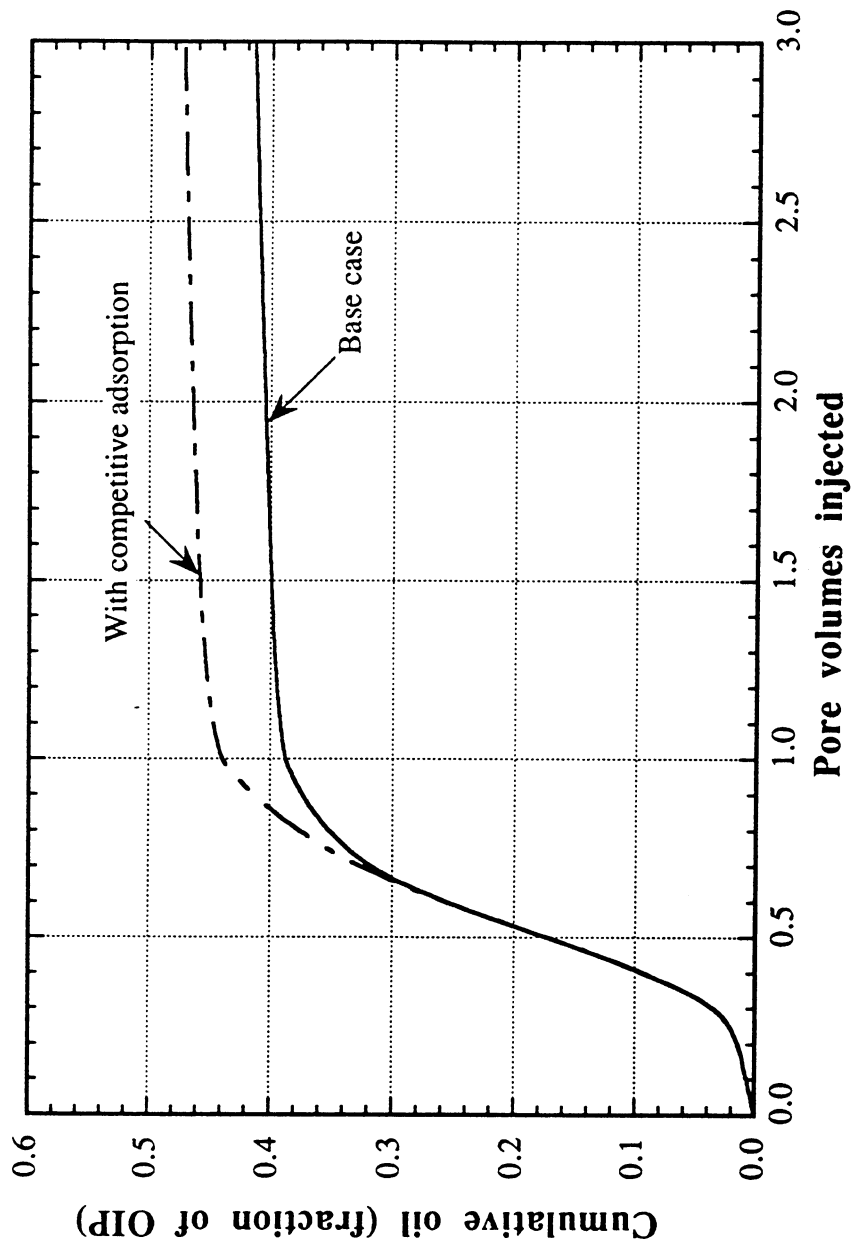


Figure 2.40. Effect of competitive adsorption on oil recovery for Reservoir I

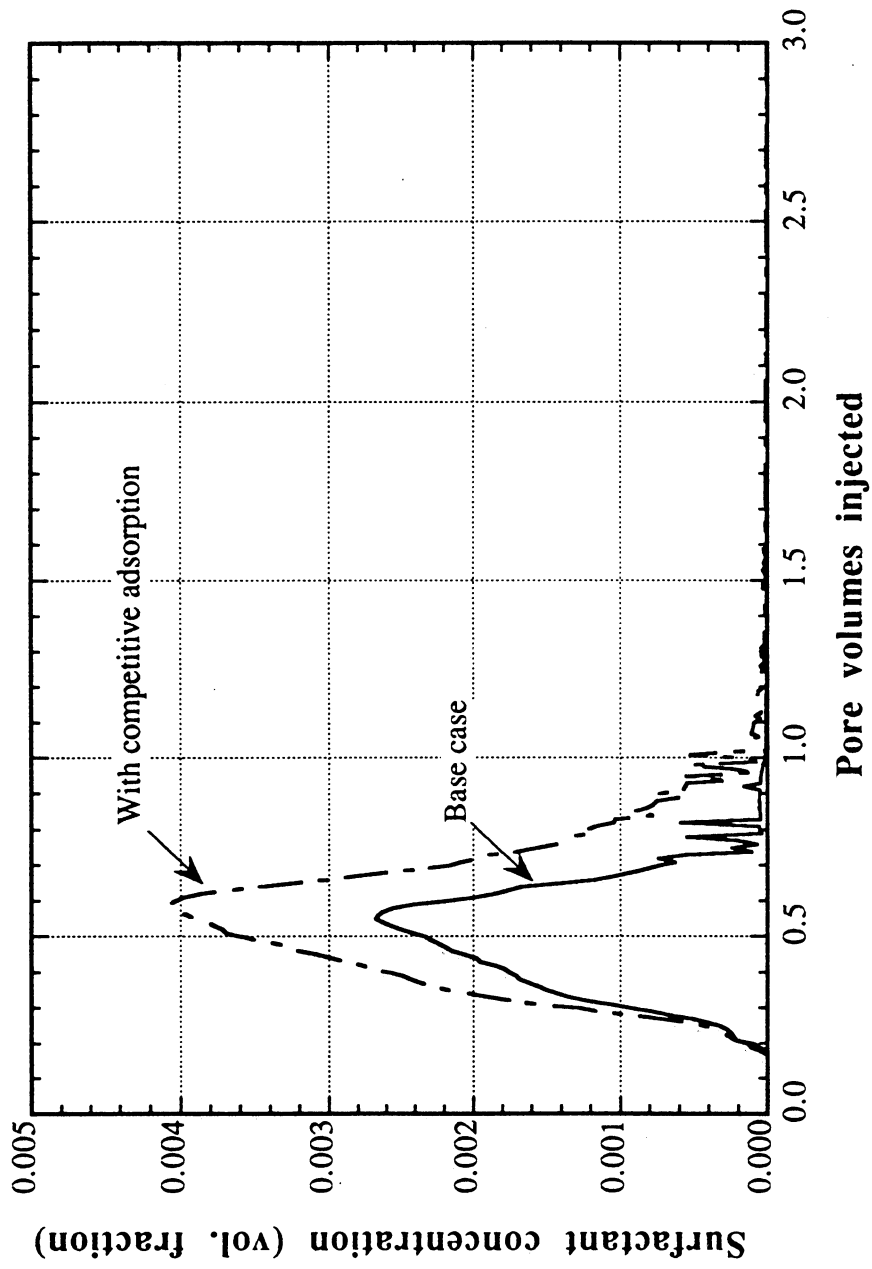


Figure 2.41. History of effluent surfactant concentration for Reservoir I

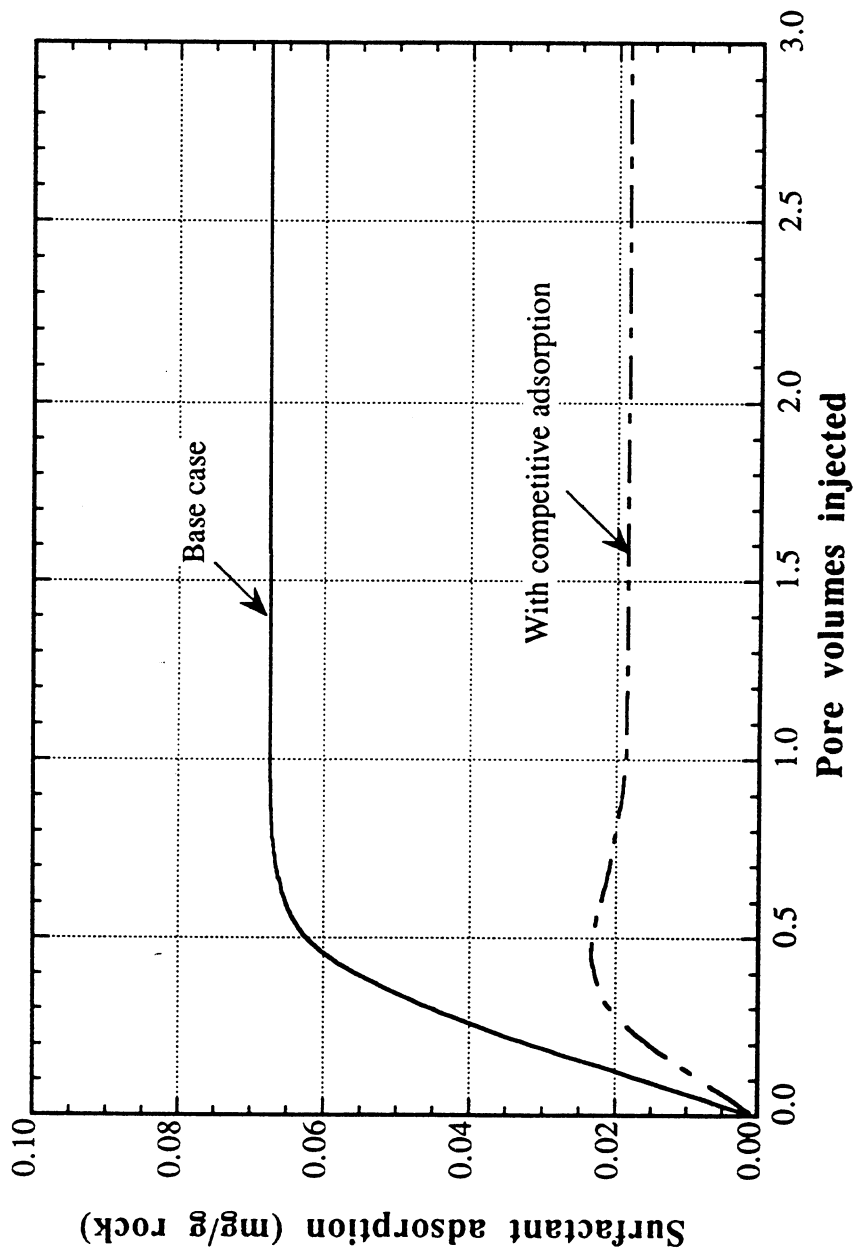


Figure 2.42. Surfactant adsorption with and without competition from polymer for Reservoir I

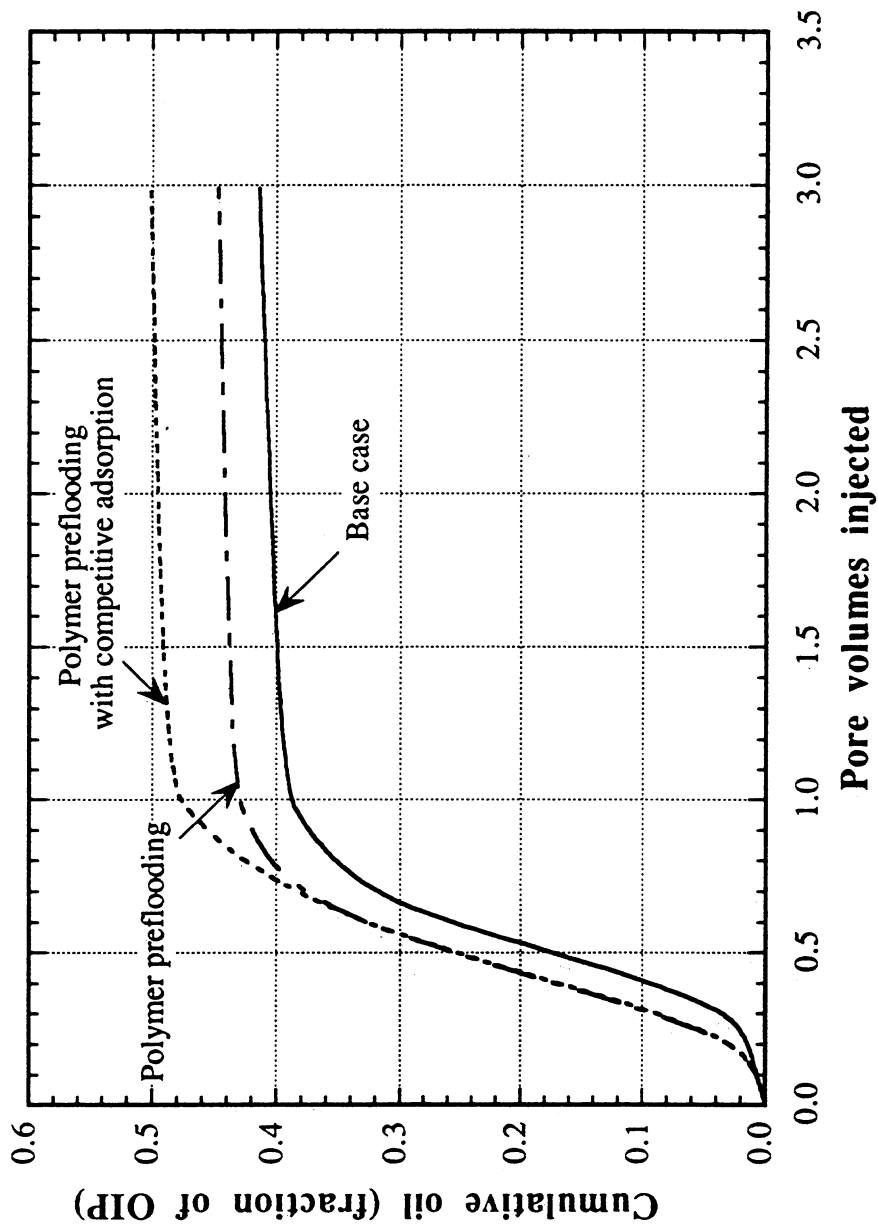


Figure 2.43. Effect of polymer preflooding on oil recovery for Reservoir I

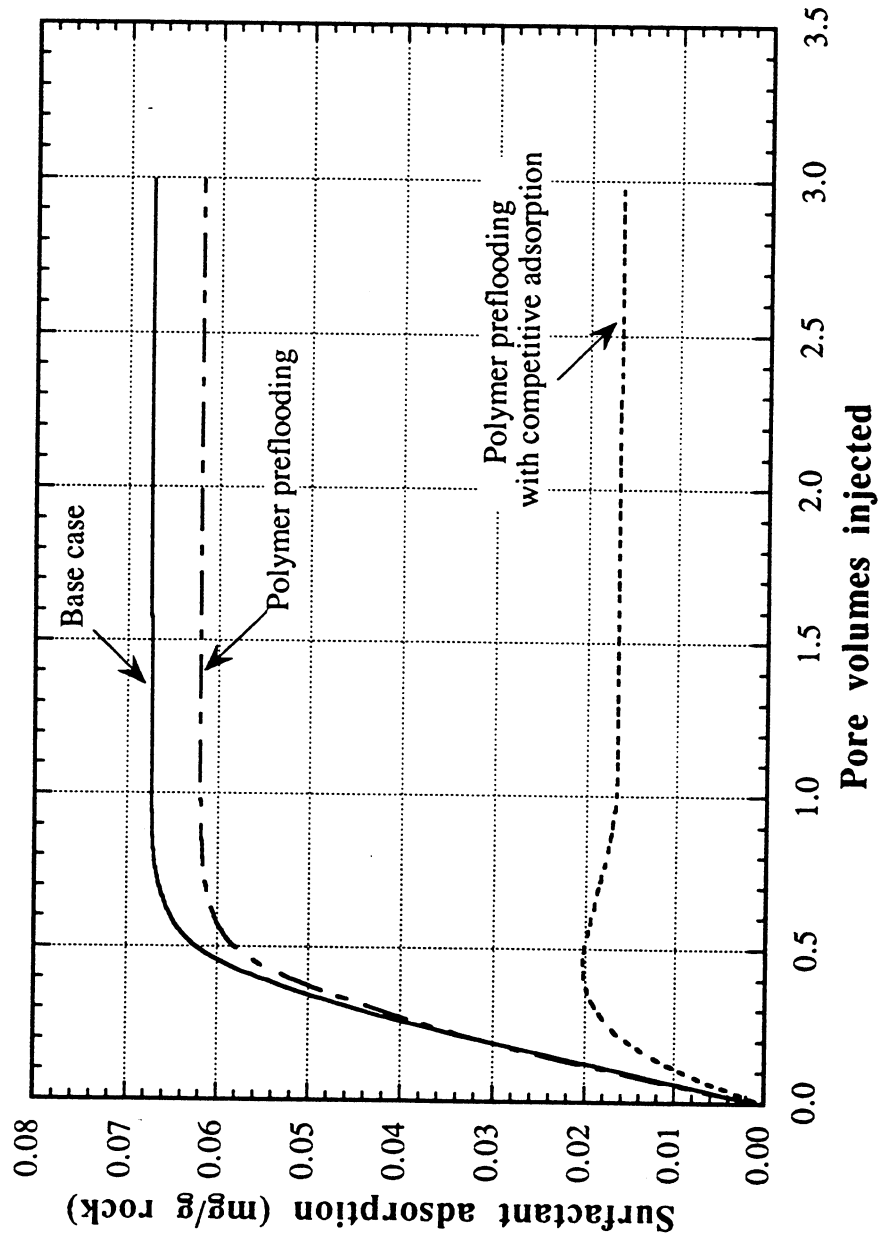


Figure 2.44. Effect of polymer preflooding on surfactant adsorption for Reservoir I

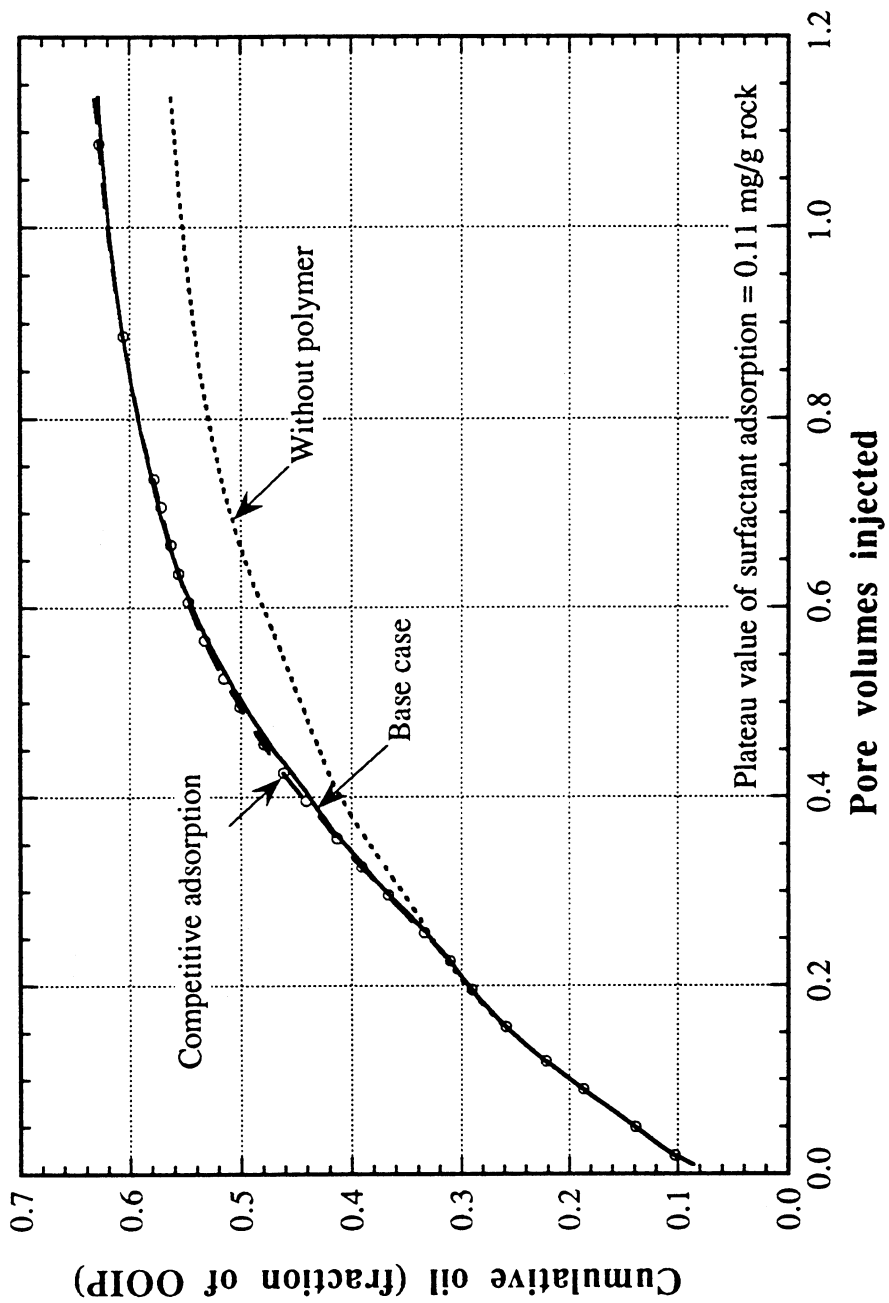


Figure 2.45. Effect of competitive adsorption on oil recovery for Reservoir II

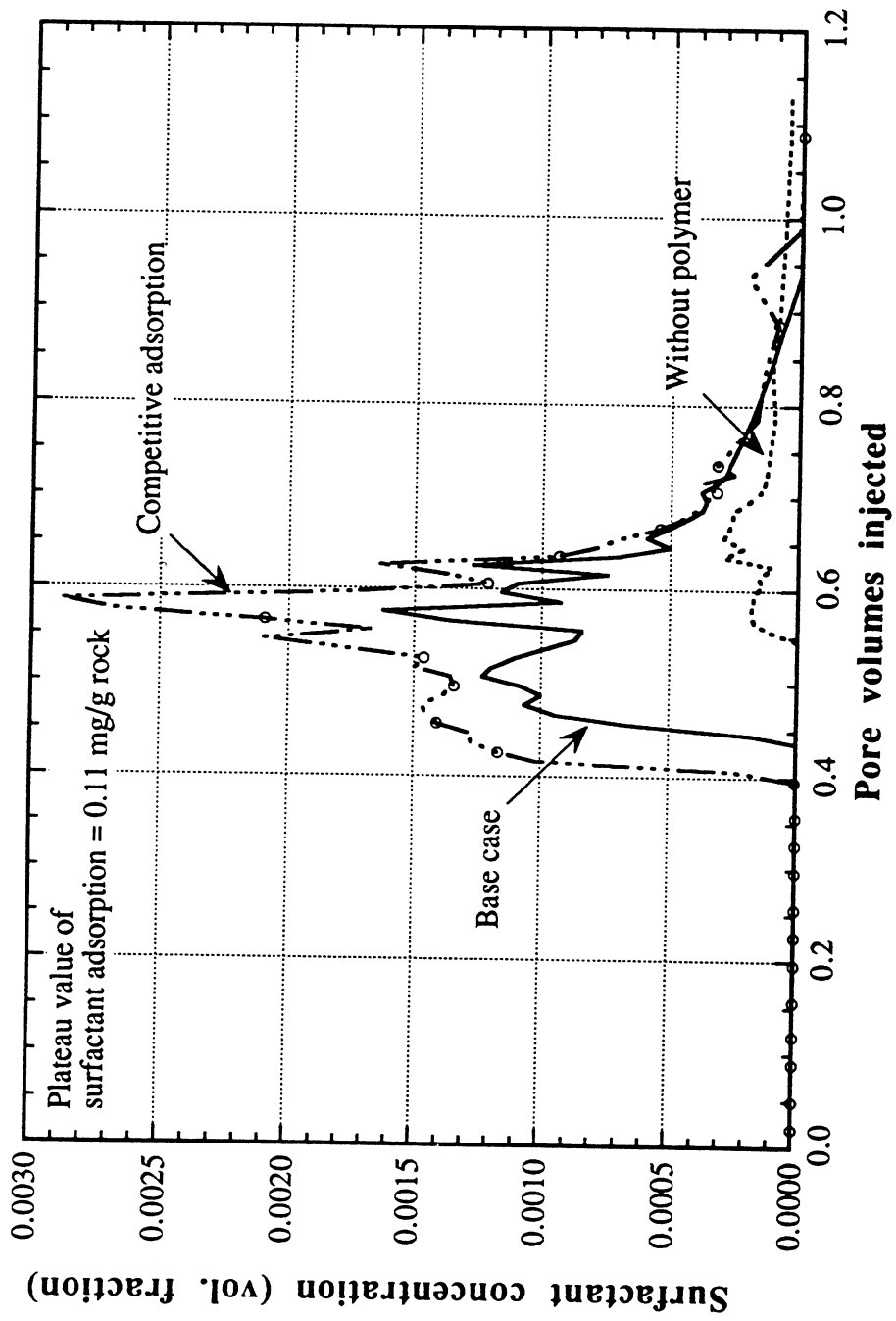


Figure 2.46. Effect of competitive adsorption on effluent surfactant concentration for Reservoir II

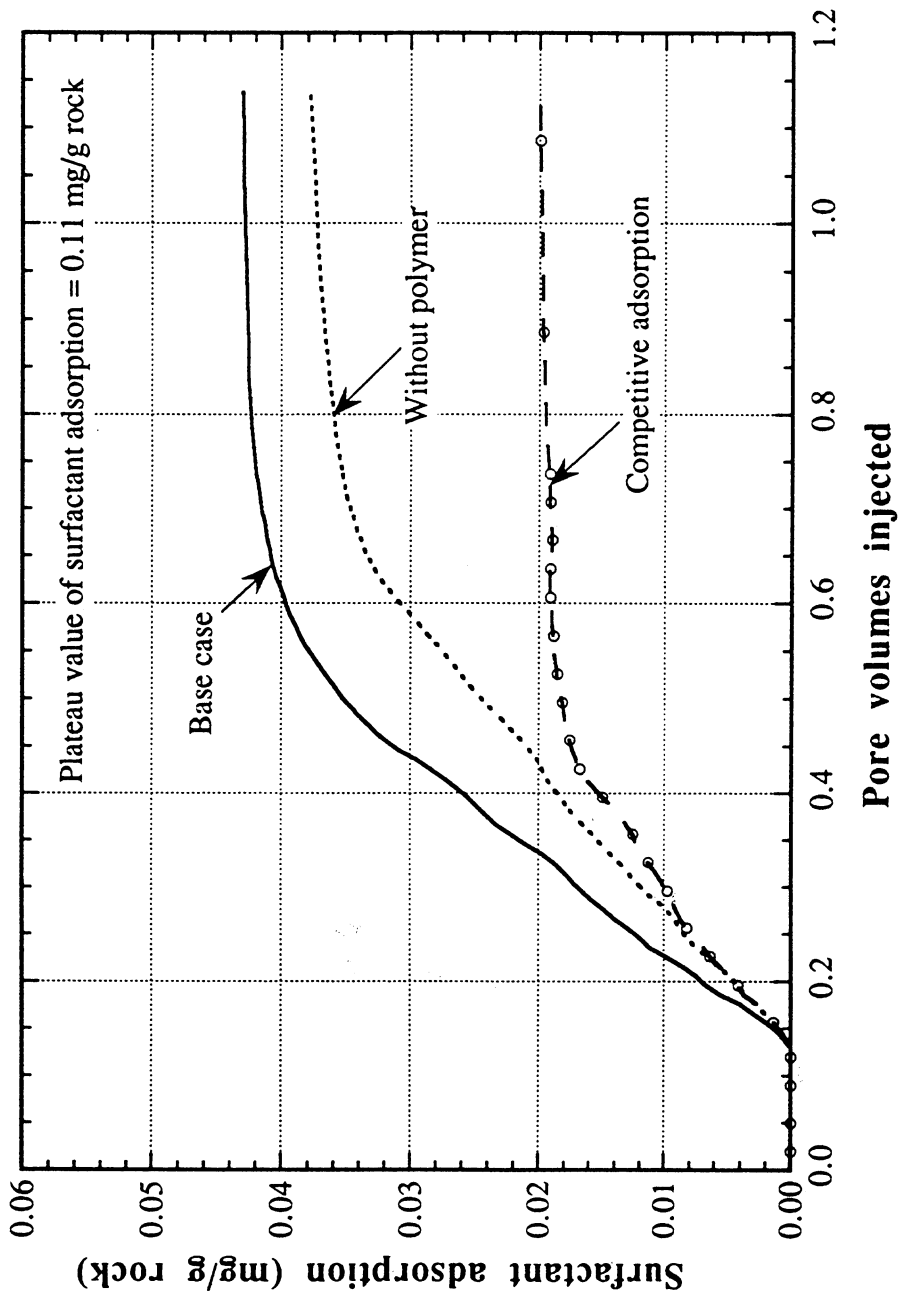


Figure 2.47. Effect of competitive adsorption on surfactant adsorption for Reservoir II

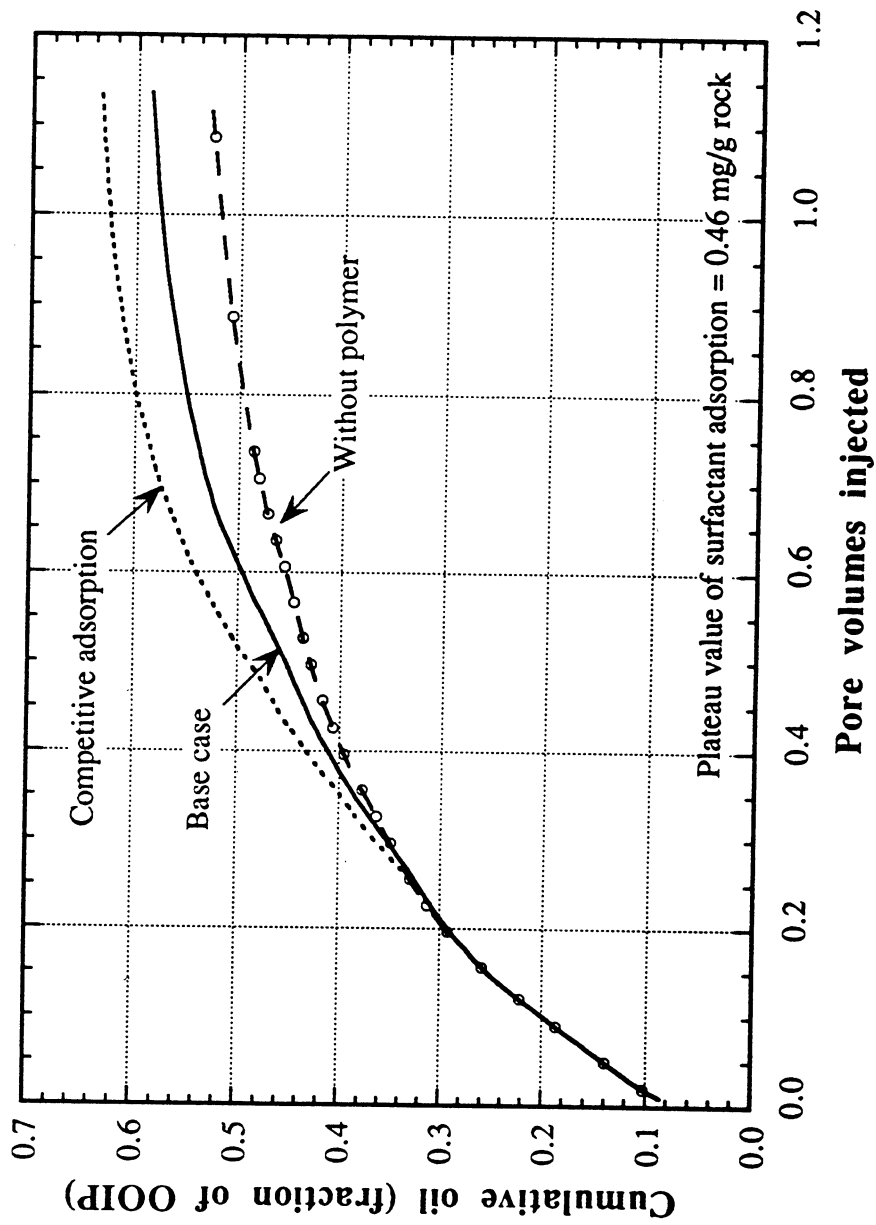


Figure 2.48. Effect of competitive adsorption on oil recovery for Reservoir II

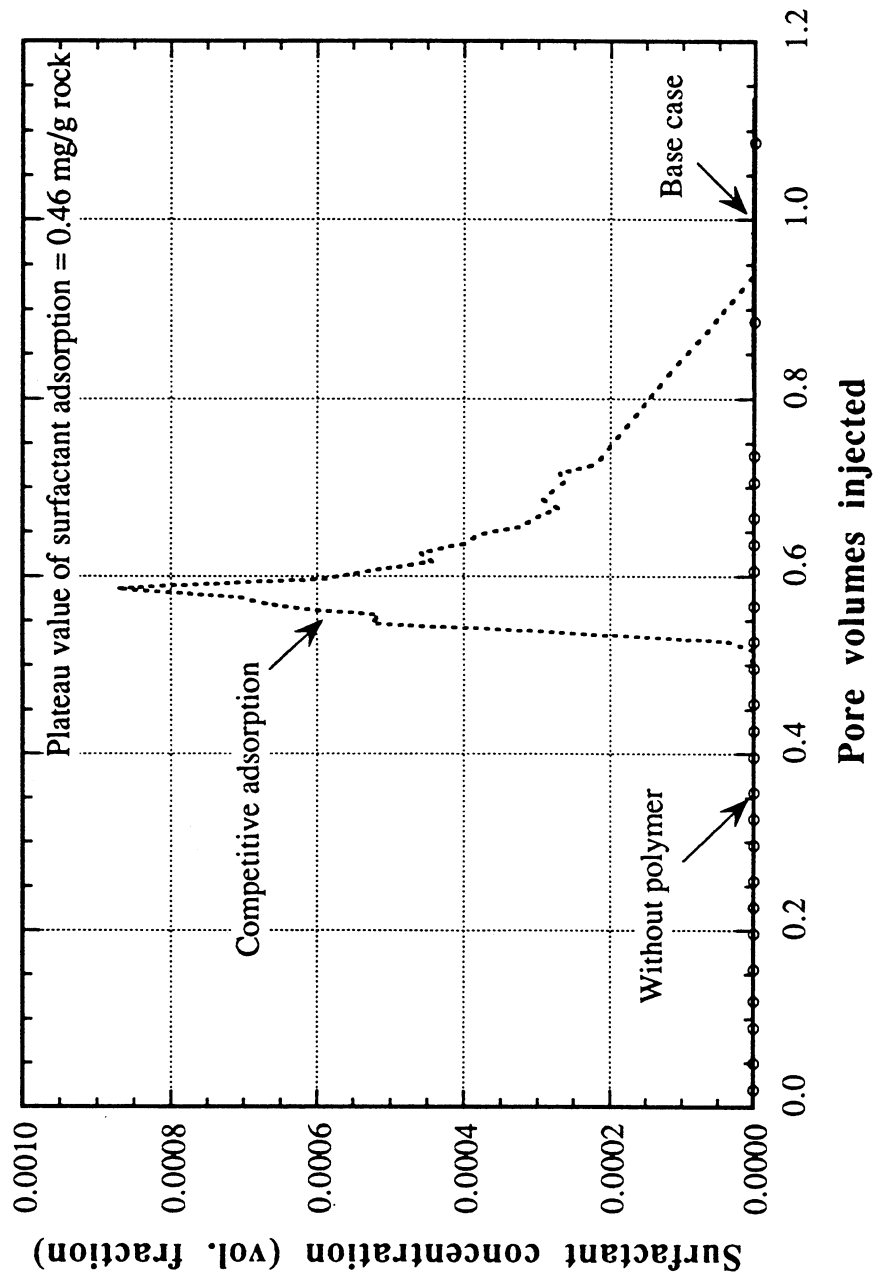


Figure 2.49. Effect of competitive adsorption on effluent surfactant concentration for Reservoir II

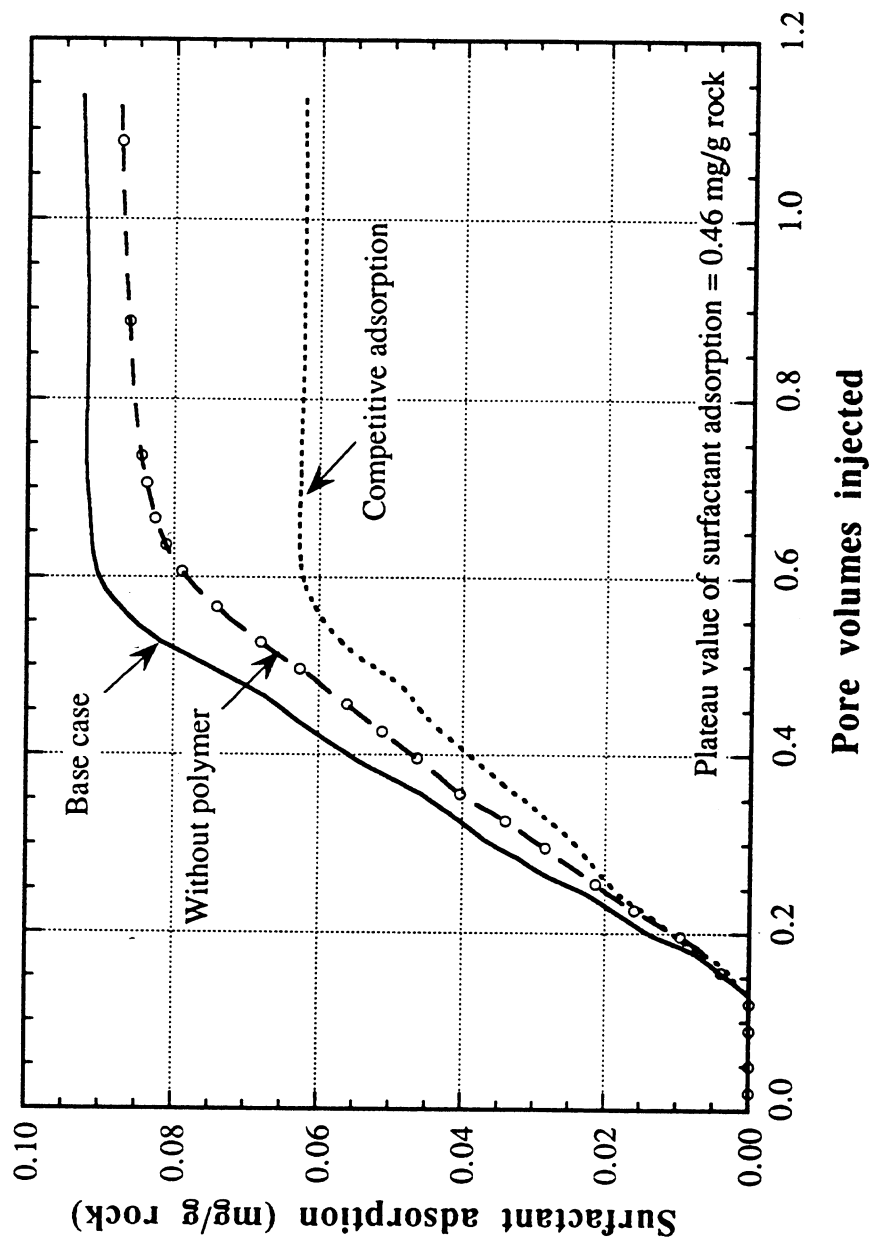


Figure 2.50. Effect of competitive adsorption on surfactant adsorption for Reservoir II

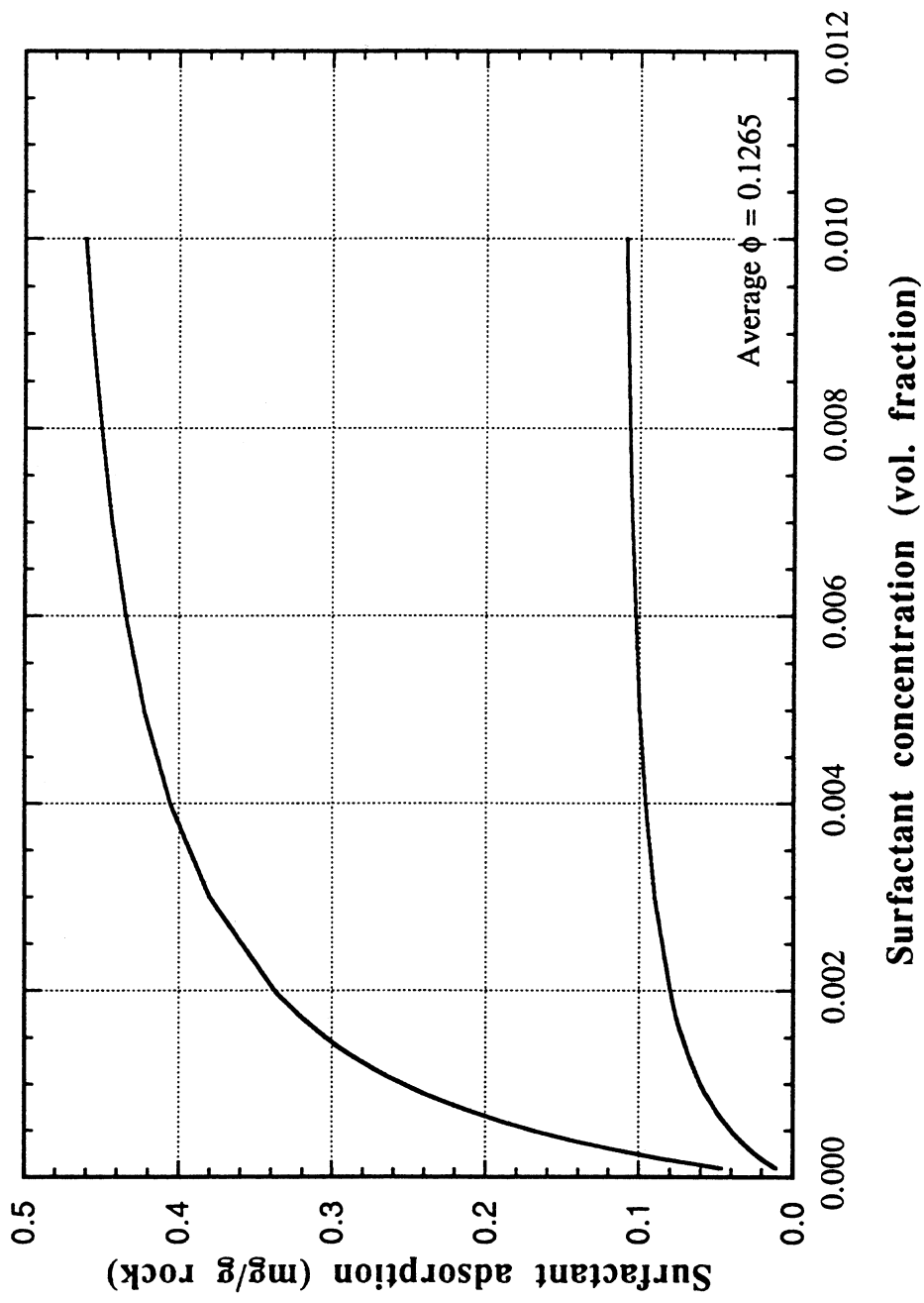


Figure 2.51. Surfactant adsorption isotherms for Reservoir II

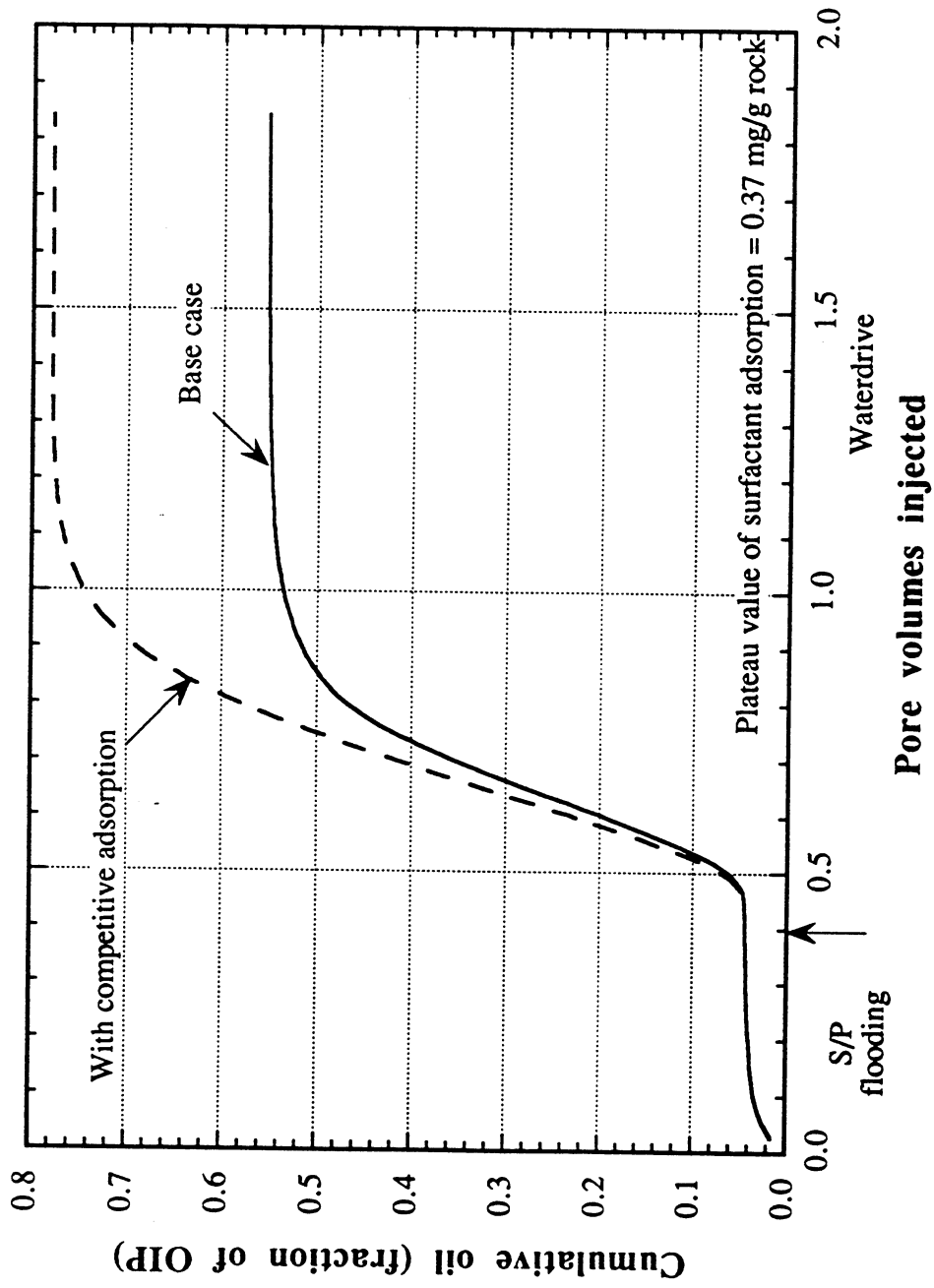


Figure 2.52. Effect of competitive adsorption on oil recovery for Reservoir III

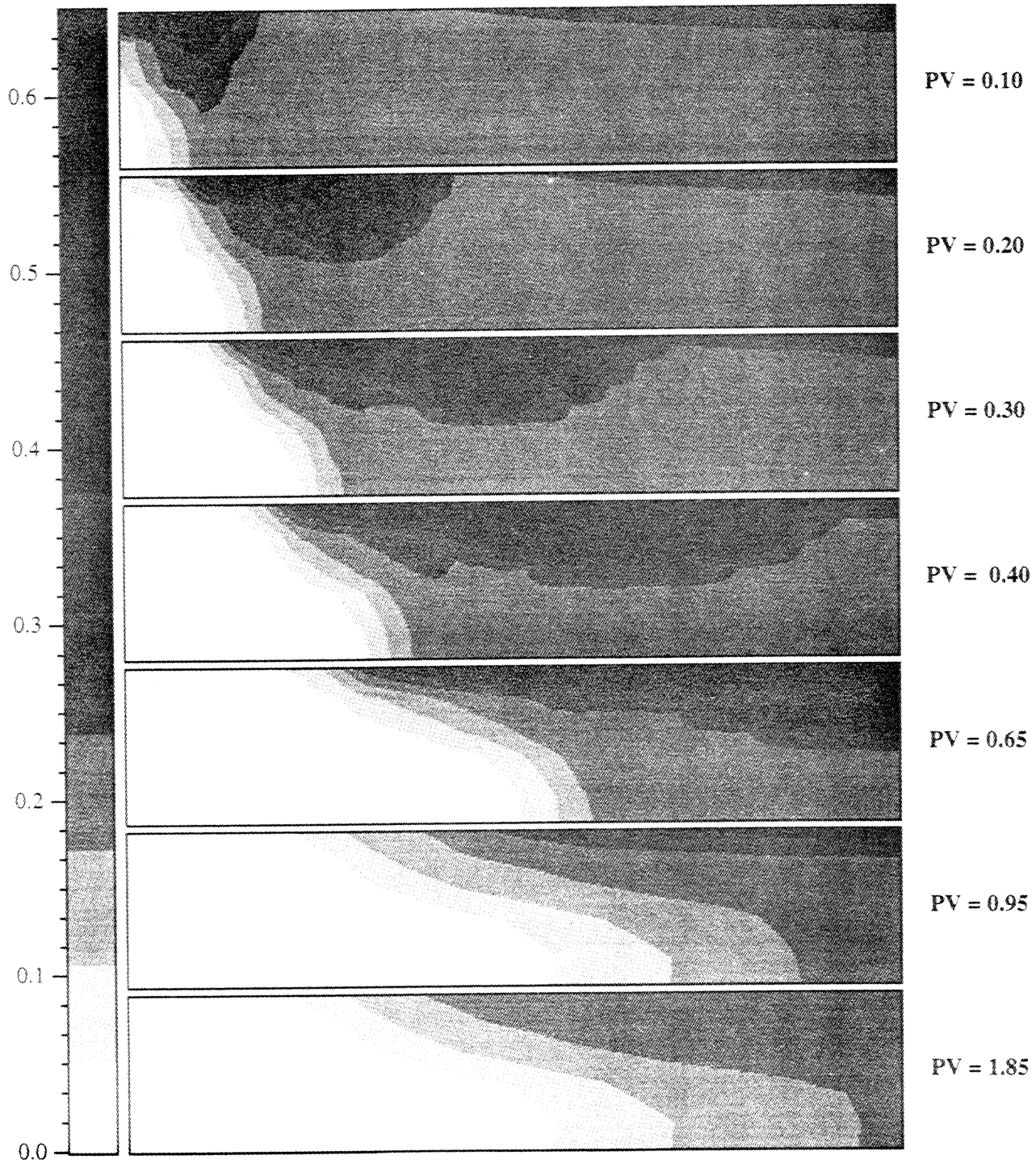
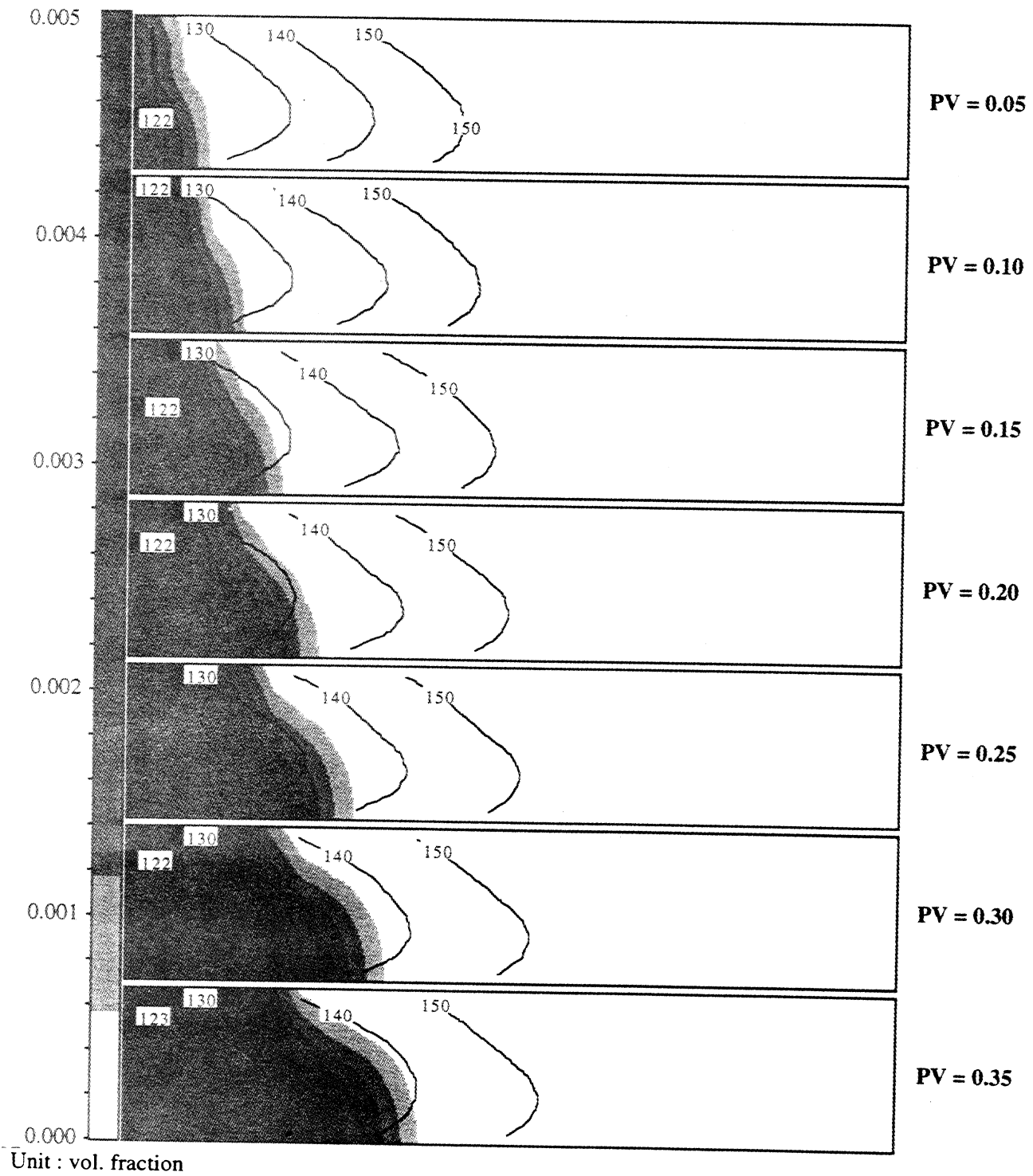
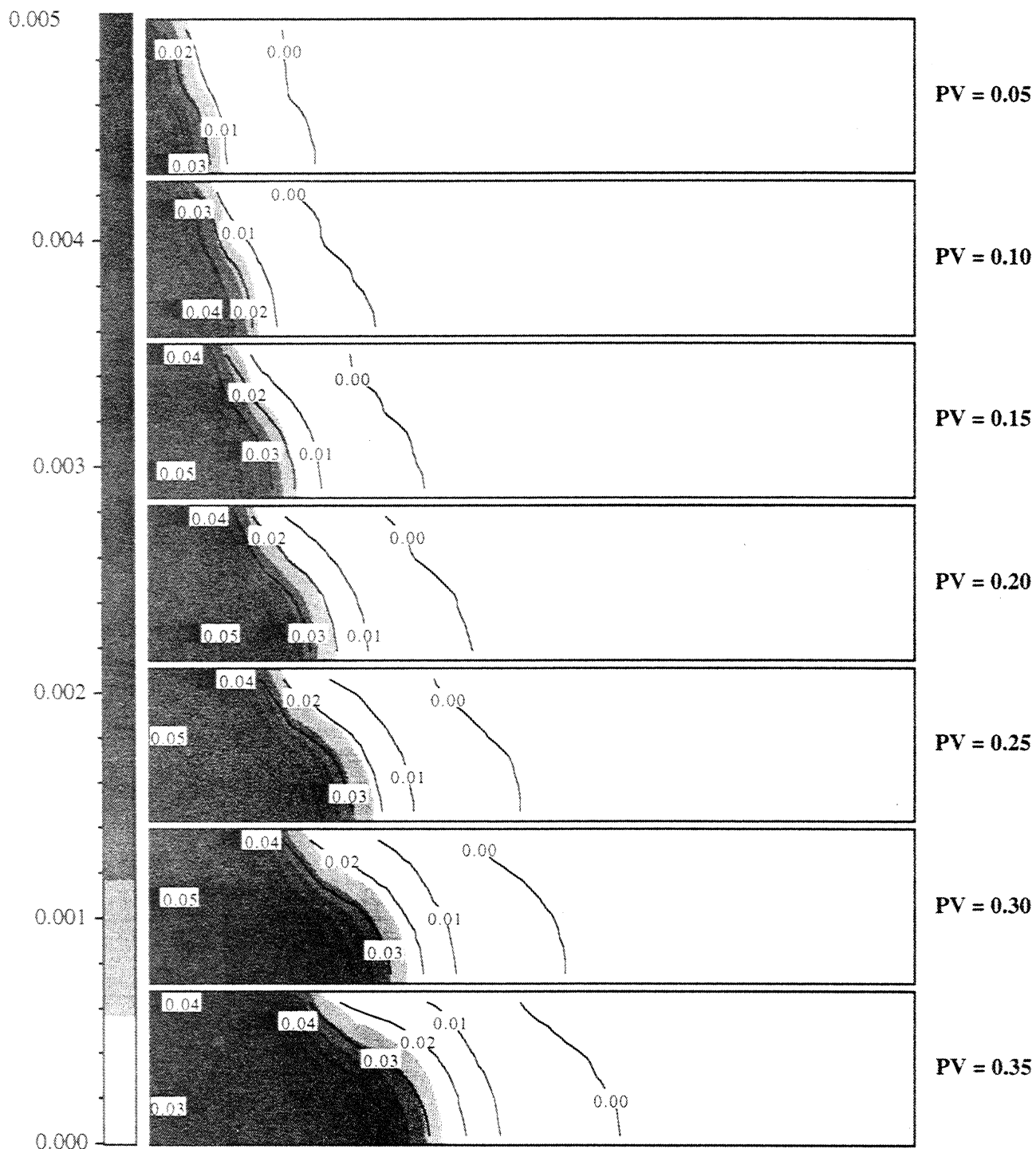


Figure 2.53. Oil concentration profiles for base case for Reservoir III





Unit : vol. fraction

Figure 2.55. Profiles of surfactant concentration overlaid by polymer concentration countours in wt% for Reservoir III

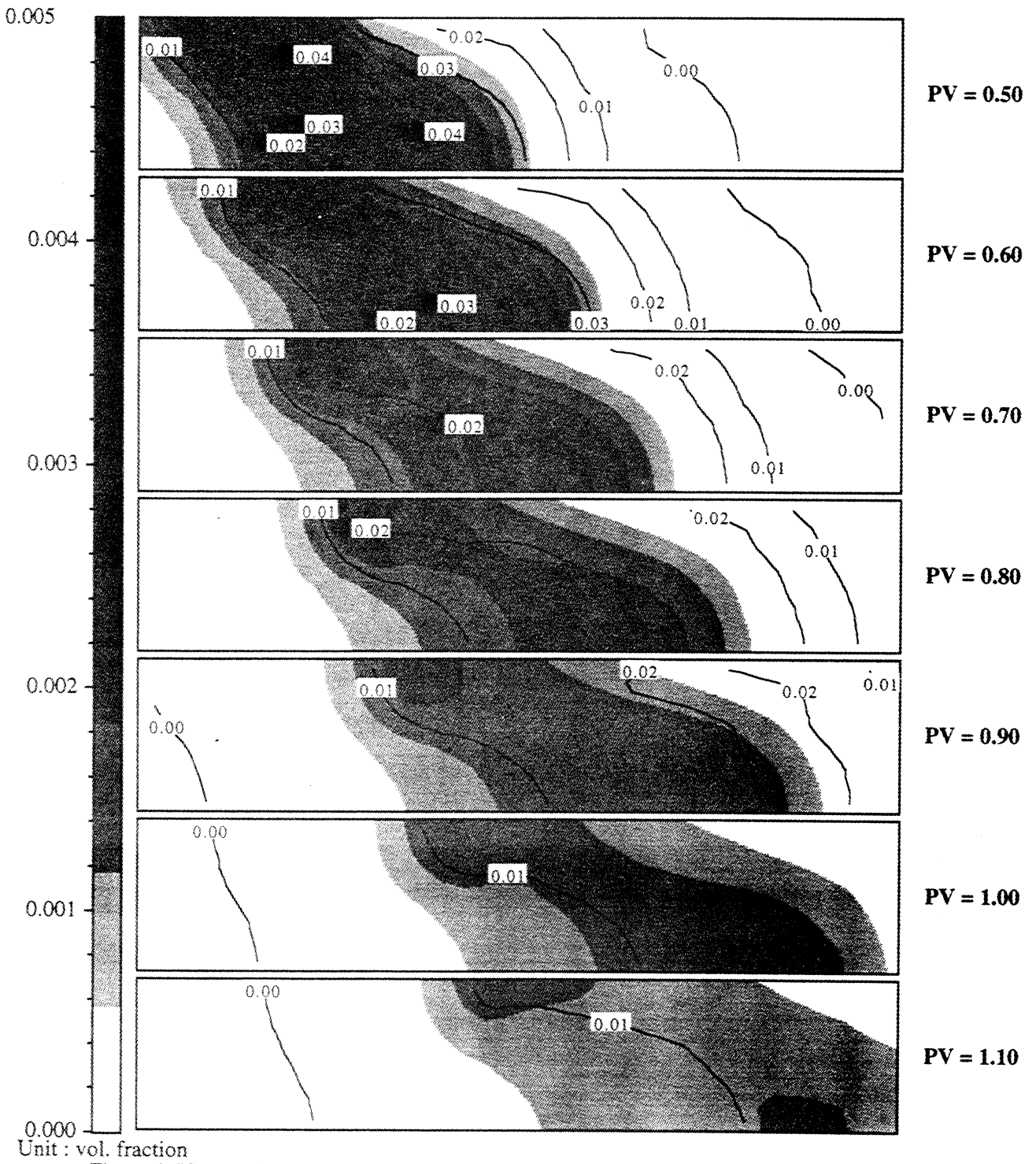


Figure 2.55. (continued) Profiles of surfactant concentration overlaid by polymer concentration contours in wt% for Reservoir III

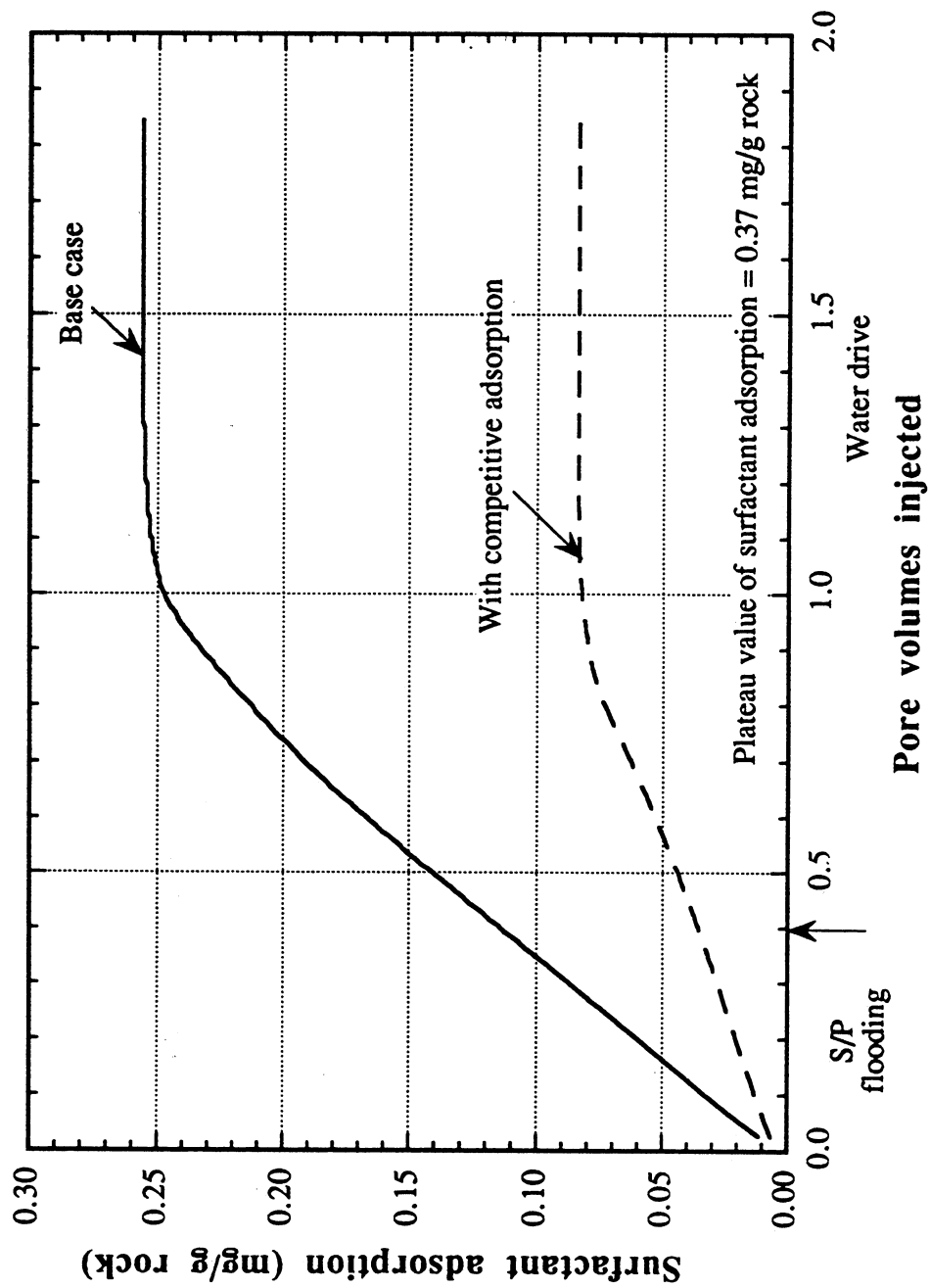


Figure 2.56. Surfactant adsorption with and without competition from polymer for Reservoir III

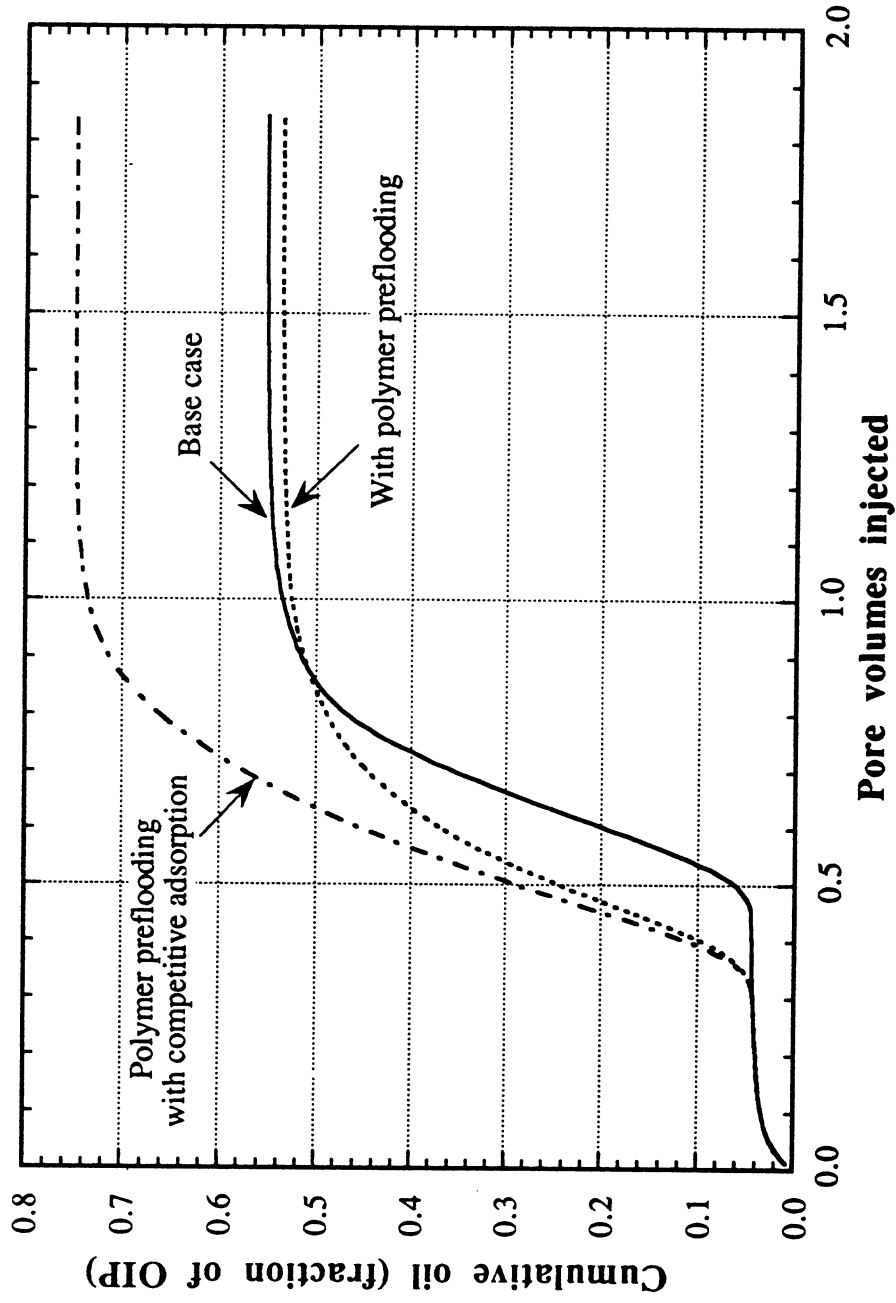


Figure 2.57. Effect of polymer preflooding on oil recovery for Reservoir III

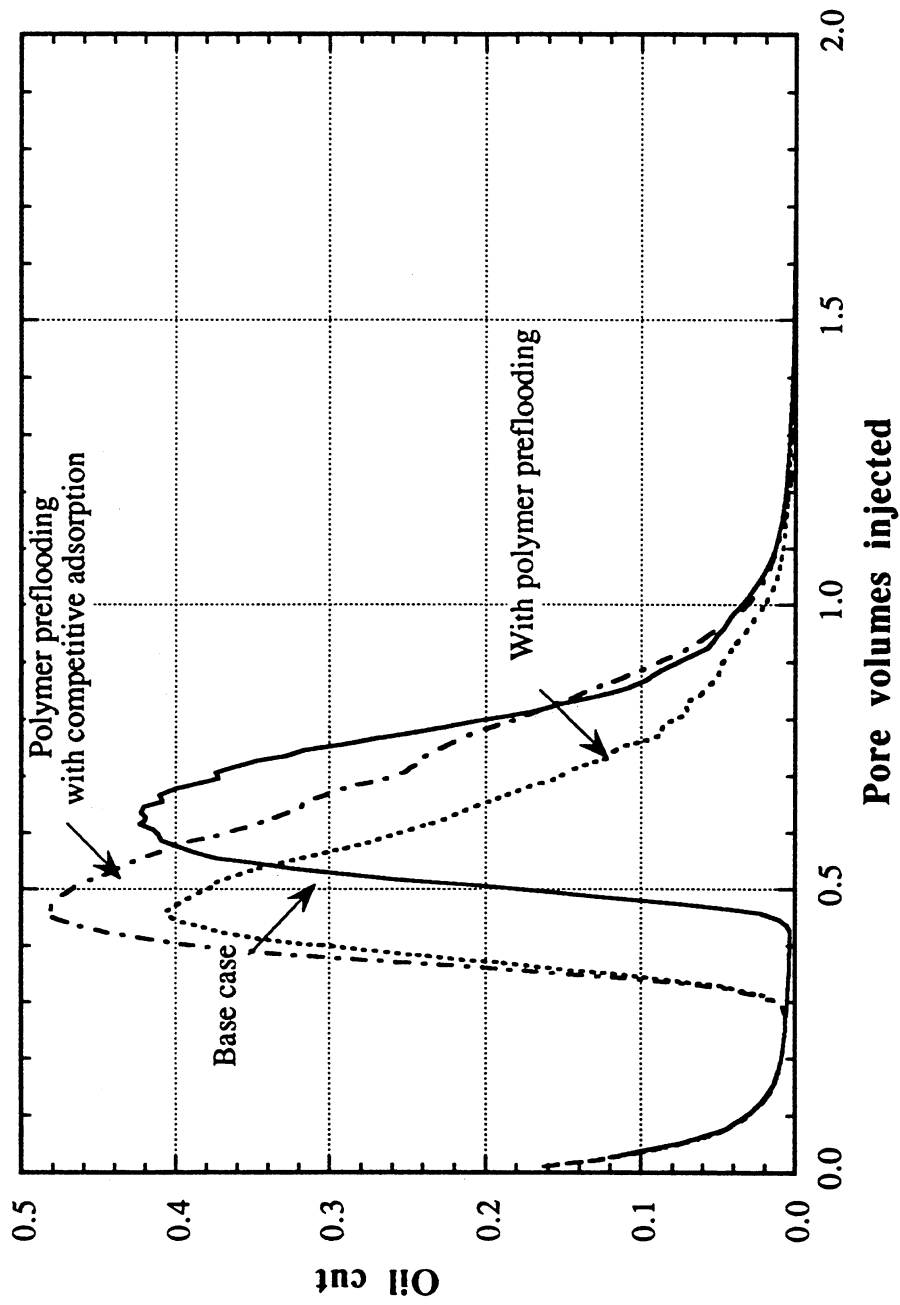


Figure 2.58. Effect of polymer preflooding on oil cut for Reservoir III

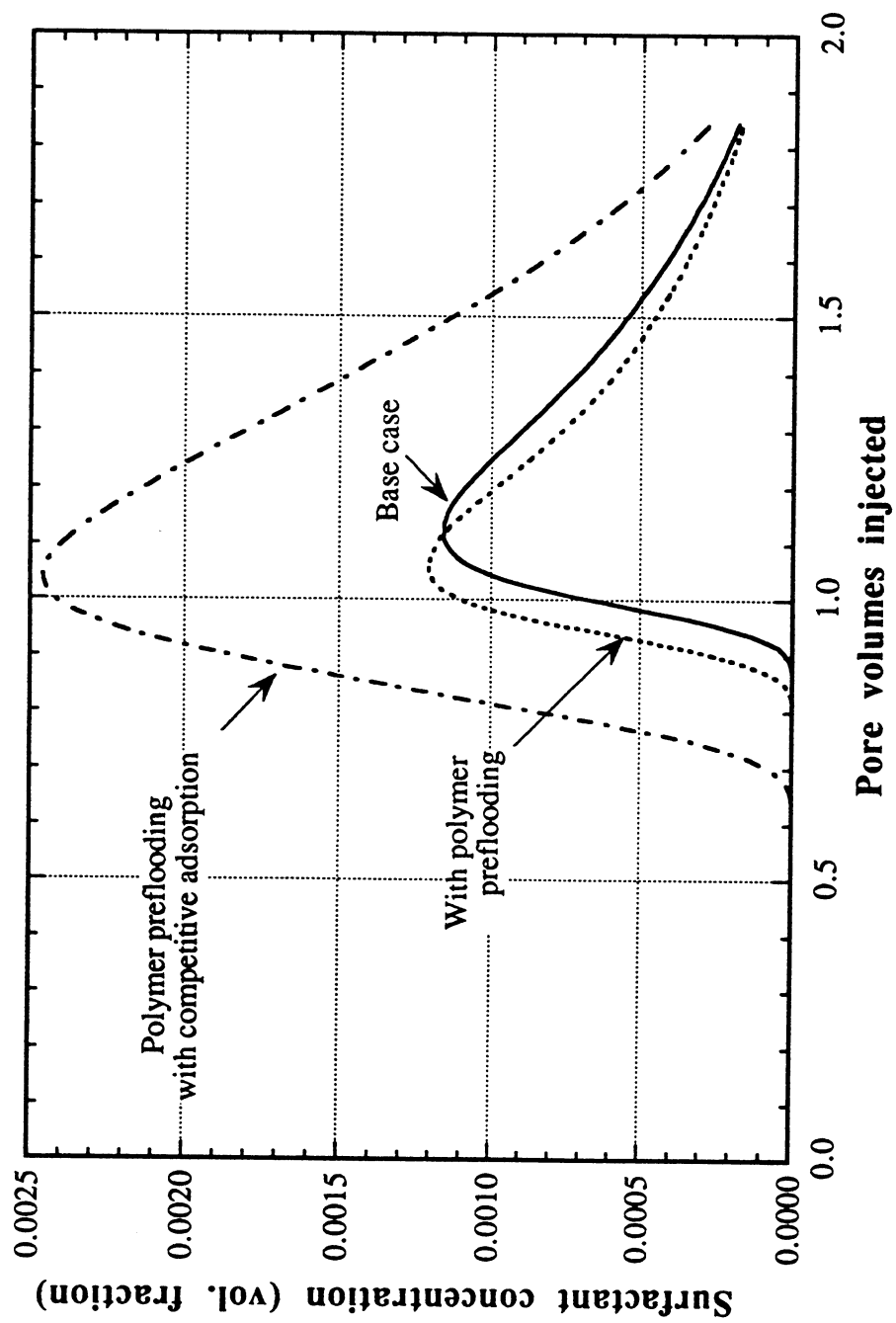


Figure 2.59. Effect of polymer preflooding on effluent surfactant concentration for Reservoir III

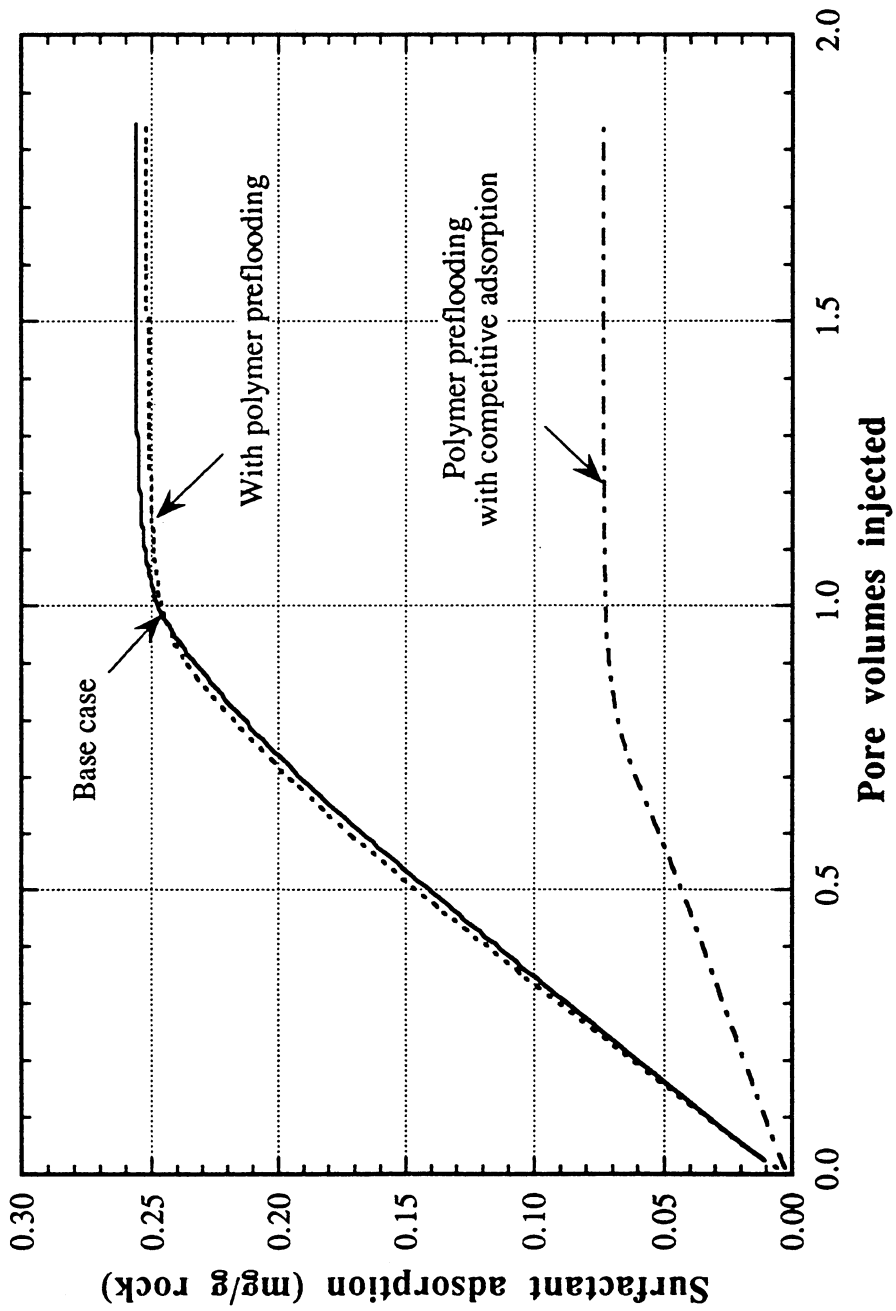


Figure 2.60. Effect of polymer preflooding on surfactant adsorption for Reservoir III

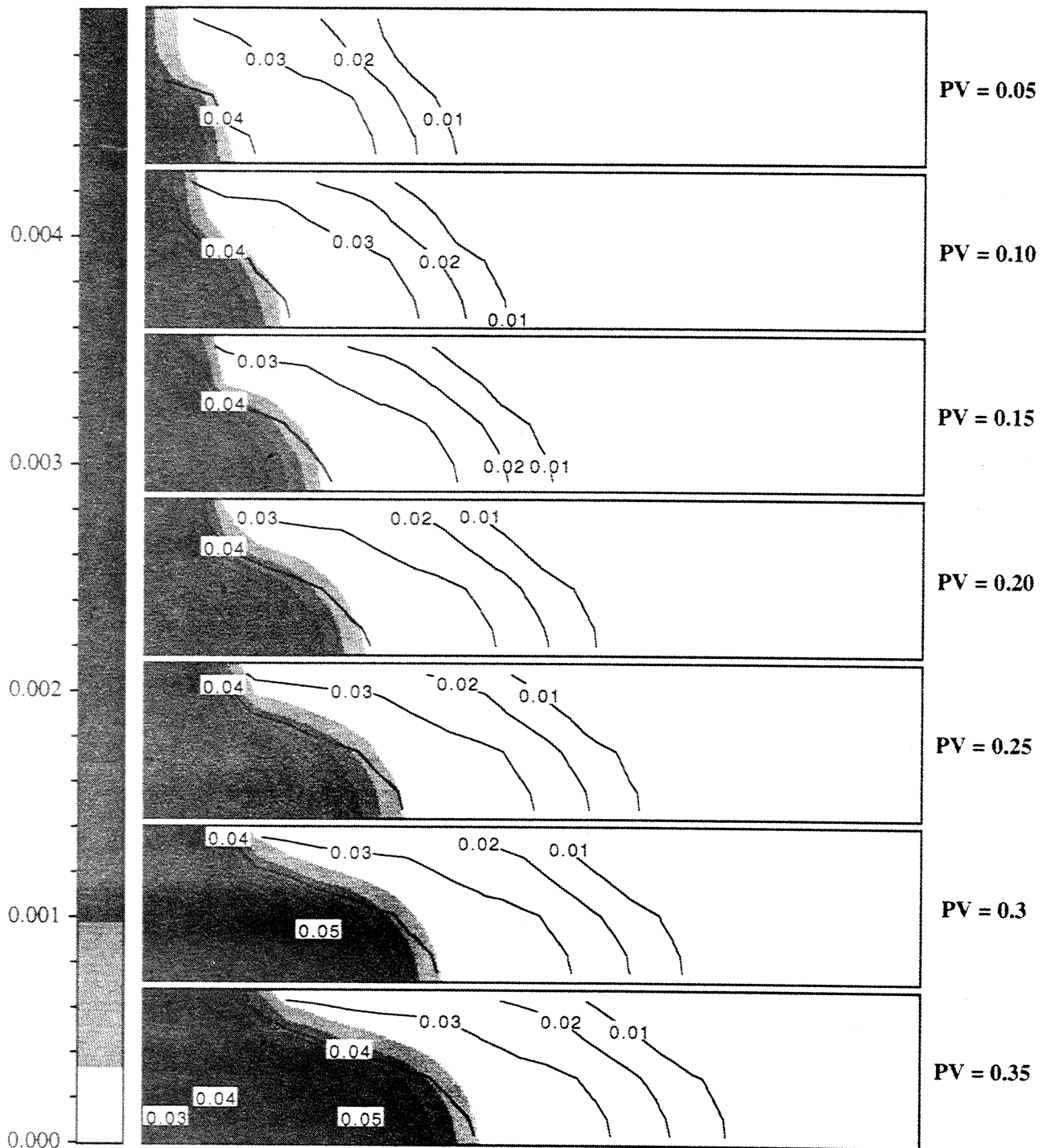


Figure 2.61. Profiles of surfactant concentration overlaid by polymer concentration contours in wt% for Reservoir III

